TÉCNICO LISBOA

Explicit Guidance Solutions for the Lunar Ascent Element of the HERACLES Mission

Leonardo Guilherme Ferreira da Cruz

Thesis to obtain the Master of Science Degree in

Aerospace Engineering

Supervisor: Prof. Paulo Jorge Soares Gil

Examination Committee

Chairperson: Prof. José Fernando Alves da Silva
Supervisor: Prof. Paulo Jorge Soares Gil
Member of the Committee: Eng. Nuno Tiago Salavessa Cardoso Hormigo Vicente

November 2018

Dedicated to my family

Acknowledgments

I want to thank all the support from my family and friends along all my academic journey. I also want to thank professor Paulo Gil and Engineer Tiago Hormigo from spin.works for all the support.

Resumo

Nesta tese, novos algoritmos explícitos baseados na teoria de controlo ótimo para um problema de subida sem atmosfera e veículos de um só estágio foram desenvolvidos e testados para o Lunar Ascent Element do conceito de missão HERACLES. Os diferentes algoritmos consistem em aproximar a estimativa de tempo de ascenção restante, através de uma aproximação do cosseno do ângulo de picada por uma função quadrática e aproximando o integral da aceleração de propulsão em função do tempo por um aproximante de Padé. O seno da picada obtido dos multiplicadores de Lagrange também é aproximado por expansões lineares e quadráticas da série de Taylor a partir de um ponto genérico, ou por polinómios de Lagrange de primeira e segunda ordem, para que uma solução explícita possa ser obtida. Os novos algoritmos são comparados com uma solução explícita da literatura [1], com dois métodos de orientação bastante testados (Orientação Polinomial e PEG) e com a solução óptima numérica para a subida da superfície da Lua para uma órbita lunar baixa usando o Lunar Ascent Element. As aproximações lineares, em particular, produzem perfis de picada próximos do óptimo sem um aumento no custo computacional da solução explícita anterior.

Palavras-chave: Lua, Orientação Explícita, Controlo Ótimo, Voo Ascendente de Foguetes

Abstract

In this thesis, new explicit algorithms based on optimal control theory for an atmosphereless single stage ascent problem were obtained and tested for the Lunar Ascent Element of the HERACLES mission concept. The different algorithms consist on approximating the remaining burntime estimation, using a quadratic approximation for the cosine of the pitch angle, and approximating the thrust acceleration integral in time by a Padé approximant. The sine of the pitch obtained from the Lagrange multipliers will also be approximated by linear and quadratic Taylor series expansions from a generic point, or linear and quadratic Lagrange polynomials, so that an explicit solution is obtained. The new algorithms are compared with an explicit solution from literature [1], with two well tested guidance methods (Polynomial Guidance and PEG) and with the optimal numerical solution for an ascent from the surface of the moon into low lunar orbit using the early design of the Lunar Ascent Element. The linear approximations in particular produced near optimal pitch profiles without an increase in computational cost from the previous explicit solution.

Keywords: Moon, Explicit Guidance, Optimal Control, Rocket Ascent.

Contents

List of Tables

List of Figures

Nomenclature

Greek symbols

α	LAE maximum pitch/yaw angular acceleration.
ζ	Out of plane perturbation angle.
θ	Pitch angle.
Λ	Full Lagrange multiplier vector in the MCI reference frame.
Λ_R	Position Lagrange multiplier vector in the MCI reference frame.
Λ_V	Velocity Lagrange multiplier vector in the MCI reference frame.
$\lambda_{u,v,w}$	Velocity Lagrange multipliers in the LVLH reference frame.
$\lambda_{x,y,z}$	Position Lagrange multipliers in the LVLH reference frame.
μ	Standard gravitational parameter of the moon.
μ_p	Standard gravitational parameter of the third body.
$\vec{\Xi}$	State vector in the MCI reference frame.
τ	Ratio between reference exhaust velocity and current acceleration from thrust $\frac{v_e m}{T}$.
χ	Downrange angle.
ψ	Yaw angle.
ω	Schuller frequency.

Roman symbols

A, B	PEG guidance constants.
a_T	Acceleration generated by thrust $\frac{T}{m}$.
$A_{1,2,3}$	Fully explicit guidance constants.
a_{J2}	Acceleration J2 gravity term.
a_{sp}	Acceleration from solar radiation pressure.

a_{3b} Acceleration from third body perturbation.

$b_0, b_1, b_2, c_0, c_1, b_2$ Thrust acceleration integrals.

C_y $g - \frac{u^2}{r}$.

$\hat{F}$ Normalized thrust vector in the MCI reference frame.

$\hat{f}$ Normalized thrust vector in the LVLH reference frame.

$\hat{f}_1, \hat{f}_2, \hat{f}_3$ Normalized thrust coordinates LVLH reference frame.

$\vec{G}$ Acceleration vector due to inverse square gravity field in the MCI reference frame.

g Acceleration due to inverse square gravity field in the LVLH reference frame.

g_0 Gravity acceleration at moon surface.

H Hamiltonian.

i Inclination.

I_{sp} LAE control maximum torque.

$I_{x,y}$ Moments of inertia of the LAE.

k LAE radius.

$k_{1,2,3,4,5,6}$ Polynomial guidance constants.

k LAE height.

M LAE maximum torque.

m Mass of the vehicle.

$\vec{P}$ Acceleration vector due to perturbations in the MCI reference frame.

$\vec{R}$ Position vector in the MCI reference frame.

$\vec{R}_p$ Position vector of the perturbing body centered on the moon.

$\vec{R}_{ps}$ Position vector of the perturbing body centered on the vehicle.

r $R_{☾} + y$.

$R_{\odot}$ Radius of the Sun.

$R_{☾}$ Radius of the moon.

T Thrust modulus.

t Time since lift-off.

t_f Insertion time.

u, v, w LVLH reference frame velocity coordinates.

$\vec{V}$ Velocity vector in the MCI reference frame.

v_e Reference exhaust velocity.

$\hat{X}, \hat{Y}, \hat{Z}$ MCI reference frame normalized position coordinates.

X, Y, Z MCI reference frame position coordinates.

x, y, z LVLH reference frame position coordinates.

Subscripts

0 At lift-off time.

f At insertion time.

Superscripts

T Transpose.

Glossary

DSG	Deep Space Gateway.
GER	Global Exploration Roadmap.
HERACLES	Human-Enhanced Robotic Architecture and Capability for Lunar Exploration and Science.
ISECG	International Space Exploration Coordination Group.
LAE	Lunar Ascent Element.
LDE	Lunar Descent Element.
LEO	Low Earth Orbit.
LLO	Low Lunar Orbit.
LVLH	Local Vertical Local Horizontal.
MCI	Moon Centered Inertial.
NRHO	Near Rectilinear Halo Orbit.
PEG	Powered Explicit Guidance.

Chapter 1

Introduction

1.1 Historical Notes

When in October 1957 Sputnik 1, the first artificial satellite, was launched into orbit bu the Soviet Union, mankind's space exploration started [2]. This caused concern to the people of the United States as it confirmed the capacity of the Soviet Union to attack the US with nuclear weapons from Europe. Thus, the space race began and culminated in the July of 1969 with the first humans landing on the surface of the moon. The Apollo 11 mission was carried out by astronauts Armstrong, Aldrin and Collins [3].

There were 5 other successful Apollo missions [4–8], but since Apollo 17, no other manned missions reached the moon. However, this might be changing soon. In 2018, the International Space Exploration Coordination Group (ISECC), released the latest installment of the Global Exploration Roadmap (GER) [9]. In this document, the main avenues of exploration beyond Low Earth Orbit (LEO) are discussed, with the main objective of human exploration of Mars. The main goals for investing in beyond LEO are discussed and consist in developing exploration technologies, engaging with the public, enhancing Earth's safety, extending human presence beyond LEO, performing science to enable human exploration and other applied sciences, searching for life and stimulating economic growth. In order to achieve these goals, ISEGC divided the prospective missions into 3 main themes, which are the exploration of a Near-Earth asteroid, having extended duration crew missions, and sending humans to the lunar surface [9].

In this work, various algorithms for the guidance of the ascending flight from the lunar surface are developed, implemented, and compared with a numerical optimal trajectory. The objective is to create guidance algorithms that can be called on a set frequency during the ascent flight, and calculate the optimal thrust direction input of the vehicle. This has application to the Lunar Ascent Element (LAE) of the HERACLES mission concept, that fits in the second and third themes mentioned above.

1.2 HERACLES Mission

The HERACLES concept was created for the GER [9]. HERACLES stands for Human-Enhanced Robotic Architecture and Capability for Lunar Exploration and Science and it consists on a new mission concept

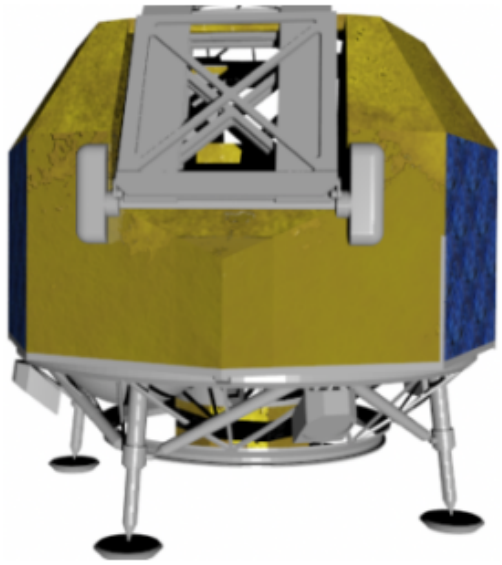

Figure 1.1: Lunar descent element model taken from [11]

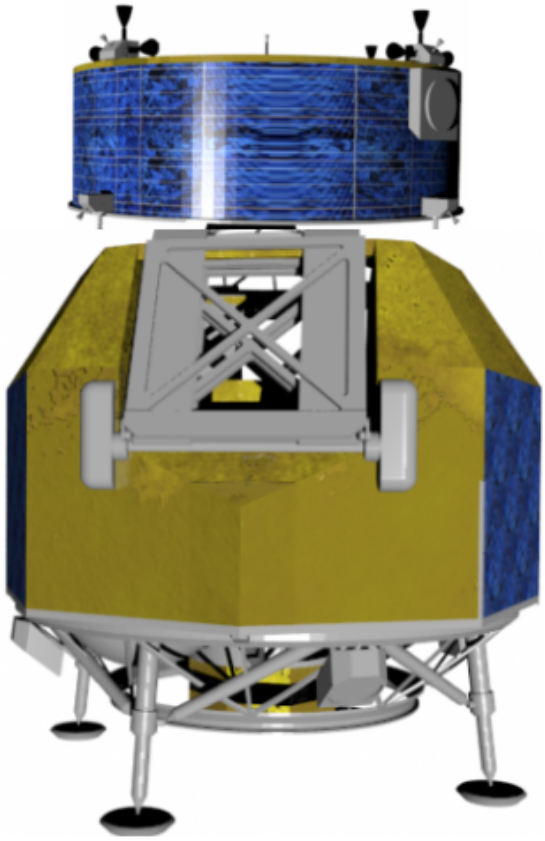

Figure 1.2: Full robotic surface system assembly model taken from [11]

to establish human presence on the moon. There are two main themes to this concept. The first is the establishment of a platform in the lunar vicinity, known as the DSG (Deep Space Gateway). This platform will have many purposes. It will allow for scientific enhancements of the solar system exploration capabilities and improve the knowledge about living outside Earth's vicinity. It will also have the purpose of operating robotic and manned missions to surface of the moon and serve as gateway for missions to mars. The platform will likely be set in a Near Rectilinear Halo Orbit (NRHO), as these types of orbits are the most promising [10]; they will be better described in section 1.3.

The DSG should be established before 2020 and have humans on it in the early 2020's, allowing for human lunar surface exploration in the late 2020's [9]. As of right now, the HERACLES mission has three main systems defined. They are the DSG, the human lander system and the robotic surface system [11, 12]. The DSG, as explained before, is a station that orbits in a NRHO to which Lunar vehicles ascending from the Moon return, from where the robotic missions are partially controlled and from where the human surface missions are conducted. The human lander system will consist of a lander element, an ascent element and pressurised rovers. The robotic surface system (Fig. 1.2) consists of a Lunar Ascent Element (LAE, Fig. 1.3), a Lunar Descent Element (LDE, Fig. 1.3), a sample container, and a rover.

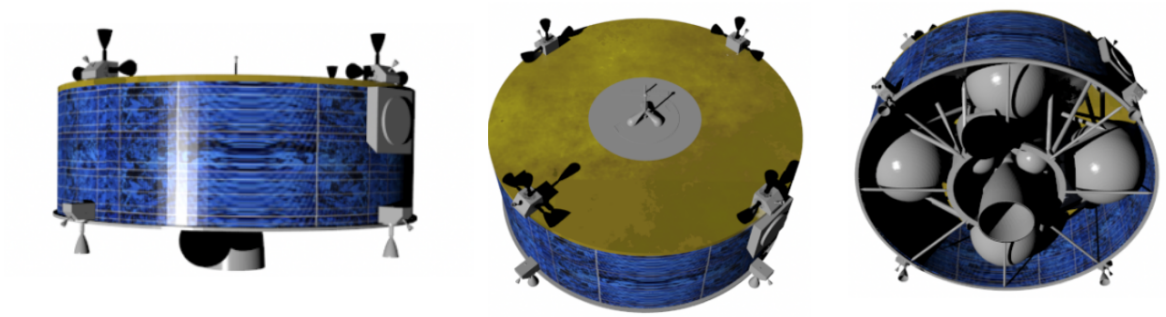

Figure 1.3: Lunar ascent element model taken from [11]

1.3 Near Rectilinear Halo Orbits

The NRHO orbits are a subset of the halo orbits in the vicinity of the colinear Lagrange points, L1 and L2 (in front of and behind the moon respectively), that expand out of the Earth-Moon plane and become close to polar orbits around the moon. A family of halo orbits around L2 can be seen in Fig 1.4. There, NRHO orbits are the near polar orbits on the left. As the halo orbits approach the moon from the Lagrange points, they become almost perpendicular to the Earth-Moon orbital plane and resemble highly elliptical polar orbits. This allows the L2 southern NRHO to have the desired features of continuous communications with the Earth and have direct line of sight with the southern hemisphere of the moon [10, 13].

While these orbits are periodic in the context of the circular restricted three body problem, in a higher-fidelity force model they are only quasi-periodic. They can, however, be kept with some maintenance without high costs if their perilune is close to the surface of the moon (current focus is for perilune between 2100 and $6500\,\mathrm{km}$) [10, 13]. Detailed information on these types of orbits and their advantages for the staging of the DSG can be found in [10, 13]. However, a very thorough understanding of these types of orbits is not required for this thesis, since the work developed here is only related to the ascent flight from the surface of the moon to the transition Polar LLO.

1.4 Guidance Algorithms

Many ascent laws for exo atmospheric problems have been developed over the past decades. In the Apollo missions a polynomial guidance scheme was used [14]. This guidance scheme is not optimal, but it is very simple and has shown good enough results. Another successful guidance scheme was Iterative Guidance Mode (IGM) [15] used on Saturn, where the thrust direction was assumed to be a linear function of time. Probably the most successful and well known ascent guidance scheme is the Powered Explicit Guidance (PEG) [16] used for the Space Shuttle [17, 18]. PEG is based on a linear tangent law for the thrust direction. It includes small angle approximations and requires solving one equation iteratively to estimate the remaining burntime. Other similar methods based on the original PEG and the linear tangent law for the thrust direction have been developed over the years by making

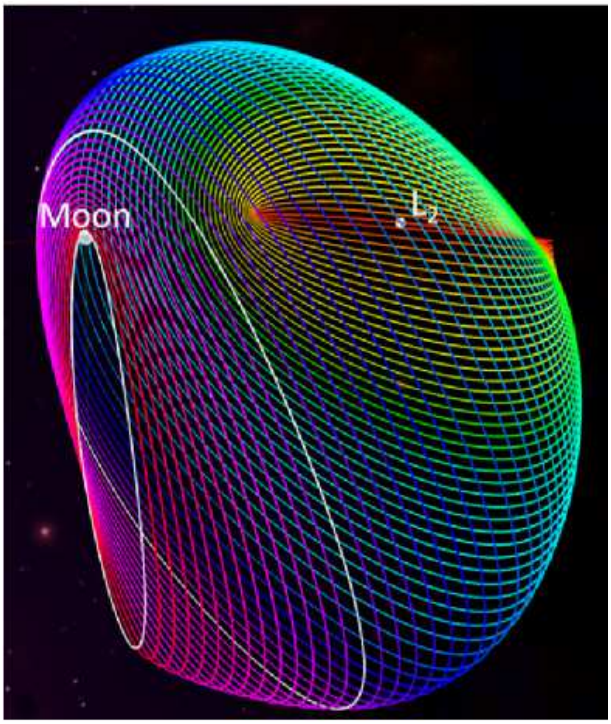

Figure 1.4: Representation of L2 Halo orbits family taken from [13]

changes to the original algorithm on the way to predict the remaining burntime, such as the guidance method proposed for the new Space Launch System [19] and for the Orion capsule [20]. Many other similar methods requiring the numerical solution of one or more equations exist [21–24].

Other than the numerical solutions, a completely analytical solution for the optimal atmosphereless ascent problem was developed in [25] using a two dimensional ascent approximation and in [1] for a three dimensional ascent, by using simplified equations of motion in the Local Vertical Local Horizontal (LVLH) reference frame considering a non-rotating spherical planetary body and some small angle approximations. This approximation has shown near optimal results [1] and the ability to handle out-of-plane pertubations [1, 26]. These guidance methods are based on optimal control theory and unlike PEG, they do not require the usage of a linear tangent law for the thrust direction. This approach to developing a guidance a law is different from the classical methods applied in the development of the PEG algorithm since it does not use a pre defined thrust direction law in its development.

Generalizing the solutions found in [1] for the ascent problem, new guidance algorithms based on different cosine of pitch and sine of pitch approximations, as well as an acceleration integral approximation, are introduced in this work. All approximations are fully analytic and explicit, which is an advantage, because an analytical solution that performs as well as (or almost) a numerical solution can be used to save valuable spacecraft computational resources, either making the mission cheaper or allowing for extra resources for the payload.

1.5 Thesis Overview

In this work an optimal reference trajectory was obtained for the ascent phase of LAE of the HERACLES mission with given orbital insertion conditions. A guidance algorithm that allows the real flight to follow said reference trajectory was also developed. In order to implement a functional guidance algorithm, various methods were compared, such as the ones used for the Space Shuttle and the Apollo missions, as well as more recent methods obtained from optimal control theory.

New algorithms were developed in this work, refining an optimal control theory based algorithm from literature. They are tested and shown to deliver better results when applied to the case of the LAE. Selection preferences for choosing a method are the algorithm speed, reliability and its fuel optimality. The results were discussed and the best guidance methods chosen accordingly.

Chapter 2

Problem definition

2.1 Introduction to the Problem

The objective of the ascent flight is to reach the chosen insertion conditions while spending the minimum fuel possible. For an exoatmospheric ascent, such as the ascent from the surface of the moon to a LLO, the main applied forces in effect are thrust and gravity. Other pertubation forces are discussed in Section 2.4.

In this work, the thrust of the LAE was assumed constant, and so, the mass flow β was also constant. This means that the fuel optimization problem is the same as minimizing the ascent time. A specific transfer LLO has not yet been chosen for the HERACLES concept. Therefore, different insertion altitudes need to be tested. This offers an opportunity to understand how the new algorithms perform as a function of the insertion altitude.

It is useful to use two reference frames, one for the reference trajectory numerical calculation, and one for the development of the guidance algorithms. The Moon centered inertial (MCI) reference frame was used for the reference trajectory calculation, as shown in 2.1. The XZ plane for the frame used is parallel to the orbit insertion plane. Any directions for the X and Y axes are valid, and are not important for the optimization problem, as long as they are consistent. The MCI reference frame is used for the numerical optimization due the simplicity of the equations of motion. This will allow for easy numerical integrations. The LVLH reference frame used to deduce the guidance law is shown in figure 2.2. The xy plane is the orbit insertion plane (assuming keplerian orbits). The definitions for x, y, u, v are the in-plane downrange, altitude, horizontal velocity component, and vertical velocity component, respectively. The coordinate z is the out-of-plane distance and w is the out-of-plane component of the velocity. The pitch (θ) and yaw (ψ) angles are defined in relation to the local horizontal. This reference frame was chosen because with some simplifications, it allows for the development of completely analytical and explicit guidance laws.

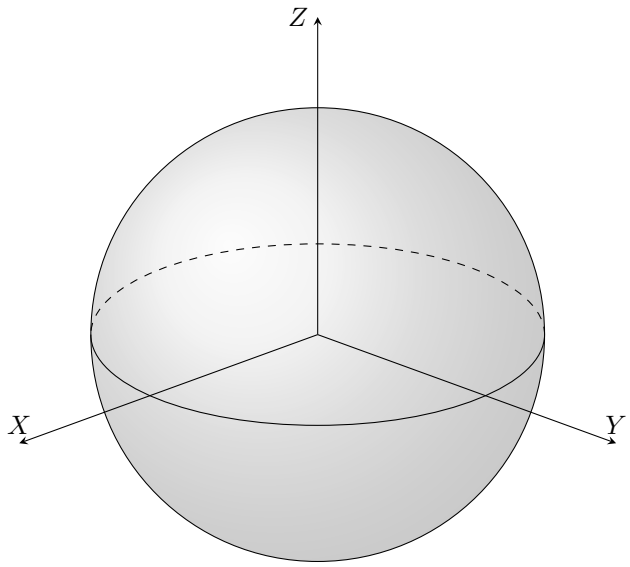

Figure 2.1: Moon centered inertial reference frame

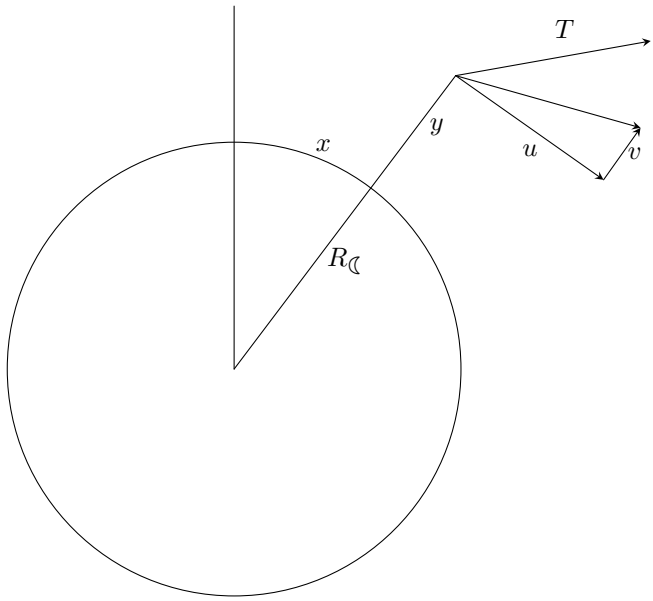

Figure 2.2: Local vertical local horizontal reference frame

2.2 Equations of Motion

2.2.1 Equations of Motion in the MCI Reference Frame

For a standard ascent problem the equations of motion in the MCI frame are:

$$\dot{\vec{R}} = \vec{V}, \tag{2.1a}$$

$$\dot{\vec{V}} = \vec{G} + a_T \hat{F} + \vec{P}, \tag{2.1b}$$

where $\vec{R}$ is the position vector, $\vec{V}$ is the velocity vector, $\vec{G}$ is the inverse square field gravity acceleration, a_T is the absolute value of the acceleration due to the thrust, $\hat{F}$ is the thrust direction and $\vec{P}$ is the acceleration due perturbations acting on the vehicle, that will be discussed in Section 2.4.

2.2.2 Equations of Motion in the LVLH Reference Frame

Assuming a spherical non-rotating moon with no third body influences, the equations of motion in the LVLH reference frame are simplified to:

$$\dot{x} = \frac{R_{☾}}{r} u, \tag{2.2a}$$

$$\dot{y} = v, \tag{2.2b}$$

$$\dot{z} = \frac{R_{☾}}{r} w, \tag{2.2c}$$

$$\dot{u} = a_T \hat{f}_1 + \frac{uw}{r} \tan(\frac{z}{R_{☾}}) - \frac{uv}{r}, \tag{2.2d}$$

$$\dot{v} = a_T \hat{f}_2 - g + \frac{u^2}{r} + \frac{w^2}{r}, \tag{2.2e}$$

$$\dot{w} = a_T \hat{f}_3 - \frac{u^2}{r} \tan(\frac{z}{R_{☾}}) - \frac{vw}{r}, \tag{2.2f}$$

where x, y, u, v are the in-plane downrange, altitude, horizontal velocity component, and vertical velocity component, respectively. The coordinate z is the out-of-plane distance and w is the out-of-plane component of the velocity, $\hat{f} = [\hat{f}_1, \hat{f}_2, \hat{f}_3]$ is the unit thrust vector, g is the acceleration of gravity at the vehicle position, $R_{☾}$ is the radius of the moon and $r = R_{☾} + y$. An optimal ascent is bidimensional, but a real ascent flight has pertubations in the z direction. However, if they are small, the terms $uw/r, vw/r$, w^2/r and $\tan(z/R_{☾})$ can be neglected. Also for low altitude ascent trajectories $R_{☾}/r \approx 1$ and $uv/r << a_T \hat{f}_1$ [1]. Neglecting these terms the equations can then be reduced to:

$$\dot{x} = u, \tag{2.3a}$$

$$\dot{y} = v, \tag{2.3b}$$

$$\dot{z} = w, \tag{2.3c}$$

$$\dot{u} = a_T \hat{f}_1, \tag{2.3d}$$

$$\dot{v} = a_T \hat{f}_2 - g + \frac{u^2}{r}, \tag{2.3e}$$

$$\dot{w} = a_T \hat{f}_3. \tag{2.3f}$$

If the term $C_y = g - \frac{u^2}{r}$ is assumed to be constant, we end up with:

$$\dot{x} = u, \tag{2.4a}$$

$$\dot{y} = v, \tag{2.4b}$$

$$\dot{z} = w, \tag{2.4c}$$

$$\dot{u} = a_T \hat{f}_1, \tag{2.4d}$$

$$\dot{v} = a_T \hat{f}_2 - C_y, \tag{2.4e}$$

$$\dot{w} = a_T \hat{f}_3. \tag{2.4f}$$

This is useful because the guidance algorithm needs to calculate the trajectory on the flight at a chosen frequency (1 Hz was chosen on this paper). To obtain analytic and explicit guidance algorithms, C_y is assumed to be cosntant every time the trajectory is calculated on the flight.

2.3 Vehicle Features

In this thesis the vehicle used for testing the algorithms was the early design version for the LAE of the HERACLES mission, as described in [11]. The main features of this vehicle can be found on Table 2.1. Other than the Bi-propellant main engine, LAE uses 16 High thrust (220 N each) engines for ascent/descent control, 8 Low thrust engines (10 N each) for DSG proximity operations and berthing and 8 Thrusters for roll control.

Specific Impulse	340 s
Wet Mass	1339 kg
Thrust	6 kN

Table 2.1: Main LAE features

In order to figure out the capabilities of the actuators in terms of pitch and yaw rate change it is necessary to estimate the LAE moment of inertia. For simplification, the vehicle was assumed to be a homogeneous cylinder of height $l = 0.9$, radius $k = 1.295$ m and mass $m = 1339 - tT/g_0 I_{sp}$ kg leading to a moment of inertia for both yaw and pitch purposes of:

$$I_x = I_y = \frac{m}{12}(3k^2 + 4l^2), \tag{2.5a}$$

$$I_x = I_y = 0.6893(1339 - 1.8t). \tag{2.5b}$$

Each of the 220 N engines is placed at the maximum radius as seen in Fig. 1.3 can produce a torque of $M = 220k = 220 \times 1.295 =$ 284.9 N m, so, the angular acceleration in $\mathrm{rad\,s^{-2}}$ that each engine can provide is:

$$\alpha = \frac{M}{I} = \frac{284.9}{0.6893(1339 - 1.8t)}. \tag{2.6}$$

Even though no actuators were modelated in this thesis, it should be kept in mind that this is the maximum angular acceleration that the vehicle can generate, and the pitch profiles generated from the new guidance algorithms comply with it.

2.4 Environment Models

For the simplyfied equations to be valid, we must confirm if the perturbations not included can be neglected. The main perturbations acting on the vehicle are the third body perturbations (mainly from the Sun and the Earth), the solar radiation pressure and the gravity perturbations due to the non sphericity of the moon.

The third body accelerations are [27]

$$a_{3b} = \mu_p \left(\frac{\vec{R}_{ps}}{||\vec{R}_{ps}||^3} - \frac{\vec{R}_p}{||\vec{R}_p||^3} \right), \tag{2.7}$$

where μ_p is the standard gravitational parameter of the perturbing body, R_{ps} is the radius vector of the perturbing body relative to the spacecraft and R_p is the radius vector of the perturbing body relative to the main body. The main body in this case will be the moon, and the perturbing bodies considered will be the earth and the Sun.

Eq. (2.7) holds a maximum value when the three bodies are on a straigth line and is

$$||a_{3b}||_{\text{max}} = \mu_p \left(\frac{-2r||\vec{R}_p|| + ||\vec{R}||^2}{||\vec{R}_p||^4 - 2||\vec{R}_p||^3||\vec{R}|| + ||\vec{R}||^2||\vec{R}_p||^2} \right), \tag{2.8}$$

where $||\vec{R}||$ is distance from the center of the main body to the spacecraft. The third body maximum perturbations can then be easily estimated assuming that R_p is constant and equal to the minimum distance between the main body and the perturbing body.

The J2 perturbation is [28]

$$a_{J2} = \frac{3J_2\mu R_{☾}^2}{2||\vec{R}||^5} \left[\left(\frac{5Z^2}{||\vec{R}||^2} - 1 \right)(X\hat{X} + Y\hat{Y}) + \left(\frac{5Z^2}{||\vec{R}||^2} - 3 \right)(Z\hat{Z}) \right]. \tag{2.9}$$

The modulus of the perturbation is maximum when $||\vec{R}|| = Z$, so this was the case studied. When this happens, Eq. (2.11) becomes:

$$a_{J2} = \frac{3J_2\mu R_{☾}^2}{||\vec{R}||^5 Z} \hat{Z}, \tag{2.10}$$

$$||a_{J2}|| = \frac{3ZJ_2\mu R_{☾}^2}{||\vec{R}||^5}. \tag{2.11}$$

The result of this calculations can be visualised in Fig. 2.3, using the characteristics of the moon found in [29].

Another perturbation that was not taken into consideration in Fig. 2.3 was the solar radiation pressure which, according to [30], can be calculated using:

$$a_{sp} = \frac{\kappa}{R_{\odot}^2}, \qquad \kappa = \frac{\eta L}{2\pi c\sigma}, \qquad \sigma = \frac{m}{A}, \tag{2.12}$$

where the solar luminosity $L = 3.842 \times 10^{26}$ W, $\eta = 0.5$ means total absorption of photons by the vehicle and η = 1 means total reflection, and the value is between both. A is the area bathed by sunlight, m is the mass of the vehicle, $R_{\odot}$ is the distance of the vehicle to the Sun and c is the speed of light. Replacing with the values of the problem,

$$a_{sp} \sim 10^{-8}\,\text{m}\,\text{s}^{-2} \tag{2.13}$$

In order to see the importance of each of these accelerations, an estimate of the velocity variation, Δv, and the position variation, Δx, caused by each of the accelerations is calculated, assuming a 6 minute

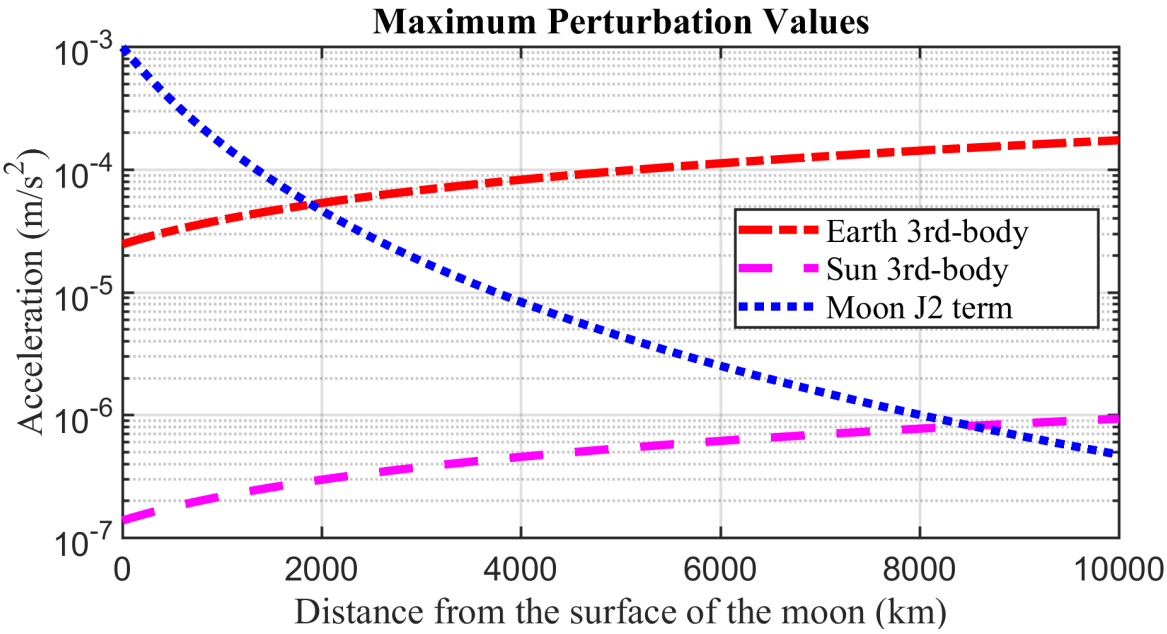

Figure 2.3: Perturbations due to Moon's J2 term and third body accelerations

ascent flight time time into orbit, and a maximum value during the whole ascent for the perturbations:

Table 2.2: Maximum effect of the perturbations during the ascent

Perturbation	Acceleration (max) $[\mathrm{m\,s^{-2}}]$	$\Delta v[\mathrm{m\,s^{-1}}]$	$\Delta x[\mathrm{m}]$
Earth third body	2×10^{-4}	0.072	12.96
Moon J2	10^{-3}	0.36	64.8
Sun third body	10^{-6}	3.6×10^{-4}	6.48×10^{-2}
Sun radiation	10^{-8}	3.6×10^{-6}	6.48×10^{-4}

The Moon's J2 and the Earth's third body pertubations might have a strong enough impact to be taken into account in the simulations, but none of the perturbations is large enough to warrant a change in the guidance techniques and increase in complexity and calculation time, as they can manage small perturbations and the small loss of optimality will not have a large effect compared to the assumptions that will be made to derive explicit equations.

In order to use the J2 gravity term in the simulation, the perturbation must be calculated in the MCI frame and then be rotated into the MCI frame, which is done in Appendix C.

Chapter 3

Obtaining a Reference Trajectory

In order to be able to compare and test the guidance algorithms, it is necessary to have a an optimal reference trajectory. Since this trajectory can be calculated before the flight, it is fine to use a numerical method. The method used is described below.

3.1 Optimal Control Approach

The approach to obtain an optimal reference trajectory used in this thesis is the one described in [31], done for a constant thrust vehicle. A brief description and the equations used are provided in this section.

Optimal control is a theory that finds the optimal input, in this case the direction of the thrust, for a given system and a required optimality criterion. In this work, the vehicle tested is always assumed to have constant thrust. This means that optimizing the fuel efficiency is equivalent to minimizing the ascent time. According to optimal control theory [32] the optimal input is obtained by solving the differential equations:

$$\frac{\partial H}{\partial \vec{\Lambda}} = \dot{\vec{\Xi}}, \tag{3.1}$$

$$\frac{\partial H}{\partial \vec{\Xi}} = -\dot{\vec{\Lambda}}, \tag{3.2}$$

where, for a time minimization problem, the Hamiltonian, H, is

$$H = \vec{\Lambda}.\dot{\vec{\Xi}} + 1, \tag{3.3}$$

In addition to these the value of the Hamiltonian must not depend on the input, that is

$$\frac{\partial H}{\partial \vec{u_c}} = 0. \tag{3.4}$$

$\vec{\Xi}$ is the state vector, $\vec{\Lambda}$ is the vector of the Lagrange multipliers and $\vec{u_c}$ is the input control vector. These equations become a two point boundary value problem. This means that as long as the values of the initial comditions, the insertion conditions and the behavior of the system are known, the problem can be solved either analitcally, if possible, or numerically.

In the algorithm described next, the gravitational acceleration is assumed to varie linearly with the distance to the center of the moon. This assumption is valid since all the altitudes to be tested are small in comparison with the Moon's radius. This allows the Lagrange multipliers to be represented by elementary transcendental functions (sines and cosines), which facilitates the numerical solution of the system by a large amount, as the pitch will be defined by elementary functions, removing the need to use an arbitrary pitch profile for the optimization. This approximation mantains the direction of the gravity acceleration vector the same as the real direction for a spherical moon. Since the distance to the center of the Moon does not change significatively for the ascent trajectories to be tested, using this approximation in a close loop scheme, where the pitch profile is calculated, every iteration will provide a trajectory that is extremelly close to the absolute optimal trajectory. This can be used to evaluate the optimality of the guidance schemes. The pitch is recalculated on a 1 Hz frequency, since increasing the frequency more than this did not have any noticeable effect on the generated trajectory. The position and velocity are calculated each second using a Runge-Kutta 4-5 algorithm, and the vehicle mass was assumed to change linearly. The method to obtain the pitch profile at each step is described next.

For the ascent problem in the spherical Moon in the MCI reference frame with no perturbing forces the Hamiltonian is [32]

$$H = \vec{\Lambda}.\dot{\vec{\Xi}} + 1, \tag{3.5}$$

where $\vec{\Xi}$ is the state vector in the MCI reference frame, $\vec{\Xi} = [\vec{R}; \vec{V}/\omega]$ and $\vec{\Lambda}$ is the vector of Lagrange multipliers. Assuming that the acceleration of gravity

$$\vec{G} = \omega^2 \vec{R}, \tag{3.6}$$

where $\omega = \sqrt{\mu/\bar{R}^3}$ is the Schuller frequency, where μ is the standard gravitational constant and $\bar{R}$ is the average of the modulus of the position vector. This linear approximation of the gravity field is good enough for low altitude ascent trajectories, like the ones studied in this thesis. Thus, the Hamiltonian is

$$H = \vec{\Lambda_R}.\vec{V} + \vec{\Lambda_V}.\left(a_T \hat{F} - \omega^2 \vec{R}\right) + 1. \tag{3.7}$$

From Eq. (3.2), the Lagrange multipliers are of the form

$$\vec{\Pi}(t) = \begin{bmatrix} \cos(\omega t) I_3 & \sin(\omega t) I_3 \\ -\sin(\omega t) I_3 & \cos(\omega t) I_3 \end{bmatrix} \vec{\Pi}_0 = \Phi(t) \vec{\Pi}_0, \tag{3.8}$$

where I_3 is a 3 by 3 identity matrix and $\vec{\Pi} = [\vec{\Lambda}_V; -\vec{\Lambda_R}/\omega]$. From Eqs. (3.4) and (3.7), it can be seen that the direction of $\vec{\Lambda}_V$ is the optimal thrust direction. This means that replacing the thrust direction with $\vec{\Lambda}_V$ in the system of Eqs. (2.1), the solution is

$$\vec{\Xi}(t) = \Phi(t) \vec{\Xi}_0 + \Gamma(t) \vec{I}(t), \tag{3.9}$$

where,

$$\vec{I}(t) = \begin{bmatrix} \int_0^\tau \hat{F}(t)\cos(\omega t) a_T(t) dt \\ \int_0^\tau \hat{F}(t)\sin(\omega t) a_T(t) dt \end{bmatrix}, \tag{3.10}$$

and

$$\Gamma(t) = \frac{1}{\omega} \begin{bmatrix} \sin(\omega t) I_3 & -\cos(\omega t) I_3 \\ \cos(\omega t) I_3 & \sin(\omega t) I_3 \end{bmatrix}. \tag{3.11}$$

The Thrust integrals, $\vec{I}(t)$, can be calculated numerically. In this case a 4 step Milne's rules is used, as is suggested in [31].

By replacing the values of the desired final conditions and the initial conditions on Eq. (3.9) we can obtain a system of equations that will give us the optimal thrust vector. By adding the boundary condition to the Hamiltonian at the insertion time, $H_f = 0$, the optimal burntime can also be determined. The system was solved with a Trust-Region method, since the value of the Jacobian was not calculated, and thus using something like Newthon's method was not possible.

3.2 Test and Validation

In this thesis the vehicle used for testing the algorithms was the early design of the LAE. The main features of this vehicle can be found on Table 2.1 The algorithm described in Section 3.1 will be tested for an insertion into a LLO with an apoapsis at $100\,\mathrm{km}$ altitude and a periapsis at $15\,\mathrm{km}$ altitude leading to the insertion conditions stated in Table 3.1. In Fig. 3.1 it can be seen that the conditions required were met after $307.1\,\mathrm{s}$ of flight. The algorithm had already been extensively tested in [31], so this brief test just intends to verify if the algorithm was well implemented, i.e. if the intended orbit was achieved. The method managed to achieve an ascent that was more optimal than the trajectories provided by the guidance methods of the Apollo missions and the Space Shuttle, displayed in Chapter 5.

Table 3.1: Orbit insertion conditions

Final vertical velocity	$0\,\mathrm{m\,s^{-1}}$
Final horizontal velocity	$1692.9\,\mathrm{m\,s^{-1}}$
Final altitude	$15\,\mathrm{km}$

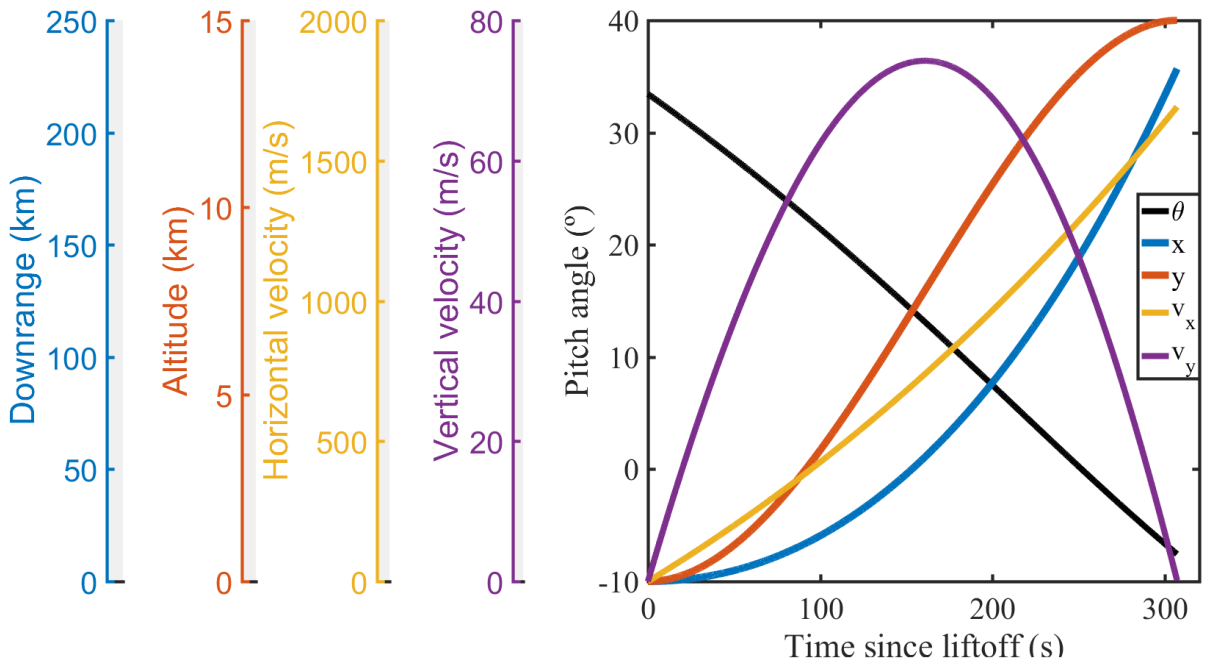

Figure 3.1: Characteristics of the optimal ascent

Chapter 4

Ascent guidance

4.1 Overview of Ascent Missions

On Earth there are usually two guidance phases in launches. The first one is open loop guidance, which is usually a list of attitude commands, that the spacecraft follows and is not updated in flight. The attitude profile is calculated and optimized before the flight. this phase is then followed by a powered guidance phase, known as closed loop guidance [33], when the optimal attitude is calculated and updated along the flight, at a set frequency. Each one of this optimizations is refered to as a guidance call. In the presence of an atmosphere it is very complicated to include all the strong forces in a fast close loop model, and in this cases an open loop phase is necessary. Since the moon does not have an atmosphere, this problem is nonexistent. Thus, the open loop guidance phase can be entirely skipped. The only reason the closed loop scheme cannot start from the surface is to avoid objects such as lunar mountains. This means that a vertical flight phase and linear pitchover are necessary, but these are a small portion of the ascent, when compared to launches from the Earth [14, 33]. This is what is usally considered, altough open loop guidance schemes can still be used on the moon. They might fail if the real trajectory deviates from the reference, which is somewhat likely to happen in the moon (the landing, and thus ascent site might not be what was predicted, mission objectives can change based on how the mission is going, etc).

4.2 Decomposition Into Mission Phases

As in the Apollo missions [14], an ascent from the surface can be decomposed into 3 different phases (Fig. 4.1). The first phase will be a vertical climb to gain altitude to be able to fly over the natural obstacles, such as mountains. The second phase is a linear pitchover where the pitch is decreased linearly as fast as possible, in order to get to the optimal guidance phase as quickly as it is feasable. The third, and longest phase of the flight, is the Powered Guidance phase. During this phase the vehicle will gain most of its speed in order to reach the desired orbit. On the vertical flight phase the pitch is simply

kept at 90° for the whole duration. From Eq. (2.3), the altitude during this phase is

$$y = y_0 + a_T - \frac{\mu}{(R_{☾} + y)^2}. \tag{4.1}$$

On the linear pitch over phase, the pitch changes linearly as fast as possible between 90° and an angle to be defined, so the pitch is

$$\theta = \theta_0 + \dot{\theta} t \tag{4.2}$$

In the simulations done in this work the vehicle was considered to be leaving the ground and entering the powered guidance phase right away. This was done to facilitate the understanding of the simulation results plots because the vertical ascent and linear pitchover would be the same for all the guidance algorithms. Since the ascent problem treated in this work is atmosphereless, this assumption will have little effect on the whole trajectory, as the powered ascent phase will be about 90% of time of the total ascent [33].

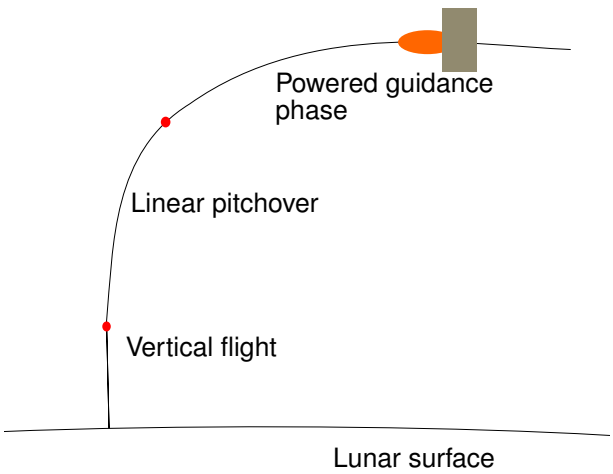

Figure 4.1: Lunar ascent flight phases

4.3 Applicable Guidance Algorithms from Literature

4.3.1 PEG

PEG was first developed for the Surveyor missions as an alternative to using open loop schemes [16]. The algorithm is based on a linear tangent law for the thrust direction and is close to a fuel optimal guidance method for a standard rocket ascent. Since then it has become a staple in ascent guidance algorithms and is mainly known for its use in the Space Shuttle. PEG was developed using the following approximations:

- Inverse square gravity field (spherical constant density planet)
- No atmospheric effects
- No third body perturbations
- Constant thrust and specific impulse

Pitch guidance

Using the approximations stated above and Eq. (2.3), the acceleration in the vertical direction is

$$\ddot{r} = \frac{u^2}{r} - \frac{\mu}{r^2} + a_T \hat{f}_2, \tag{4.3}$$

where $r = y + R_{☾}$ in the LHLV reference frame, the u^2/r term is the centrifugal force term, μ/r^2 is the gravity term, a_T is the acceleration due to thrust and $\hat{f}_2$ the projection of the thrust unit vector in the local vertical direction. The pitch guidance law used is:

$$\hat{f}_2 = A + Bt + \frac{\mu/r^2 - u^2/r}{a_T}, \tag{4.4}$$

so, from Eq. (4.3) and Eq.(4.4) we get

$$\ddot{r} = (A + Bt)a_T. \tag{4.5}$$

Equation (4.5) can be integrated twice leading to

$$\dot{r}_f = \dot{r}_0 + b_0 A + b_1 B, \tag{4.6a}$$

$$r_f = r_0 + \dot{r}_0 t_f + c_0 A + c_1 B, \tag{4.6b}$$

where:

$$b_0 = \int_0^{t_f} a_T(t)\,dt = -v_e \log\left(1 - \frac{t_f}{\tau}\right) \tag{4.7a}$$

$$b_1 = \int_0^{t_f} t a_T(t)\,dt = -b_0\tau - v_e t_f, \tag{4.7b}$$

$$c_0 = \int_0^{t_f} \int_0^{t} a_T(s)\,ds\,dt = b_0 t_f - b_1, \tag{4.7c}$$

$$c_1 = \int_0^{t_f} \int_0^{t} s a_T(s)\,ds\,dt = c_0\tau - \frac{v_e t_f}{2}, \tag{4.7d}$$

Where v_e is the reference exhaust velocity and $\tau = v_e m/T$ is the ratio between the reference exhaust velocity and the acceleration generated from the thrust. Now, the System of Eqs. (4.6) can be analytically solved as long as r_f, $\dot{r}_f$, and t_f are known. The solution is

$$\begin{bmatrix} A \\ B \end{bmatrix} = \frac{1}{c_1 b_0 - b_1 c_0} \begin{bmatrix} -b_1 & c_1 \\ -b_0 & c_0 \end{bmatrix} \begin{bmatrix} \dot{r}_f - \dot{r}_0 \\ r_f - r_0 - \dot{r}_0 t_f \end{bmatrix}. \tag{4.8}$$

Since the value of $\hat{f}_2$ must not exceed 1 in order to assure the values for the pitch angle are real, its value at the ascent start time is limited by

$$|A + \frac{\mu/r_0^2 - u_0^2/r_0}{a_{t0}}| = A + C < 1. \tag{4.9}$$

This will impose a condition on the remaining burntime for which the desired insertion conditions can be obtained. That is, there is a maximum value of remaining burntime for which the algorithm can produce real trajectories. This means that for certain insertion conditions the PEG algorithm is unable to produce real trajectories. If the initial velocity, the starting altitude and the vertical velocity at insertion are assumed to be zero, then the expression for the maximum insertion altitude is

$$y < \frac{(b_1 c_0 - b_0 c_1)(1 - C)}{b_1}. \tag{4.10}$$

The inequality in Eq. (4.10) is plotted in Fig. 4.2. If the estimated remaining burntime ends up being smaller than the limit, then this version of PEG is not a suitable algorithm for the guidance. We can compare this with the optimal burntimes obtained from the method described in Chapter 3 and have an overview of what insertion altitudes are suitable for using PEG. This comparison can be seen on Fig. 4.2 where we notice that this version of PEG is not even close to the optimal value for the $100\,\mathrm{km}$ insertion altitude trajectory. PEG has, however, the capability to guide multistage rockets. This means it can be used for vehicles with more than one booster stage. It has, however, the disadvantage of requiring solving one equation iteratively.

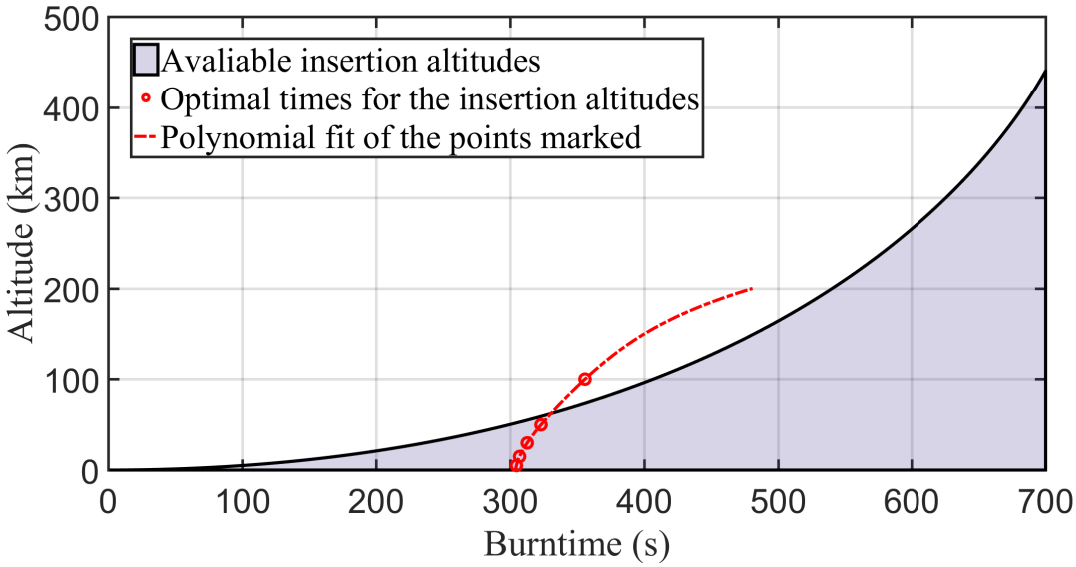

Figure 4.2: PEG altitude limit versus burntime

Remaining Burntime Estimation

As mentioned before, in order for A and B from Eqs. (4.8) to be calculated, the remaing burntime, t_f, needs to be estimated. This done using the method described in [16]. To start, $\hat{f}_2$ is assumed to be a linear function of time.

$$\hat{f}_2 = (\hat{f}_2)_0 + \dot{\hat{f}}_2 t, \tag{4.11}$$

where

$$\dot{\hat{f}}_2 = \frac{(\hat{f}_2)_f - (\hat{f}_2)_0}{t_f}, \tag{4.12}$$

and

$$(\hat{f}_2)_0 = A + \frac{\mu/r_0^2 - u_0^2/r_0}{(a_t)_0}, \tag{4.13a}$$

$$(\hat{f}_2)_f = A + \frac{\mu/r_f^2 - u_f^2/r_f}{(a_t)_f}, \tag{4.13b}$$

Since $\hat{f}$ is a unit vector, then

$$\hat{f}_1 = \sqrt{1 - \hat{f}_2^2}. \tag{4.14}$$

Equation (4.14) can be approximated by its Taylor series expansion around zero. Using only the two first terms the expression obtained for $\hat{f}_1$ is

$$\hat{f}_1 \approx 1 - \frac{\hat{f}_2^2}{2} = 1 - \frac{(\hat{f}_2)_0^2}{2} - (\hat{f}_2)_0 \dot{\hat{f}}_2 t - \frac{\dot{\hat{f}}_2^2}{2} t^2, \tag{4.15}$$

thus $\hat{f}_1$ can be expressed as a second order polynomial function with time

$$\hat{f}_1 = \hat{f}_1 + \dot{\hat{f}}_1 t + \ddot{\hat{f}}_1 t^2. \tag{4.16}$$

The vehicle is inserted in the desired orbit when the angular momentum for the desired orbit is reached. The angular momentum can be obtained from the required insertion velocity and altitude from

$$h_f = r_f v_f, \tag{4.17}$$

its time derivative is

$$\dot{h} = a_T r \hat{f}_1, \tag{4.18}$$

and therefore, the change in angular momentum required is

$$\Delta h = \int_0^{t_f} a_T r \hat{f}_1 \, dt. \tag{4.19}$$

Since the altitudes tested are much smaller than the radius of the Moon the value of r does not vary much (less than 6% for the highest altitude tested). If r is considered constant during the ascent (the average value $\bar{r}$ is used), then the required change in angular momentum is

$$\Delta h = \bar{r}[(\hat{f}_1)_0 b_0 + \dot{\hat{f}}_1 b_1 + \ddot{\hat{f}}_1 b_2], \tag{4.20}$$

and Eq. (4.20) can be expressed in terms of b_0

$$\Delta h = \bar{r}\Big\{[(\hat{f}_1)_0 \tau + \dot{\hat{f}}_1 \tau + \ddot{\hat{f}}_1 \tau^2] b_0 - v_e t_f (\dot{\hat{f}}_1 + \ddot{\hat{f}}_1 \tau) - \frac{v_e \ddot{\hat{f}}_1 t_f^2}{2}\Big\}, \tag{4.21}$$

inverting Eq. (4.21) we obtain

$$b_0 = \frac{\Big[\frac{\Delta h}{\bar{r}} + v_e t_f (\dot{\hat{f}}_1 + \ddot{\hat{f}}_1 \tau) + v_e \ddot{\hat{f}}_1 t_f^2 / 2\Big]}{[(\hat{f}_1)_0 \tau + \dot{\hat{f}}_1 \tau + \ddot{\hat{f}}_1 \tau^2]}. \tag{4.22}$$

The updated t_f from the previous guidance call can be used to estimate the new b_0 and this value can be used to calculate a new estimate of the remaining burntime

$$t_f = \tau(1 - e^{b_0/v_e}). \tag{4.23}$$

4.3.2 Polynomial Guidance

Polynomial guidance was first used in the Apollo missions. Even though it is extremely simple it is capable of reaching the desired final conditions, within some limits. For the derivation of this guidance law the acceleration in the LVLH frame is assumed to be a known function of time. As was assumed in the Apollo missions [14], the algorithm uses a linear function of time for the acceleration of the vehicle in all directions, $\dot{u} = k_1 t + k_2$, $\dot{v} = k_3 t + k_4$ and $\dot{w} = k_5 t + k_6$. This means that the equations of motion in

the LVLH reference frame are

$$\dot{x} = u, \tag{4.24a}$$

$$\dot{y} = v, \tag{4.24b}$$

$$\dot{z} = w, \tag{4.24c}$$

$$\dot{u} = k_1 t + k_2, \tag{4.24d}$$

$$\dot{v} = k_3 t + k_4, \tag{4.24e}$$

$$\dot{w} = k_5 t + k_6. \tag{4.24f}$$

Where k_1 through k_6 are the constants that determine the attitude of the vehicle and need to be determined. Equations (4.24) can be integrated twice leading to:

$$u_f - u_0 = \frac{1}{2} k_1 t_f^2 + k_2 t_f, \tag{4.25a}$$

$$v_f - v_0 = \frac{1}{2} k_3 t_f^2 + k_4 t_f, \tag{4.25b}$$

$$w_f - w_0 = \frac{1}{2} k_5 t_f^2 + k_6 t_f, \tag{4.25c}$$

$$x_f - x_0 = \frac{1}{6} k_1 t_f^3 + \frac{1}{2} k_2 t_f^2 + u_0 t_f, \tag{4.25d}$$

$$y_f - y_0 = \frac{1}{6} k_3 t_f^3 + \frac{1}{2} k_4 t_f^2 + v_0 t_f, \tag{4.25e}$$

$$z_f - z_0 = \frac{1}{6} k_5 t_f^3 + \frac{1}{2} k_6 t_f^2 + w_0 t_f. \tag{4.25f}$$

The System of Eqs. (4.25) can be solved analytically for k_1 through k_6 and the solution is:

$$k_1 = \frac{6(u_f + u_0)t_f - 12(x_f - x_0)}{t_f^3}, \tag{4.26a}$$

$$k_2 = \frac{-2(u_f + 2u_0)t_f + 6(x_f - x_0)}{t_f^2}, \tag{4.26b}$$

$$k_3 = \frac{6(v_f + v_0)t_f - 12(y_f - y_0)}{t_f^3}, \tag{4.26c}$$

$$k_4 = \frac{-2(v_f + 2v_0)t_f + 6(y_f - y_0)}{t_f^2}, \tag{4.26d}$$

$$k_5 = \frac{6(w_f + w_0)t_f - 12(z_f - z_0)}{t_f^3}, \tag{4.26e}$$

$$k_6 = \frac{-2(w_f + 2w_0)t_f + 6(z_f - z_0)}{t_f^2}, \tag{4.26f}$$

determining the acceleration completely, and therefore the thrust vector can be calculated.

If the engine does not have a throttle capability, i.e the modulus of the thrust is constant, then only the direction has to be calculated. This can be done if the downrange and the total burntime are not prescribed making the problem solvable. The vertical acceleration is still assumed to be a linear function of time and the remaining burntime is determined as a function of velocity to be gained, b_0. This b_0 function can be calculated through different methods, bur for the sake of simplicty, it will be calculated

using Eq. (4.46). The yaw guidance can be calculated using the same logic and thus the guidance angles at the time of each guidance call are:

$$\theta = \arcsin\left(\frac{k4 + C_y}{a_T}\right), \tag{4.27a}$$

$$\psi = \arcsin\left[\frac{k_6}{\cos(\theta)a_T}\right]. \tag{4.27b}$$

From Eq. (4.27a) it can be seen that there is a limit to k_4 so that

$$\left(\frac{k4 + C_y}{a_T}\right) \leq 1. \tag{4.28}$$

Substituting Eqs. (4.26d) in Eq. (4.28)

$$\left(\frac{-2(v_f + 2v_0)t_f + 6(y_f - y_0)}{t_f^2} + C_y\right)\frac{m}{T} \leq 1, \tag{4.29}$$

replacing t_f using Eq. (4.46) and assuming that the maximum pitch is at the start of the ascent (happens for regular ascents) one can plot the necessary sine of the pitch angle at $t = 0$ versus the insertion altitude, for a zero vertical velocity insertion. From Fig. 4.3 it can be seen that insertion altitudes greater than 40 km would not be reachable using polynomial guidance with constant thrust for the LAE vehicle specifications.

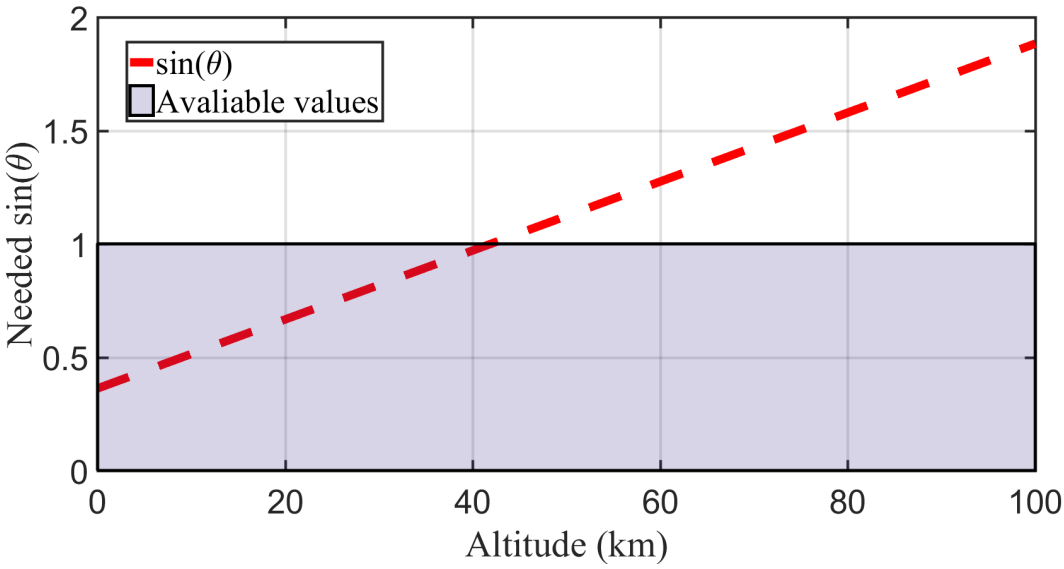

Figure 4.3: Polynomial guidance altitude limit

4.3.3 Hull's Solution for the Lunar Ascent Problem

The optimal control approach for a quasi-planar ascent lunar trajectory approximation was developed in [1], and is explained below, as it is necessary to understand the new approximations developed in this work. The derivation done here is slightly different and simpler, but leads to the same guidance

algorithm.

As is explained in Chapter 3, in order to obtain the optimal controls, i.e. the optimal pitch and yaw angles, the differential equations for the Lagrange multipliers, Eqs. (3.1), (3.2) and (3.4) must be solved.

The thrust will be considered constant, therefore $a_T = T/m$ and $m = m_0 - \beta t$, where β is the contant mass flow rate, the thrust is $T = I_{sp} g_0 \beta$ and g_0 is the acceleration of gravity at the surface of the moon. Since we have a constant mass flow rate, minimizing the time will minimize the fuel expended.

In order to calculate the optimal thrust direction inputs, the Hamiltonian of the system needs to be calculated, and is in this case

$$H = \lambda^T \dot{X} + 1, \tag{4.30}$$

where λ is the Lagrange multiplier vector and the X is the state vector. Expanding Eq. (4.30) with Eq. (2.4) we have

$$H = \lambda_x u + \lambda_y v + \lambda_z w + \lambda_u (a_T \hat{f}_1) + \lambda_v (a_T \hat{f}_2 - C_y) + \lambda_w (a_T \hat{f}_3) + 1. \tag{4.31}$$

The differential equations for the Lagrange multipliers, Eqs. (3.2) and (3.1) are easily solved and the solution is:

$$\lambda_u = -\lambda_x t + A_1, \tag{4.32a}$$

$$\lambda_v = -\lambda_y t + A_2, \tag{4.32b}$$

$$\lambda_w = -\lambda_z t + A_3, \tag{4.32c}$$

where $\lambda_{x,y,z}$ are constant and $A_{1,2,3}$ are integration constants. These are the variables that determine the optimal attitude of the vehicle, and need to be dtermined.

The optimality condition, Eq. (3.4), leads to the thrust having the same direction as the velocity Lagrange multiplier [32], that is

$$\hat{f}_{1,2,3} = \frac{\pm \lambda_{u,v,w}}{\sqrt{\lambda_u^2 + \lambda_v^2 + \lambda_w^2}} \tag{4.33}$$

The signal ambiguity is not important, since the constants that need to be determined can have any real value, any choice of signal will work. For simplicity, the positive sign will be chosen. In order to solve Eqs. (3.1) and (3.2), the intial and final conditions are required. The initial state vector at $t = 0$ is

$$X(0) = \begin{bmatrix} x_0 \\ y_0 \\ z_0 \\ u_0 \\ v_0 \\ w_0 \end{bmatrix}, \tag{4.34}$$

the state vector at insertion, $t = t_f$ is

$$X(t_f) = \begin{bmatrix} x_f \\ y_f \\ z_f \\ u_f \\ v_f \\ w_f \end{bmatrix}, \tag{4.35}$$

and the boundary condition for t_f is [32]

$$H_f = 0. \tag{4.36}$$

The system of Eqs. (2.4) can then be integrated twice for the position and once for the velocity, using the boundary condtions in Eqs. (4.34) and (4.35). Joining these with Eq. (4.36) we get.

$$x_f = x_0 + u_0 t + \int_0^{t_f} \int_0^t a_T(s) \hat{f}_1 \, ds \, dt, \tag{4.37a}$$

$$y_f = y_0 + v_0 t - \frac{C_y t^2}{2} + \int_0^{t_f} \int_0^t a_T(s) \hat{f}_2 \, ds \, dt, \tag{4.37b}$$

$$z_f = z_0 + \int_0^{t_f} \int_0^t a_T(s) \hat{f}_3 \, ds \, dt, \tag{4.37c}$$

$$u_f = u_0 + \int_0^{t_f} a_T(t) \hat{f}_1 \, dt, \tag{4.37d}$$

$$v_f = v_0 + \int_0^{t_f} a_T(t) \hat{f}_2 \, dt - C_y t, \tag{4.37e}$$

$$w_f = w_0 + \int_0^{t_f} a_T(t) \hat{f}_3 \, dt, \tag{4.37f}$$

$$H_f = 0, \tag{4.37g}$$

The guidance algorithm speed and complexity will depend on how the system of Eqs. (4.37) is solved, that is, what approximations are used to calculate the integral terms. The goal is to obtain an explicit analytical solution because the guidance will be used in a close loop scheme, i.e. the attitude needs to be calculated every guidance call during the ascent flight (at a 1 Hz frequency in our case). Therefore the guidance scheme should be as fast and simple as possible.

The thrust direction can be expressed in terms of pitch(θ) and yaw(ψ) angles as

$$\hat{f} = [\cos(\theta)\cos(\psi); \sin(\theta); \cos(\theta)\sin(\psi)]. \tag{4.38}$$

From Eqs. (4.33) and (4.38) and since $-\pi/2 < \theta < \pi/2$ (the spacecraft will not fly backwards):

$$\sin(\theta) = \frac{\lambda_v}{\sqrt{\lambda_u^2 + \lambda_v^2 + \lambda_w^2}}. \tag{4.39a}$$

$$\cos(\theta) = \frac{\sqrt{\lambda_u^2 + \lambda_w^2}}{\sqrt{\lambda_u^2 + \lambda_v^2 + \lambda_w^2}}, \tag{4.39b}$$

$$\sin(\psi) = \frac{\lambda_w}{\sqrt{\lambda_u^2 + \lambda_w^2}}, \tag{4.39c}$$

$$\cos(\psi) = \frac{\lambda_u}{\sqrt{\lambda_u^2 + \lambda_w^2}}. \tag{4.39d}$$

The typical orbit insertion conditions do not require a specific value of downrange, so according to optimal control theory it is required that $\lambda_x = 0$ [1, 32]. This leaves us with a constant $\lambda_u = A_1$. It is also possible to eliminate the calculation of A_1 and (4.36). This happens because from Eq. (4.33) it can be seen that it is the ratio between the multipliers that matters, and not the individual multipliers themselves, i.e. the thrust direction can be written as a function of only the ratios between the multipliers

$$\hat{f}_{2,3} = \frac{\lambda_{v,w}}{\sqrt{A_1^2 + \lambda_v^2 + \lambda_w^2}} = \frac{\lambda_{v,u}/A_1}{\sqrt{1 + \left(\lambda_v/A_1\right)^2 + \left(\lambda_w/A_1\right)^2}}. \tag{4.40}$$

For this reason, the new variables that are the ratios between the multipliers are introduced to the system

$$\bar{\lambda}_v = \frac{\lambda_v}{A_1} = \frac{-\lambda_y t + A_2}{A_1} = -\bar{\lambda}_y t + \bar{A}_2, \tag{4.41a}$$

$$\bar{\lambda}_w = \frac{\lambda_w}{A_1} = \frac{-\lambda_z t + A_3}{A_1} = -\bar{\lambda}_z t + \bar{A}_3. \tag{4.41b}$$

The thrust directions are then defined as:

$$\hat{f}_{2,3} = \frac{\bar{\lambda}_{v,w}}{\sqrt{1 + \bar{\lambda}_v^2 + \bar{\lambda}_w^2}}, \tag{4.42}$$

and so we can define the cosines and sines of the pitch and yaw angles as such:

$$sin(\theta) = \frac{\bar{\lambda}_v}{\sqrt{1 + \bar{\lambda}_v^2 + \bar{\lambda}_w^2}}, \tag{4.43a}$$

$$cos(\theta) = \frac{\sqrt{1 + \bar{\lambda}_w^2}}{\sqrt{1 + \bar{\lambda}_v^2 + \bar{\lambda}_w^2}}, \tag{4.43b}$$

$$sin(\psi) = \frac{\bar{\lambda}_w}{\sqrt{1 + \bar{\lambda}_w^2}}, \tag{4.43c}$$

$$cos(\psi) = \frac{1}{\sqrt{1 + \bar{\lambda}_w^2}}. \tag{4.43d}$$

These simplyfications lead to:

$$y_f = y_0 + v_0 t - \frac{C_y t^2}{2} + \int_0^{t_f} \int_0^t a_T(s) \hat{f}_2 \, ds \, dt \tag{4.44a}$$

$$z_f = z_0 + \int_0^{t_f} \int_0^t a_T(s) \hat{f}_3 \, ds \, dt \tag{4.44b}$$

$$u_f = u_0 + \int_0^{t_f} a_T(t) \hat{f}_1 \, dt \tag{4.44c}$$

$$v_f = v_0 - C_y t + \int_0^{t_f} a_T(t) \hat{f}_2 \, dt \tag{4.44d}$$

$$w_f = w_0 + \int_0^{t_f} a_T(t) \hat{f}_3 \, dt \tag{4.44e}$$

The System of Eqs. (4.44a) does not have an explicit analytical solution and the 5 by 5 system can only be solved numerically to get the values for λ_y, λ_z, A_2, A_3 and t_f. This happens because the integrals of the thrust acceleration are complicated, non polynomial functions. The system can however be simplified and solved analytically if some approximations are taken into account. An explicit analytical solution can likely be used on the flight for closed loop guidance due to its speed, which is not true for a numerical solution.

4.3.4 Hull's Explicit Approximate Solutions

It is possible to obtain an approximate analytical solution to the system of Eqs. (4.44). As a first approximation, since the deviations in the z axis are supposed to be small, $sin(\psi) \approx \bar{\lambda}_w$ and $\cos(\psi) \approx 1$. If the pitch angle is also small then $sin(\theta) \approx \bar{\lambda}_v$ and $\cos(\theta) \approx 1$. Although this is only reasonable for low altitudes, with these assumptions the System of Eqs. (4.44) can be solved analytically. With these approximations the system of Eqs. (4.44) simplifies to

$$y_f = y_0 + v_0 t - \frac{C_y t^2}{2} + c_0 \bar{A}_2 - c_1 \bar{\lambda}_y, \tag{4.45a}$$

$$z_f = z_0 + c_0 \bar{A}_3 - c_1 \bar{\lambda}_z, \tag{4.45b}$$

$$u_f = u_0 + b_0, \tag{4.45c}$$

$$v_f = v_0 + b_0 \bar{A}_2 - b_1 \bar{\lambda}_y - C_y t, \tag{4.45d}$$

$$w_f = w_0 + b_0 \bar{A}_3 - b_1 \bar{\lambda}_z. \tag{4.45e}$$

Eq. (4.45c) can be solved explicitly for t_f,

$$t_f = \tau \left[1 - e^{(u_0 - u_f)/v_e} \right]. \tag{4.46}$$

From Eqs. (4.45a) and (4.45d we can obtain $\bar{\lambda_y}$ and A_2 and from Eqs. (4.45a) and (4.45d) we can obtain $\bar{\lambda_z}$ and A_3:

$$\begin{bmatrix} \bar{A_2} \\ \bar{\lambda_y} \end{bmatrix} = \frac{1}{c_1 b_0 - b_1 c_0} \begin{bmatrix} -b_1 & c_1 \\ -b_0 & c_0 \end{bmatrix} \begin{bmatrix} Y \\ V \end{bmatrix}, \tag{4.47}$$

$$\begin{bmatrix} \bar{A_3} \\ \bar{\lambda_z} \end{bmatrix} = \frac{1}{c_1 b_0 - b_1 c_0} \begin{bmatrix} -b_1 & c_1 \\ -b_0 & c_0 \end{bmatrix} \begin{bmatrix} Z \\ W \end{bmatrix}, \tag{4.48}$$

where $Y = y_f - y_0 - v_0 t_f + C_y t_f^2/2$, $Z = z_f - z_0 - w_0 t_f$, $V = v_f - v_0 + C_y t_f$, $W = w_f - w_0$ and b_0, b_1, c_0 and c_1 are the thrust integrals used in PEG in Eq. (4.7).

This algorithm has the advantage of not requiring the solution of any equation numerically, unlike the PEG, that requires solving one equation iteratively.

4.4 Fully Explicit Algorithms Based on New Approximations

In Section 4.3.4 one fully explicit solution for a free downrange and free ascent time was presented. This approximation has the limitiation of requiring the pitch angle to be small, which is not true for all the trajectories at all times. For example, the optimal trajectory for a $15\,\mathrm{km}$ insertion altitude calculated in Chapter 3 has a starting pitch angle of $33°$, and an error of about 6 % in the sine of the pitch when using Hull's approximation. In this Section, more accurate approximations will be developed in order to better approximate the pitch angle, while still obtaining a closed-form analytic solution.

The new approximations consist in approximating the sine and the cosine of the pitch in different ways from Hull. The cosine will be approximated by a quadratic function, instead of $\cos(\theta) = 1$, and because of this, the acceleration integral will be calculated using a Padé approximant, in order to still be able to obtain t_f from a single equation and keep the solution closed-form. The sine will be approximated in four different ways: by a linear Taylor series expansion (around a general point, instead of just using zero), by a quadratic Taylor series expansion (once again, around a general point) and by a linear or quadractic Lagrange polynomial. The linear approximations have a similar solution to Eq. (4.47) but with different coefficients. The second order aproximations still allow for a closed form-solution, even though they require the solution of a fourth degree polynomial in order to solve the system of Eqs. (4.44).

4.4.1 Improved Approximation of the Cosine

Hull [1] approximates the cosine of the pitch by a constant value of one. That approximation can be improved. In order to do this we can try to use a polynomial function to approximate it. The value of the polynomial at the time of the guidance call can be assumed to be value at the previous call because the time between guidance calls is small enough for the angle not to change a lot. Since the function that we are trying to approximate is a cosine, then its maximum value should be one. If we know were the

maximum value is situated, then we will have three equations and be able to generate a second order polynomial. The cosine of the pitch angle is for this reason assumed to be of the form

$$\cos(\theta) = at^2 + bt + c. \tag{4.49}$$

Keep in mind that this not a Taylor series expansion and is merely a general polynomial approximation. Using Eq. (4.49), the acceleration integral becomes:

$$\begin{aligned}
\int_0^t a_T \cos(\theta)\, dt &= \int_0^{t_f} a_T (at^2 + bt + c)\, dt \\
&= \int_0^{t_f} \frac{t(at^2 + bt + c)}{m_0(1 - t/\tau)} dt \\
&= \frac{t}{m_0}\Big[a \log\Big(1 - \frac{t}{\tau}\Big)\tau^3 - at\tau^2 \\
&- \frac{at^2\tau}{2} - b \log\Big(1 - \frac{t}{\tau}\Big)\tau^2 \\
&- bt\tau - c \log\Big(1 - \frac{t}{\tau}\Big)\tau\Big].
\end{aligned} \tag{4.50}$$

The values of the coefficients of the quadratic approximation of the cosine depend on the type of approximations. Since the objective is to use this in closed loop guidance, the value for c is defined to be the value of the cosine of the pitch angle from the previous guidance call. The value for c on the first guidance call was assumed to be zero for all the simulations for simplicity (values closer to the real initial value were also tested and the pitch profile was unaffected). To define a and b more assumptions are required. The maximum value of the parabola must be at the most one, as this is attempting to approximate a cosine. This value is typically obtained close to the end of the ascent. Thus, it is reasonable to make the assumption

$$at_f^2 + bt_f + c = 1, \tag{4.51}$$

As this is a maximum, the derivative at this point must be zero, so

$$2at_f + b = 0, \tag{4.52}$$

Equations (4.51) and (4.52) can be solved for a and b as a function of t_f:

$$a = \frac{c - 1}{2t_f^2}, \tag{4.53a}$$

$$b = \frac{2(1 - c)}{t_f}. \tag{4.53b}$$

While these conditions will not be accurate in all cases, the resulting approximation is a clear improvement from assuming the cosine of the pitch is constant and equal to one. In order to verify the validity of the approximation for a typical insertion altitude, the optimal pitch profile calculated in Chapter 3 was used. In Fig. 4.4 the real value of the cosine is compared with the approximated function at various times

during the ascent. It can be seen that the new approximation is a lot more accurate than assuming the cosine of the pitch is constant and equal to one for throughout all the ascent. Replacing Eqs. (4.49),

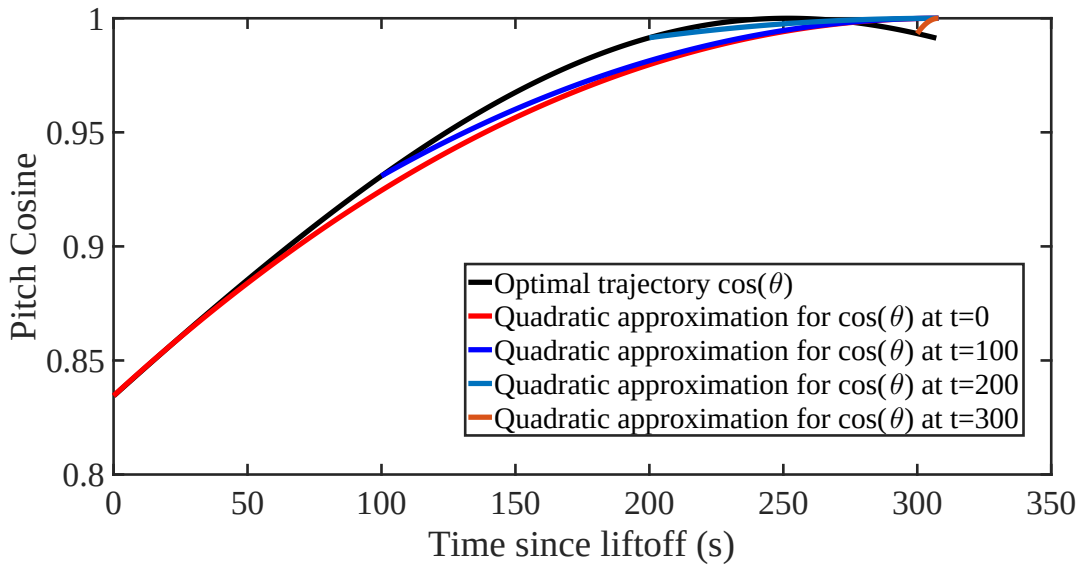

Figure 4.4: Comparison of the quadratic cosine approximation with the optimal profile for the trajectory represented in Fig. 3.1

(4.53b) and (4.53a) in Eq. (4.50), we obtain

$$
\begin{aligned}
f(t_f) = \int_0^{t_f} \frac{t(at^2+bt+c)}{m_0(1-t/\tau)} dt = \frac{t}{m_0}\Big[& \frac{c-1}{{}^2t_f^2}\log\left(1-\frac{t_f}{\tau}\right)\tau^3 \\
& - \frac{c-1}{{}^2t_f}\tau^2 - \frac{(c-1)\tau}{2} \\
& - \frac{2(1-c)}{t_f}\log\left(1-\frac{t_f}{\tau}\right)\tau^2 \\
& - 2(1-c)\tau - c\log\left(1-\frac{t_f}{\tau}\right)\tau\Big]
\end{aligned}
\quad . \tag{4.54}
$$

In order to obtain an analytic solution for t_f we can approximate $f(t_f)$ by a Padé approximant. Padé approximants are alternatives to Taylor series expansions. Instead of represeting a function with one polynomial, a ratio of two polynomials is used [34]. This useful because Eq. (4.44c), that needs to be solved to obtain t_f, will be a polynomial of order equal to the highest order of the Padé approximant. For this reason, two options will be presented. The options studied are an order 2 by 2 and order 1 by 1 Padé approximants, since the solution of a first and second order degree polynomials are easy to obtain. A more complicated, yet analytic, solution can also be calculated using order up to 4 by 4. This would increase the complexity of the solution and was deemed unnecessary, as order 2 by 2 already approximates the function closely. The 2 by 2 option does require the choice between two solutions for the burntime due to the quadratic nature of the resulting equation, so the correct option for the burntime must be chosen.

To obtain the approximant of order 2 by 2, a Taylor series expansion of Eq. (4.54) on a generic point up to order 4 is used. The expressions for the coefficients will not be shown, as they are extensive

and very easy to obtain using any symbolic calculus tool, such as the ones avaliable in *Matlab* [35] or *Wolfram Mathematica* [36]. The Taylor series will from now on be referred as

$$T_4(t) = a_0 + a_1 t + a_2 t^2 + a_3 t^3 + a_4 t^4, \tag{4.55}$$

where a_0 through a_4 are the coefficients of the Taylor series around a generic point (already expanded). The Padé approximant of order 1 by 1 is of the type

$$A_1^1(t) = \frac{p_0 + p_1 t}{q_0 + q_1 t}. \tag{4.56}$$

The coefficients are then obtained by saying that the Taylor series and the Padé approximant have the same value, that is

$$T_4(t) - A_1^1(t) = 0, \tag{4.57}$$

from Eq. (4.57) we get

$$p_0 = a_0, \tag{4.58a}$$

$$p_1 = a_0 q_1 + a_1, \tag{4.58b}$$

$$q_0 = 1, \tag{4.58c}$$

$$a_2 + a_1 q_1 = 0. \tag{4.58d}$$

System of Eqs. (4.58) is linear and can be solved to obtain the coefficients for the Padé approximant. For a Padé approximation of order 2 by 2, of the form

$$A_2^2(t) = \frac{p_0 + p_1 t + p_2 t^2}{q_0 + q_1 t + q_2 t^2}. \tag{4.59}$$

The coefficients are obtained by equalling the Taylor series and the Padé approximant

$$T_4(t) - A_2^2(t) = 0, \tag{4.60}$$

from Eq. (4.60) we get

$$p_0 = a_0, \tag{4.61a}$$

$$p_1 = a_0 q_1 + a_1, \tag{4.61b}$$

$$p_2 = a_0 q_2 + a_1 q_1 + a_2 q_0, \tag{4.61c}$$

$$q_0 = 1, \tag{4.61d}$$

$$a_3 + a_2 q_1 + a_1 q_2 = 0, \tag{4.61e}$$

$$a_4 + a_3 q_1 + a_2 q_2 = 0. \tag{4.61f}$$

System of Eqs. (4.61) is also a linear system and can be solved to obtain the coefficients for the Padé

approximant.

In order to choose which approximation should be used and which expansion point should be chosen, we can compare the approximations with the exact function. We did this using the expansion point as a parameter and minimizing the integral of the square of the absolute error,

$$\int_0^{t_f} [f(t) - g(t)]^2 dt, \tag{4.62}$$

where f is the exact function, Eq. (4.54) calculated numerically with an absolute error tolerance of 10^{-10}, and g is each approximation. This is done for values of c, the previous cosine of the pitch, ranging from 0 to 1, to make sure the approximation is good at any point in the trajectory. The value of t_f will go up to $400\,\mathrm{s}$, since the ascent time of the trajectories to be tested is expected not to be larger than that. This is done before the flight in order to set the parameters of the guidance algorithm. The parameters that need to be chosen before the flight are the initial point for the Taylor series expansion (therefore the initial expansion point for the Padé approximant) and the order of the Padé approximant. In Fig. 4.5 the

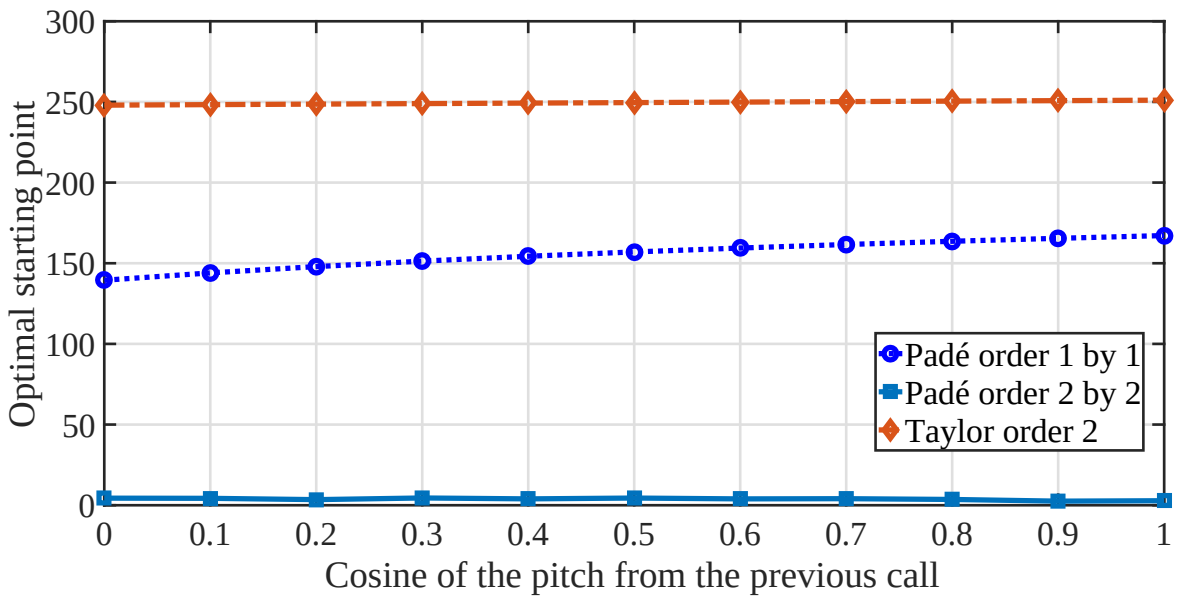

Figure 4.5: Otimal expansion point for each value of c

values of the optimal expansion point for each value the previous cosine of the pitch are plotted. These values were obtained by using a line search algorithm to calculate the expansion point that leads to the minimum integral of the error squared. It can be seen that for all the approximations, the value does not change drastically with c and thus a single expansion point can be used for any value of the previous cosine of the pitch, i.e. no matter what the current pitch angle of the spacecraft is, the Padé approximant will be accurate. Figure 4.6 shows the integral of the absolute error of each approximation for each value of the previous cosine of the pitch and the optimal values for the expansion point shown in Fig. 4.5. The order 2 by 2 Padé is a good approximation for any value of the previous cosine of the pitch, and so, even though it requires the solution of a quadratic equation, it will be the one selected. An expansion point of 3.81 will be used (average of optimal points). As an example, the exact functions and the approximations

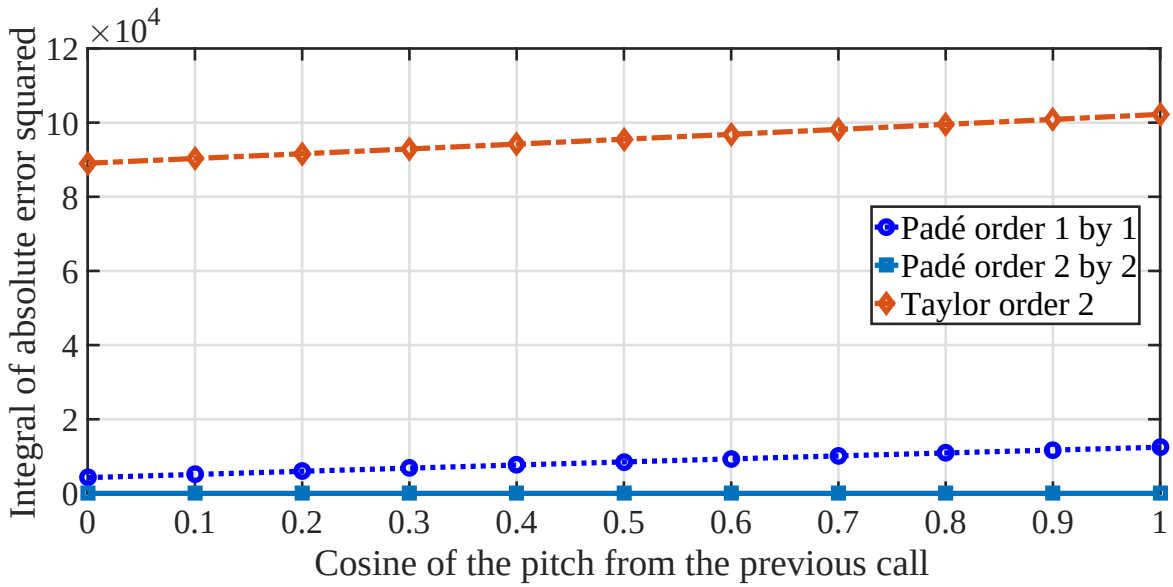

Figure 4.6: Minimum integral of the absolute error of the approximations for each value of c

for previous the cosine of the pitch, $c = 0$, $c = 0.5$ and $c = 1$ are shown in Fig. 4.7. Keep in mind that

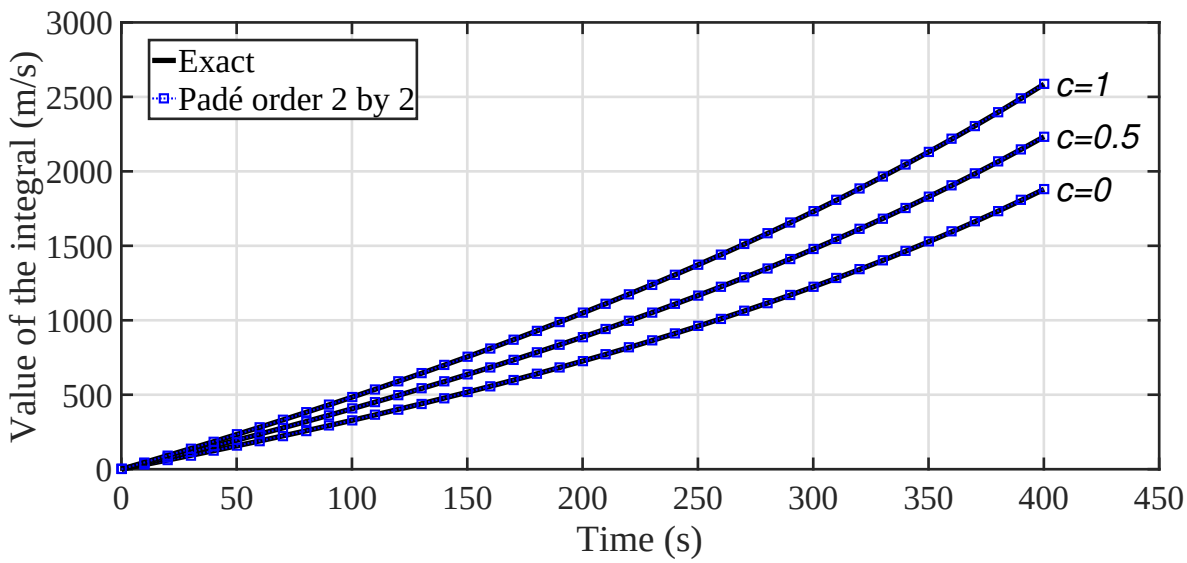

Figure 4.7: Value of the exact integral compared with the Padé 2 by 2 approximation for expansion point 3.81

the exact function in this image already takes into account the approximation of the cosine, meaning the exact function also changes with c. This does not demonstrate that the angle approximation is good, it simply shows that the resulting integral, if the quadratic cosine approximation is used, can indeed be well represented by a low order Padé approximation in the interval of interest. For the Padé 2 by 2, the

remaining burntime can be calculated using the quadratic formula.

$$a = p_2 + q_2 \frac{(u_f - u_0)\tau}{v_e}, \tag{4.63}$$

$$b = p_1 + q_1 \frac{(u_f - u_0)\tau}{v_e}, \tag{4.64}$$

$$c = p_0 + q_0 \frac{(u_f - u_0)\tau}{v_e}, \tag{4.65}$$

$$t_f = \frac{-b \pm \sqrt{b^2 - 4ac}}{2a} \tag{4.66}$$

Since there are two solutions, in Eq. (4.66), some attention must be paid to the choice of the correct one. For this case the Padé approximant of order 2 by 2 was selected. However, if the Padé approximant of order 1 by 1 is used, the burntime will be given by

$$t_f = \frac{v_e p_0 - q_0 \tau (u_f - u_0)}{\tau q_1 (u_f - u_0) - v_e p_1}. \tag{4.67}$$

Another important factor that needs to be taken into account when using Padé approximants is the poles of the function. In order to have a valid approximation, the poles must be sufficiently far away from the interval of interest. This condition is met for the expansion point chosen, 3.81, when plotting the graphs in Fig. 4.7. The condition is usually automatically met if the integral of the square of the absolute error is minimized, but nonetheless, it should be considered for each set of parameters.

4.4.2 Improved Approximations of the Sine

In [1] a Taylor series expansion for Eq. (4.43a) at the origin is used to approximate the sine as a function of $\bar{\lambda}_v$ (assuming that $\bar{\lambda}_w$ is negletable, i.e the perturbations out of plane can be discarded). We considered linear and quadratic Taylor series expansions at an arbitrary point. We also considered first and second order Lagrange polynomials to approximate the sine of the pitch, with $\bar{\lambda}_v$ as the variable.

For all the above approximations, one or more parameters must be determined. For the Taylor series expansions, the initial point needs to be chosen, and for the Lagrange polynomial approximations, the exact points must be selected. In order to minimize large deviations from the exact function the approximation parameters can be chosen by minimizing the integral of the square of absolute error between a selected interval, i.e. between two selected angles

$$\int_a^b \left[\frac{x}{\sqrt{x^2+1}} - g(x) \right]^2 dx, \tag{4.68}$$

where g is the sine approximation chosen, and a and b can be calculated from the angle interval chosen using the exact function. The angle interval can be chosen by looking at the reference trajectory. In the cases where no reference trajectory was calculated, the angle interval can be predicted intuitively from looking at prior similar trajectories. The minimization needs to be done for each of the approximations and can be done easily using a line search algorithm. Keep in mind that for $a = b$, there will be two minimum values for the Taylor series expansion options, so one must be chosen. For the sake of

simplicity, the positive value of $\bar{\lambda}_v$ was always selected. The function g can be a Taylor series expansion or a Lagrange polynomial.

Determining the Coefficients for the Approximations

The coefficients of the Taylor series can be calculated by hand or with the aid of a symbolic calculus tool such as the ones avaliable in *Matlab* [35] or *Wolfram Mathematica* [36]. The coefficients of the Taylor series of the sine of the pitch at an arbitrary point up until second order are:

$$\begin{aligned} n_0 =& \frac{\bar{\lambda}_{v0}}{\sqrt{\bar{\lambda}_{v0}^2+1}} - \bar{\lambda}_{v0}^2 \left\{ \frac{\bar{\lambda}_{v0}}{\left(\bar{\lambda}_{v0}^2+1\right)^{3/2}} + \frac{\bar{\lambda}_{v0}\left[1/\sqrt{\bar{\lambda}_{v0}^2+1} - 3\,\bar{\lambda}_{v0}^2/\left(\bar{\lambda}_{v0}^2+1\right)^{3/2}\right]}{2\,\left(\bar{\lambda}_{v0}^2+1\right)} \right\} \\ & -\bar{\lambda}_{v0}\left[\frac{1}{\sqrt{\bar{\lambda}_{v0}^2+1}} - \frac{\bar{\lambda}_{v0}^2}{\left(\bar{\lambda}_{v0}^2+1\right)^{3/2}}\right], \end{aligned} \tag{4.69a}$$

$$\begin{aligned} n_1 =& \frac{1}{\sqrt{\bar{\lambda}_{v0}^2+1}} - \frac{\bar{\lambda}_{v0}^2}{\left(\bar{\lambda}_{v0}^2+1\right)^{3/2}} \\ & +2\,\bar{\lambda}_{v0}\left\{ \frac{\bar{\lambda}_{v0}}{\left(\bar{\lambda}_{v0}^2+1\right)^{3/2}} + \frac{\bar{\lambda}_{v0}\left[1/\sqrt{\bar{\lambda}_{v0}^2+1} - 3\,\bar{\lambda}_{v0}^2/\left(\bar{\lambda}_{v0}^2+1\right)^{3/2}\right]}{2\,\left(\bar{\lambda}_{v0}^2+1\right)} \right\}, \end{aligned} \tag{4.69b}$$

$$n_2 = -\frac{\bar{\lambda}_{v0}}{\left(\bar{\lambda}_{v0}^2+1\right)^{3/2}} - \frac{\bar{\lambda}_{v0}\left[1/\sqrt{\bar{\lambda}_{v0}^2+1} - 3\,\bar{\lambda}_{v0}^2/\left(\bar{\lambda}_{v0}^2+1\right)^{3/2}\right]}{2\,\left(\bar{\lambda}_{v0}^2+1\right)}, \tag{4.69c}$$

where, $\bar{\lambda}_{v0}$ is the chosen expansion point for the Taylor series.

The linear Lagrange polynomial is interpolated from 2 chosen points. After the points are chosen the Lagrange polynomial can be obtained by adding the auxiliary polynomials for each point

$$L = L_1 f(x_1) + L_2 f(x_2), \tag{4.70}$$

where

$$L_{1,2} = \frac{x - x_{1,2}}{x_{2,1} - x_{1,2}}. \tag{4.71}$$

To obtain a quadratic Lagrange polynomial interpolation 3 points need to be chosen. After the points are chosen the polynomial is obtained by adding the auxiliary polynomials for each point

$$L = L_1 f(x_1) + L_2 f(x_2) + L_3 f(x_3), \tag{4.72}$$

where

$$L_{1,2,3} = \frac{(x - x_{2,3,1})(x - x_{3,1,2})}{(x_{1,2,3} - x_{2,3,1})(x_{1,2,3} - x_{3,1,2})}. \tag{4.73}$$

It should be noted, that since the sine of the pitch is an odd function, then if $a = b$ in Eq. (4.68) the optimal Lagrange polynomial won't have a second order term. This is not an issue since the solution of the problem is actually much simpler for the case where the sine of the pitch is linear.

Solution of the Approximated Systems

The first solution presented is for both the linear Taylor series and the linear Lagrange polynomial approximations. In either of this cases, the sine of the pitch is approximated by

$$\sin(\theta) = \frac{\bar{\lambda}_v}{\sqrt{1+\bar{\lambda}_v^2+\bar{\lambda}_w^2}} \approx \frac{\bar{\lambda}_v}{\sqrt{1+\bar{\lambda}_v^2}} \approx n_0 + n_1\bar{\lambda}_v, \tag{4.74}$$

with only the coefficients changing between each of the Taylor series and the Lagrange approximations. Replacing Eq. (4.74) in Eqs. (4.44a) and (4.44d) , we get

$$\frac{Y - c_0 n_0}{n_1} = c_0\bar{A}_2 - c_1\bar{\lambda}_y, \tag{4.75a}$$

$$\frac{V - b_0 n_0}{n_1} = b_0\bar{A}_2 - b_1\bar{\lambda}_y, \tag{4.75b}$$

with solution

$$\begin{bmatrix} \bar{A}_2 \\ \bar{\lambda}_y \end{bmatrix} = \frac{1}{c_1 b_0 - b_1 c_0} \begin{bmatrix} -b_1 & c_1 \\ -b_0 & c_0 \end{bmatrix} \begin{bmatrix} \frac{Y - c_0 n_0}{n_1} \\ \frac{V - b_0 n_0}{n_1} \end{bmatrix}. \tag{4.76}$$

Replacing these back in Eq. (4.33), we get the direction of the necessary thrust vector.

The solution for the second order Taylor series and Lagrange polynomial approximations was calculated in the same way. Saying

$$\sin(\theta) = \frac{\bar{\lambda}_v}{\sqrt{1+\bar{\lambda}_v^2+\bar{\lambda}_w^2}} \approx \frac{\bar{\lambda}_v}{\sqrt{1+\bar{\lambda}_v^2}} \approx n_0 + n_1\bar{\lambda}_v + n_2\bar{\lambda}_v^2. \tag{4.77}$$

with only the coefficients changing between each of the Taylor series and the Lagrange approximations. By replacing Eq. (4.77) in Eqs. (4.44a) and (4.44d) we get the quadratic system:

$$a_{00} + a_{10}\bar{A}_2 + a_{20}\bar{A}_2^2 + a_{01}\bar{\lambda}_y + a_{02}\bar{\lambda}_y^2 + a_{11}\bar{\lambda}_y\bar{A}_2 = 0, \tag{4.78a}$$

$$b_{00} + b_{10}\bar{A}_2 + b_{20}\bar{A}_2^2 + b_{01}\bar{\lambda}_y + b_{02}\bar{\lambda}_y^2 + b_{11}\bar{\lambda}_y\bar{A}_2 = 0, \tag{4.78b}$$

where:

$$a_{00} = n_0 b_0 - V, \tag{4.79a}$$

$$a_{10} = n_1 b_0, \tag{4.79b}$$

$$a_{20} = n_2 b_0, \tag{4.79c}$$

$$a_{01} = -n_1 b_1, \tag{4.79d}$$

$$a_{02} = n_2 b_2, \tag{4.79e}$$

$$a_{11} = -n_2 b_1, \tag{4.79f}$$

and

$$b_{00} = n_0 c_0 - Y, \tag{4.80a}$$

$$b_{10} = n_1 c_0, \tag{4.80b}$$

$$b_{20} = n_2 c_0, \tag{4.80c}$$

$$b_{01} = -n_1 c_1, \tag{4.80d}$$

$$b_{02} = n_2 c_2, \tag{4.80e}$$

$$b_{11} = -n_2 c_1, \tag{4.80f}$$

where $b_0, b1, c_0$ and c_1 are the same as in Eqs. (4.7) and b_2 and c_2 are:

$$b_2 = \int_0^{t_f} t^2 a_T(t) dt = -b_1 \tau - \frac{v_e t_f^2}{2}, \tag{4.81a}$$

$$c_2 = \int_0^{t_f} \int_0^t s^2 a_T(s) ds dt = c_1 \tau - \frac{v_e t_f^3}{6}, \tag{4.81b}$$

The system of Eqs. (4.78) can then be turned in a quartic equation, which can still be solved analytically:

$$\bar{\lambda}_y = \frac{-K_1 \pm \sqrt{I_1}}{J_1}, \tag{4.82a}$$

$$\bar{\lambda}_y = \frac{-K_2 \pm \sqrt{I_2}}{J_2}, \tag{4.82b}$$

where:

$$I_1 = (a_{01} + a_{11}\bar{A}_2)^2 - 4[a_{02}(a_{20}\bar{A}_2^2 + a_{10}\bar{A}_2 + a_{00})], \tag{4.83a}$$

$$J_1 = 2a_{02}, \tag{4.83b}$$

$$K_1 = (a_{01} + a_{11}\bar{A}_2), \tag{4.83c}$$

$$I_2 = (b_{01} + b_{11}\bar{A}_2)^2 - 4[(b_{02}(b_{20}\bar{A}_2^2 + b_{10}\bar{A}_2 + b_{00})], \tag{4.84a}$$

$$J_2 = 2b_{02}, \tag{4.84b}$$

$$K_2 = (b_{01} + b_{11}\bar{A}_2). \tag{4.84c}$$

By equaling the two equations in the System of Eqs. (4.82) we get:

$$\frac{-K_1}{J_1} + \frac{K_2}{J_2} = \mp\frac{\sqrt{I_1}}{J_1} \pm \frac{\sqrt{I_2}}{J_2}. \tag{4.85a}$$

Squaring both sides:

$$\frac{K_1^2}{J_1^2} + \frac{K_2^2}{J_2^2} - 2\frac{K_1 K_2}{J_1 J_2} = \frac{I_1}{J_1^2} + \frac{I_2}{J_2^2} \pm 2\sqrt{\frac{I_1 I_2}{J_1 J_2}}, \tag{4.85b}$$

$$(M + N - P)^2 = \frac{4 I_1 I_2}{J_1 J_2}, \tag{4.85c}$$

$$M^2 + N^2 + P^2 + 2MN - 2MP - 2NP - \frac{4 I_1 I_2}{J_1 J_2} = 0, \tag{4.85d}$$

where

$$M = \frac{K_1 - I_1}{J_1^2}, \tag{4.86a}$$

$$N = \frac{K_2 - I_2}{J_2^2}, \tag{4.86b}$$

$$P = \frac{K_1 K_2}{J_1 J_2}. \tag{4.86c}$$

In order to get the values for $\bar{A}_2$ and $\bar{\lambda}_y$, Eq. (4.85d) must be solved and the correct solution must be chosen. The correct solution only depends on the sign of n_2 in Eq. (4.77). As long as the sign stays the same, which is the case for all the trajectories tested, the correct solution is always the same. Two proposed methods for solving the quartic equation are the mehods found in [37] and in [38], but any other general method for solving a quartic equation can be used.

Validity of the Sine Approximations

A comparison between the sine approximations and the exact function and Hull's approximation can be found in Figs. 4.8, 4.9, 4.10 and 4.11.

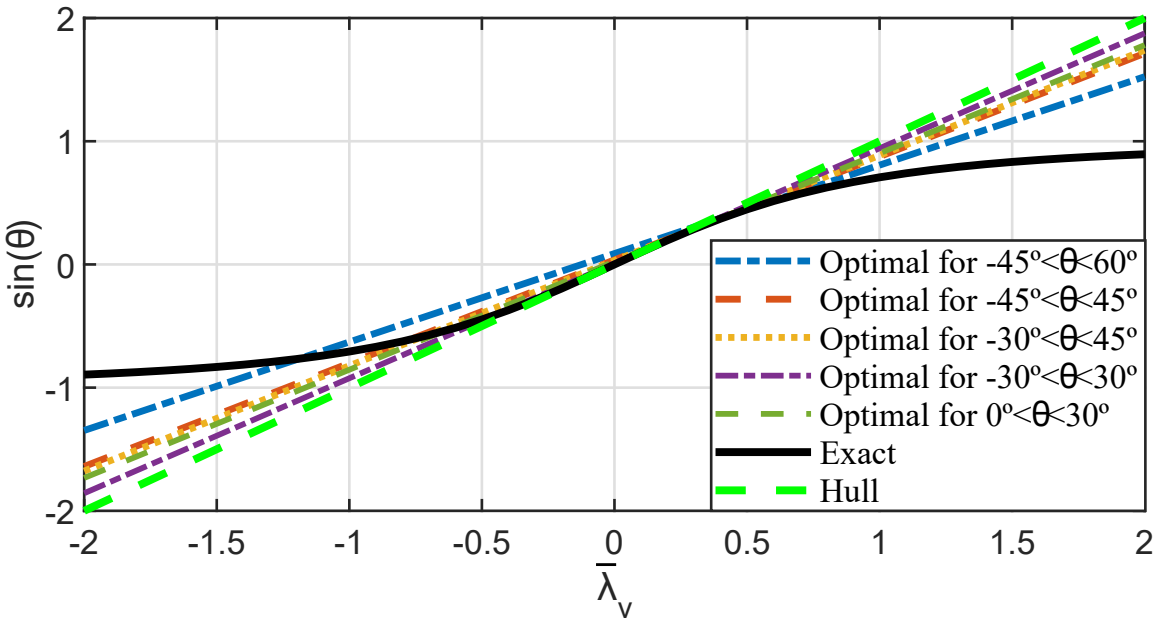

Figure 4.8: Optimal linear series expansion approximations for various angle intervals

In Figs. 4.9 and 4.11 it can be seen that due to the fact that quadratic funtions are not injective

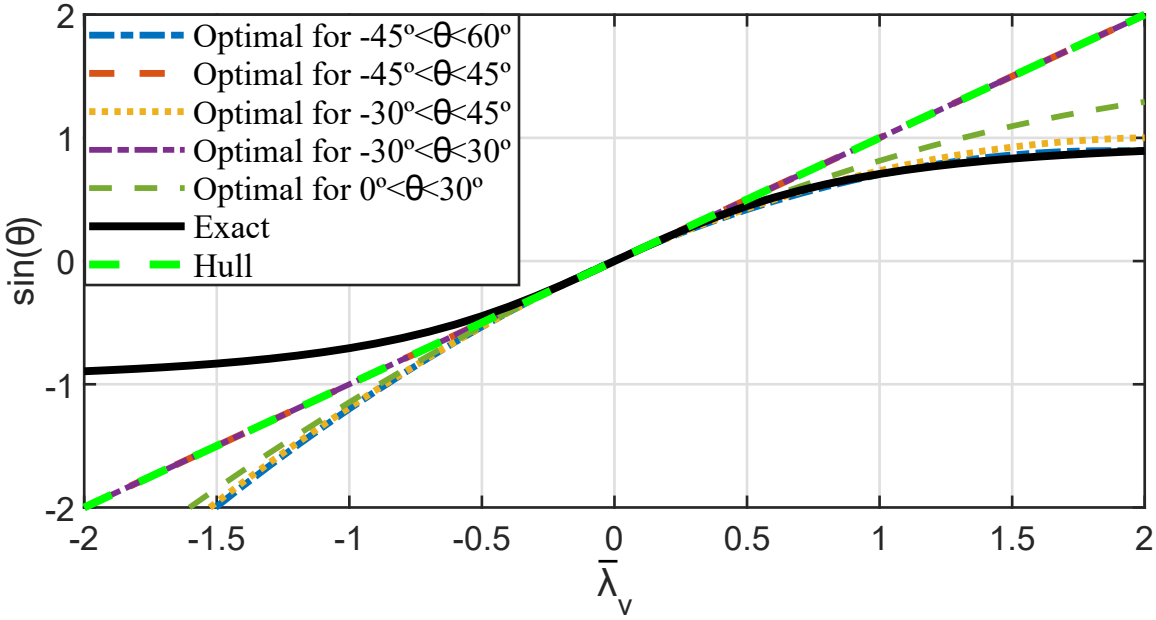

Figure 4.9: Optimal quadratic series expansion approximations for various angle intervals

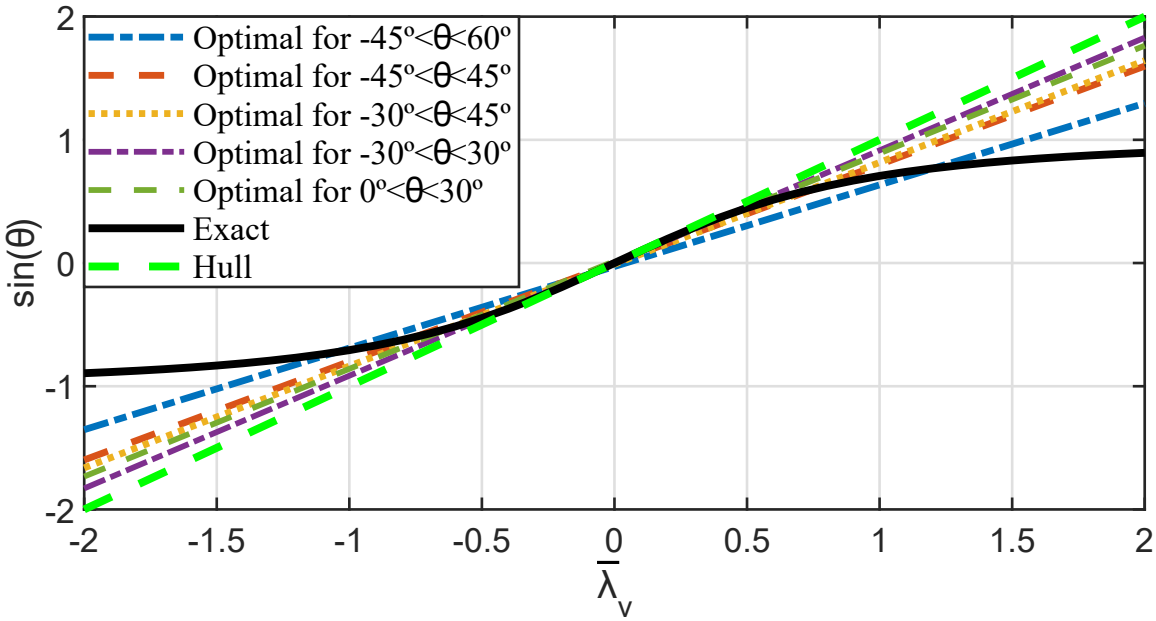

Figure 4.10: Optimal linear Lagrange polynomial approximations for various angle intervals

Table 4.1: Integral of the absolute error of each approximation for the selected angle interval

Integral of the square of the absolute error in the interval Eq. (4.68)					
	Hull	Linear	Quadratic	Linear Lagrange	Quadratic Lagrange
$-45° < \theta < 60°$	0.2849	0.0379	0.0430	0.0283	0.0087
$-45° < \theta < 45°$	0.0302	0.0071	0.0302	0.0033	0.0033
$-30° < \theta < 45°$	0.0156	0.0061	0.0016	0.0023	6.5×10^{-4}
$-30° < \theta < 30°$	0.0011	3.0×10^{-4}	0.0011	1.5×10^{-4}	1.5×10^{-4}
$0° < \theta < 30°$	5.4×10^{-4}	9.2×10^{-5}	1.4×10^{-5}	4.0×10^{-5}	5.0×10^{-7}

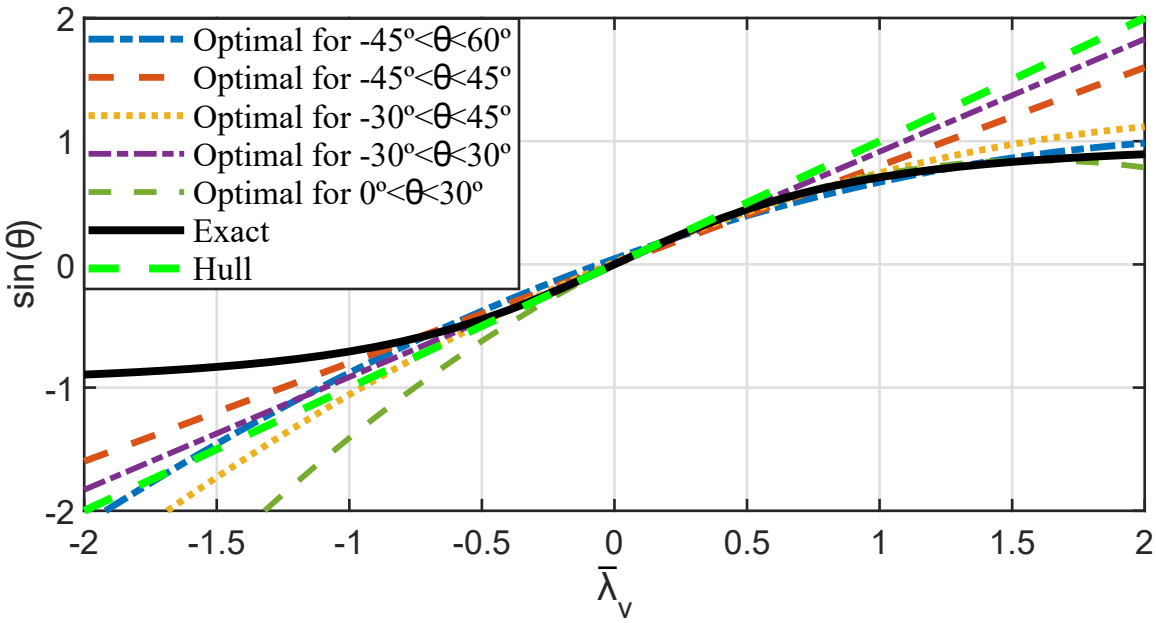

Figure 4.11: Optimal quadratic Lagrange polynomial approximations for various angle intervals

(not strictly growing, unlike the case with linear functions with positive slope), some of the quadratic approximations (Taylor series and Lagrange polynomials) do not completely cover the full codomain of the sine function, i.e. some approximations do not reach a value of one. This means they have no real solution for certain higher values of $\sin(\theta)$, becoming unsafe to use. A way to solve this is to only choose approximations where that does not happen. Another problem with a quadratic approximation for an odd bounded function is the fact that for some values the approximation will be worse than any linear approximation because of the slope.

From Table 4.1 it can be seen that all the approximations have a smaller integral of absolute error for every angle interval tested. This is a general property for any angle interval, since Hull's approximation is a particular case of any of the other approximations. Therefore it is more likely to obtain trajectories closer to optimal using the new approximations than using Hull's approximation.

4.4.3 New Guidance Algorithms

From the approximations found in Sections 4.4.1 and 4.4.2 eight different guidance algorithms can be defined. The guidance algorithms are gonna be called on a 1 Hz frequency and calculate new guidance constants $\bar{A}_2$ and $\bar{\lambda}_y$ every second.

Algorithm I- Algorithm I uses Hull's cosine approximation described in Section 4.3.4 and the linear Taylor series sine approximation described in Section 4.4.2, meaning that t_f is calculated with Eq. (4.46), and the guidance constants $\bar{A}_2$ and $\bar{\lambda}_y$ are calculated with Eq. (4.76).

Algorithm II- Algorithm II uses Hull's cosine approximation described in Section 4.3.4 and the linear Lagrange polynomial sine approximation described in Section 4.4.2, meaning that t_f is calculated with

Eq. (4.46), and the guidance constants $\bar{A}_2$ and $\bar{\lambda_y}$ are calculated with Eq. (4.76).

Algorithm III- Algorithm III uses the cosine approximation described in Section 4.4.1 and the linear Taylor series sine approximation described in Section 4.4.2, meaning that t_f is calculated with Eq. (4.66), and the guidance constants $\bar{A}_2$ and $\bar{\lambda_y}$ are calculated with Eq. (4.76).

Algorithm IV- Algorithm IV uses the cosine approximation described in Section 4.4.1 and the linear Lagrange polynomial sine approximation described in Section 4.4.2, meaning that t_f is calculated with Eq. (4.66), and the guidance constants $\bar{A}_2$ and $\bar{\lambda_y}$ are calculated with Eq. (4.76).

Algorithm V- Algorithm V uses Hull's cosine approximation described in Section 4.3.4 and the quadratic Taylor series sine approximation described in Section 4.4.2, meaning that t_f is calculated with Eq. (4.46), and the guidance constants $\bar{A}_2$ and $\bar{\lambda_y}$ are calculated with Eq. (4.85d).

Algorithm VI- Algorithm VI uses Hull's cosine approximation described in Section 4.3.4 and the quadratic Lagrange polynomial sine approximation described in Section 4.4.2, meaning that t_f is calculated with Eq. (4.46), and the guidance constants $\bar{A}_2$ and $\bar{\lambda_y}$ are calculated with Eq. (4.85d).

Algorithm VII- Algorithm VII uses the cosine approximation described in Section 4.4.1 and the quadratic Taylor series sine approximation described in Section 4.4.2, meaning that t_f is calculated with Eq. (4.66), and the guidance constants $\bar{A}_2$ and $\bar{\lambda_y}$ are calculated with Eq. (4.85d).

Algorithm VIII- Algorithm VIII uses the cosine approximation described in Section 4.4.1 and the quadratic Lagrange polynomial sine approximation described in Section 4.4.2, meaning that t_f is calculated with Eq. (4.66), and the guidance constants $\bar{A}_2$ and $\bar{\lambda_y}$ are calculated with Eq. (4.85d).

4.4.4 Algorithms Runtime

All the approximations actually require different computational times, so the time to compute the guidance constants will be calculated and compared between the newly developed guidance algorithms. To do this the average runtime for a guidance call is calculated by running it with the same parameters and conditions for each type of algorithm 100000 times. The results are presented in Table 4.2. The simulations were run on a computer with the specifications found in Appendix A. It can be seen that the linear sine approximations without the Padé approximations are two orders of magnitude faster than the algorithms that use a quadratic approximation for the sine. The use of the Padé approximant increases the runtime by one order of magnitude, so, if one of the linear approximations without using the Padé approximant provides good enough results, it is highly prefered to use it. This was expectable due to the exponential growth in the number of operations required to analitically solve a polynomial as its degree increases.

Table 4.2: Average runtime for guidance

	Algorithms I and II	Algorithms III and IV	Algorithms V and VI	Algorithms VII and VIII
Runtime [s]	5.57×10^{-7}	5.56×10^{-6}	4.05×10^{-5}	4.10×10^{-5}

Chapter 5

The Case of HERACLES Mission

5.1 Dynamic Simulation Tools

All simulations were done using *Simulink* and *Matlab* version 2016a. The block diagram that was used for simulating the ascent of the LAE into a polar LLO can be seen below.

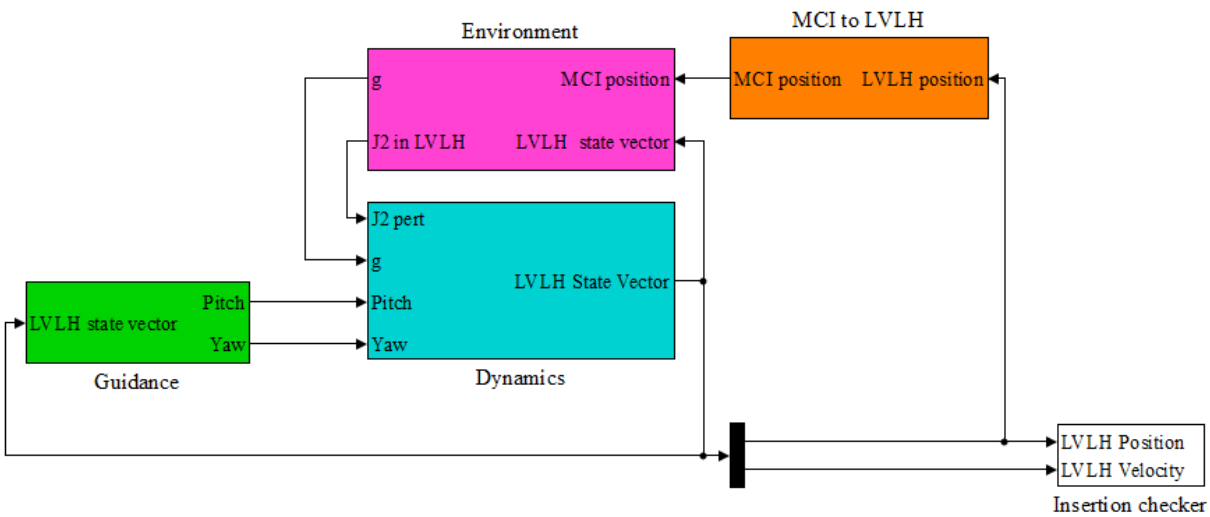

Figure 5.1: Block diagram used for the simulations

There are three main blocks in the diagram in Fig. 5.1, the Guidance block in green, the Dynamics block in blue and the Environment block in pink. The guidance block is responsable for calculating the necessary vehicle attitude to reach the final conditions based on the current state vector in the LVLH reference frame. The guidance is calculated according to each of the algorithms described in Section 4.4.3. This block outputs the pitch and the yaw angles, which are updated on a 1 Hz frequency. Since there is still no concrete information on the guidance computational cabability of the LAE, the frequency was the same as the Space Launch System from NASA [19], which uses a more complex algorithm. This is very conservative, because even the Space Shuttle updated its guidance twice as fast [19], with older technology and a slower algorithm. This block requires the state vector (and the pitch angle for some of the guidance algorithms) to be fedback on the same frequency as the guidance is updated. The

dynamics block propagates the state vector in the LVLH reference frame by integrating Eqs. (2.2), with the addition of the J2 perturbation in the perturbed cases, for the chosen timestep of $0.1\,\mathrm{s}$. This value was chosen conservatively, as there are faster inertial motion untis avaliable, such as the one proposed for Orion that works four times faster [39]. The environment block calculates the outside accelerations that the vehicle undergoes, and needs to receive the state vector in both the MCI and LVLH reference frames. In section 5.3 the only outside acceleration considered is the main gravity term and in 5.4 the J2 gravity perturbation is added. The other two blocks are the orange block that converts the position vector from the LVLH reference frame to the MCI reference frame and the white block that checks wether or not the required insertion conditions are met. As can be seen, the actuators are not simulated, i.e. the attitude profile provided by the guidance block is assumed to be followed perfectly by the vehicle. For the sake of accuracy and to assure the algorithms work in real scenarios, the actuators should be simulated at a later date.

5.2 Scenario Description

In order to validate the guidance algorithms developed in this work, they need to be tested. First the algorithms were tested and compared with others, including the optimal numerical solution. The tests were conducted in perfect condition bi-dimensional trajectories using an inverse square gravity field as the only force other than the thrust. Different insertion conditions were tested, i.e. different insertion altitudes. The capacity (and optimallity) to handle perturbations also needs to be tested, which was done by simulating an ascent using various different out-of-plane starting conditions, as well as including the J2 gravity term in the dynamics.

In order to understand the advantages and disadvantages of each algorithm, they were compared using simulations with no perturbations, i.e. in a spherical non rotating moon environment, with no third body influences. The unperturbed simulations can be found in Section 5.3. In Section 5.4 perturbations were added. All the algorithms described in Section 4.4.3 were tested against the optimal and Hull's solution for five insertion altitudes: very low ($5\,\mathrm{km}$) low ($15\,\mathrm{km}$), medium ($30\,\mathrm{km}$), high ($50\,\mathrm{km}$) and very high ($100\,\mathrm{km}$) altitude insertions. The plots for these orbits can be found in Appendix D, except for the $15\,\mathrm{km}$ altitude, which is the most plausible insertion. In addition to this, the PEG and polynomial guidance algorithms were also tested and compared.

For simplicity, the destination orbits were inserted at periapsis and the apoapsis was kept at $100\,\mathrm{km}$ for all cases. For all the guidance algorithms a sample and hold scheme, updated on a $1\,\mathrm{Hz}$, was used.

5.3 Analysis of Results From Bi-dimensional Simulations

In this section, the various algorithms are compared using simulations with no perturbations, i.e. in a spherical non rotating moon environment, with no forces acting over the body other than inverse square law gravity. This allows us to have a sense of wether or not the guidance techniques developed can

outperform the older algorithms and be worth testing under perturbed conditions. The best performing guidance algorithms were chosen based on performance and computational power required.

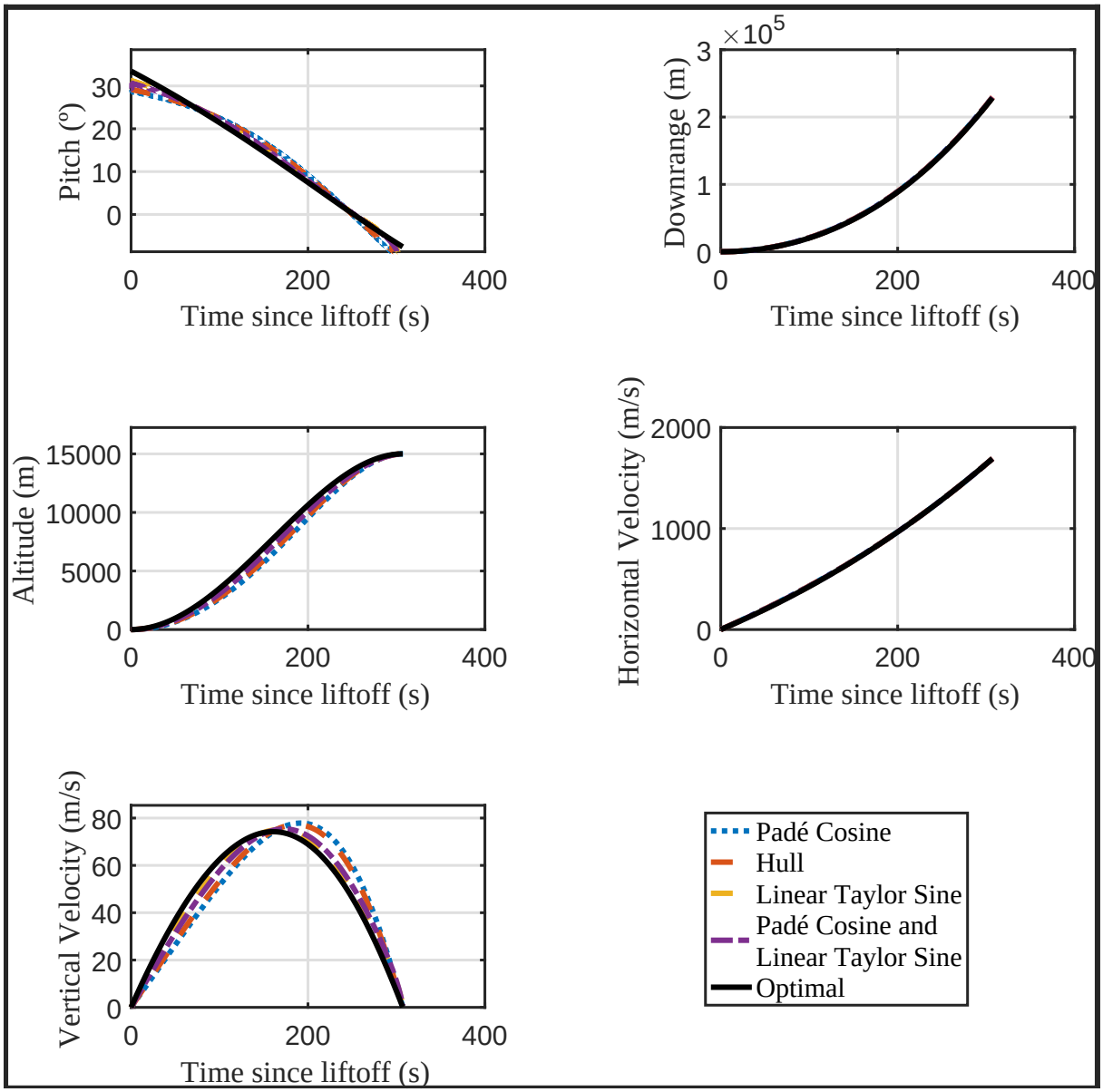

Figure 5.2: Comparison of parameters for 15 km altitude insertion using algorithms I and III

Table 5.1: Insertion times [s] comparison for linear Taylor series approximation for the sine for the different altitudes of insertion

	5 km	15 km	30 km	50 km	100 km
Hull	304. 8	307. 4	313. 0	323. 5	363. 3
Cosine approximation	304. 8	307. 4	313. 2	323. 9	370. 6
Algorithm I	304. 8	307. 2	312. 8	323. 1	356. 5
Algorithm III	304. 8	307. 3	312. 9	323. 1	356. 3
Optimal	304. 6	307. 1	312. 7	323. 0	355. 8

From Tables 5.1, 5.2 5.3, 5.4, 5.5 and 5.6 it can be seen that all the new approximations for the sine of the pitch outperform Hull's for low insertion altitudes, and the quadratic approximations start to get

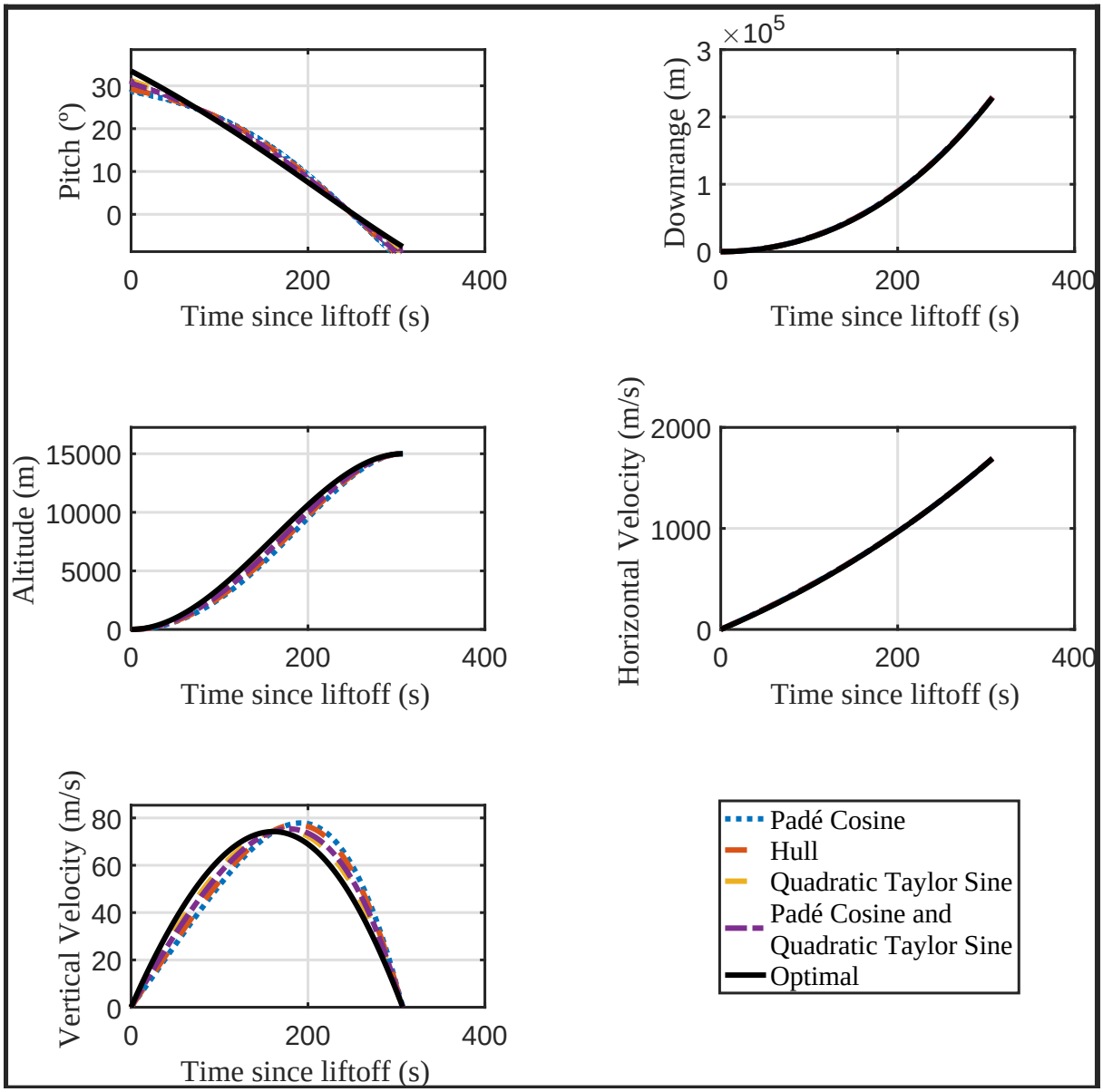

Figure 5.3: Comparison of parameters for 15 km altitude insertion using algorithms V and VII

Table 5.2: Insertion times [s] comparison for quadratic Taylor series approximation for the sine for the different altitudes of insertion

	5 km	15 km	30 km	50 km	100 km
Hull	304. 8	307. 4	313. 0	323. 5	363. 3
Cosine approximation	304. 8	307. 4	313. 2	323. 9	370. 6
Algorithm V	304. 8	307. 3	312. 9	323. 4	363. 6
Algorithm VII	304. 8	307. 3	313. 0	323. 7	370. 0
Optimal	304. 6	307. 1	312. 7	323. 0	355. 8

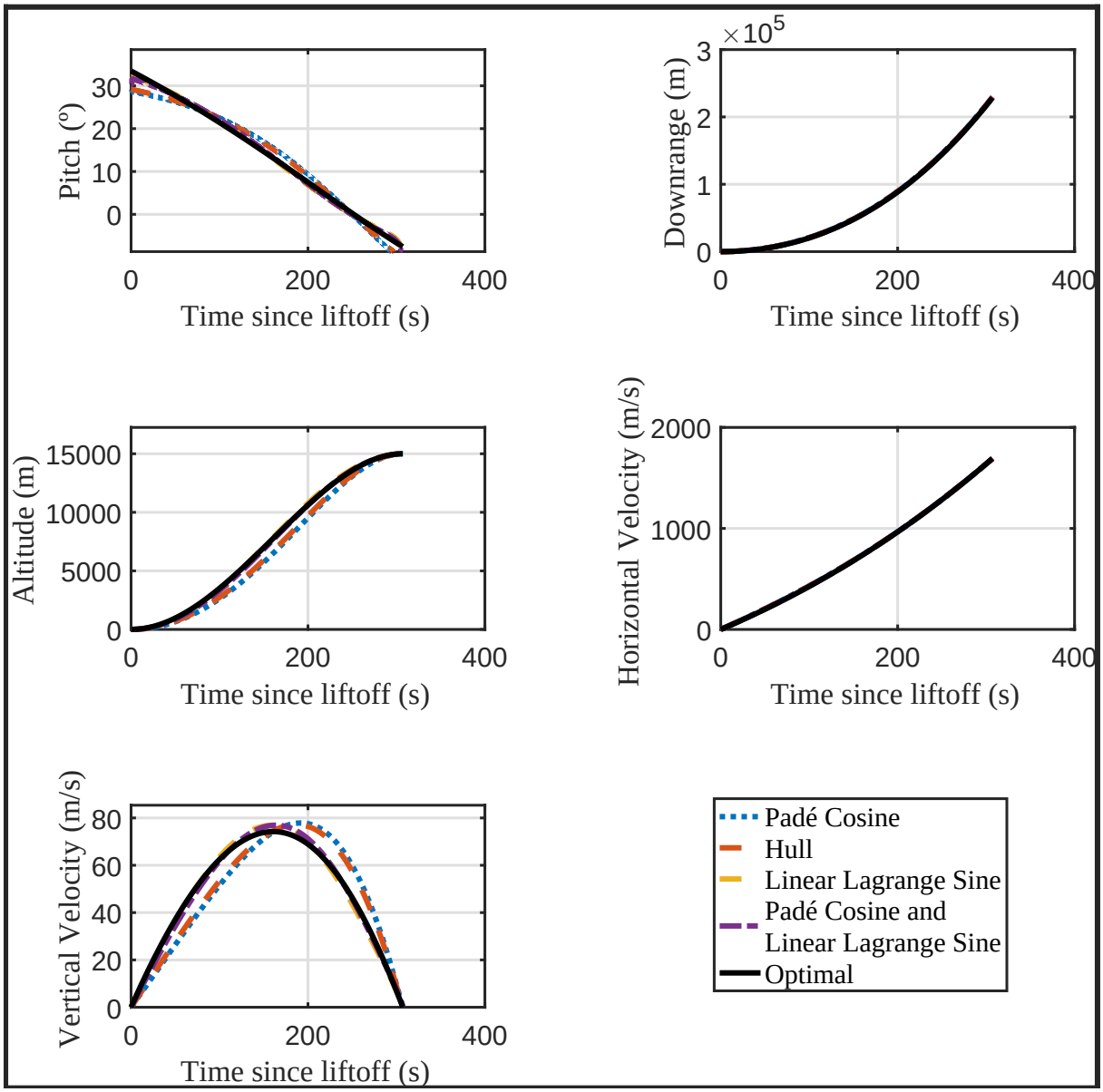

Figure 5.4: Comparison of parameters for 15 km altitude insertion using algorithms II and IV

Table 5.3: Insertion times [s] comparison for quadratic Lagrange polynomial approximation for the sine for the different altitudes of insertion

	5 km	15 km	30 km	50 km	100 km
Hull	304. 8	307. 4	313. 0	323. 5	363. 3
Cosine approximation	304. 8	307. 4	313. 2	323. 9	370. 6
Algorithm II	304. 7	307. 2	312. 9	323. 3	357. 9
Algorithm IV	304. 7	307. 3	312. 9	323. 1	356. 3
Optimal	304. 6	307. 1	312. 7	323. 0	355. 8

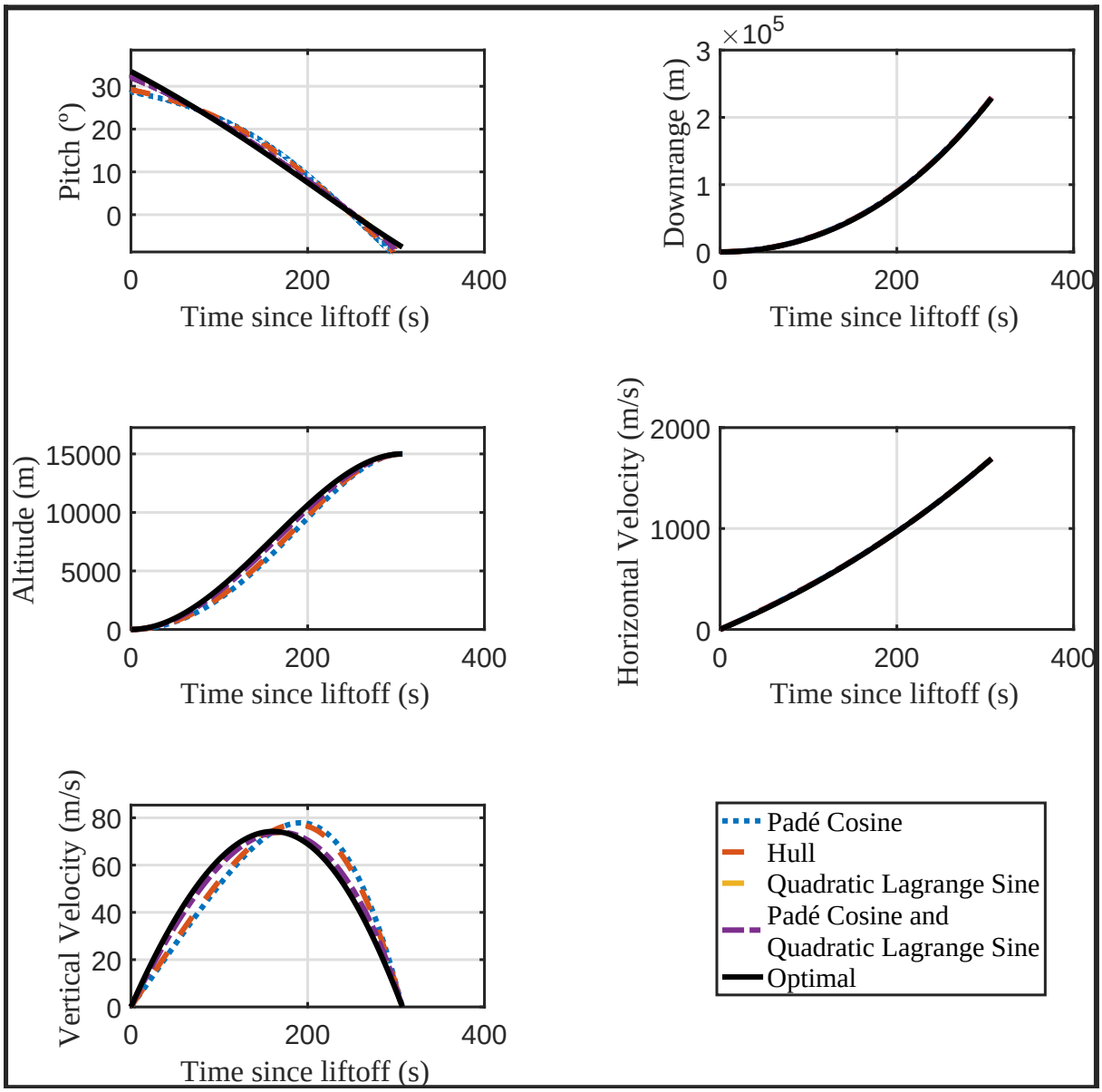

Figure 5.5: Comparison of parameters for 15 km altitude insertion using algorithms VI and VIII

Table 5.4: Insertion times [s] comparison for linear Lagrange polynomial approximation for the sine for the different altitudes of insertion

	5 km	15 km	30 km	50 km	100 km
Hull	304. 8	307. 4	313. 0	323. 5	363. 3
Cosine approximation	304. 8	307. 4	313. 2	323. 9	370. 6
Algorithm VI	304. 7	307. 2	312. 9	323. 4	358. 0
Algorithm VIII	304. 7	307. 2	312. 8	323. 2	356. 9
Optimal	304. 6	307. 1	312. 7	323. 0	355. 8

Table 5.5: Insertion times [s] comparison for PEG

	5 km	15 km	30 km	50 km	100 km
Hull	304. 8	307. 4	313. 0	323. 5	363. 3
PEG	304. 7	307. 2	313	323. 1	356. 3
Optimal	304. 6	307. 1	312. 7	323. 0	355. 8

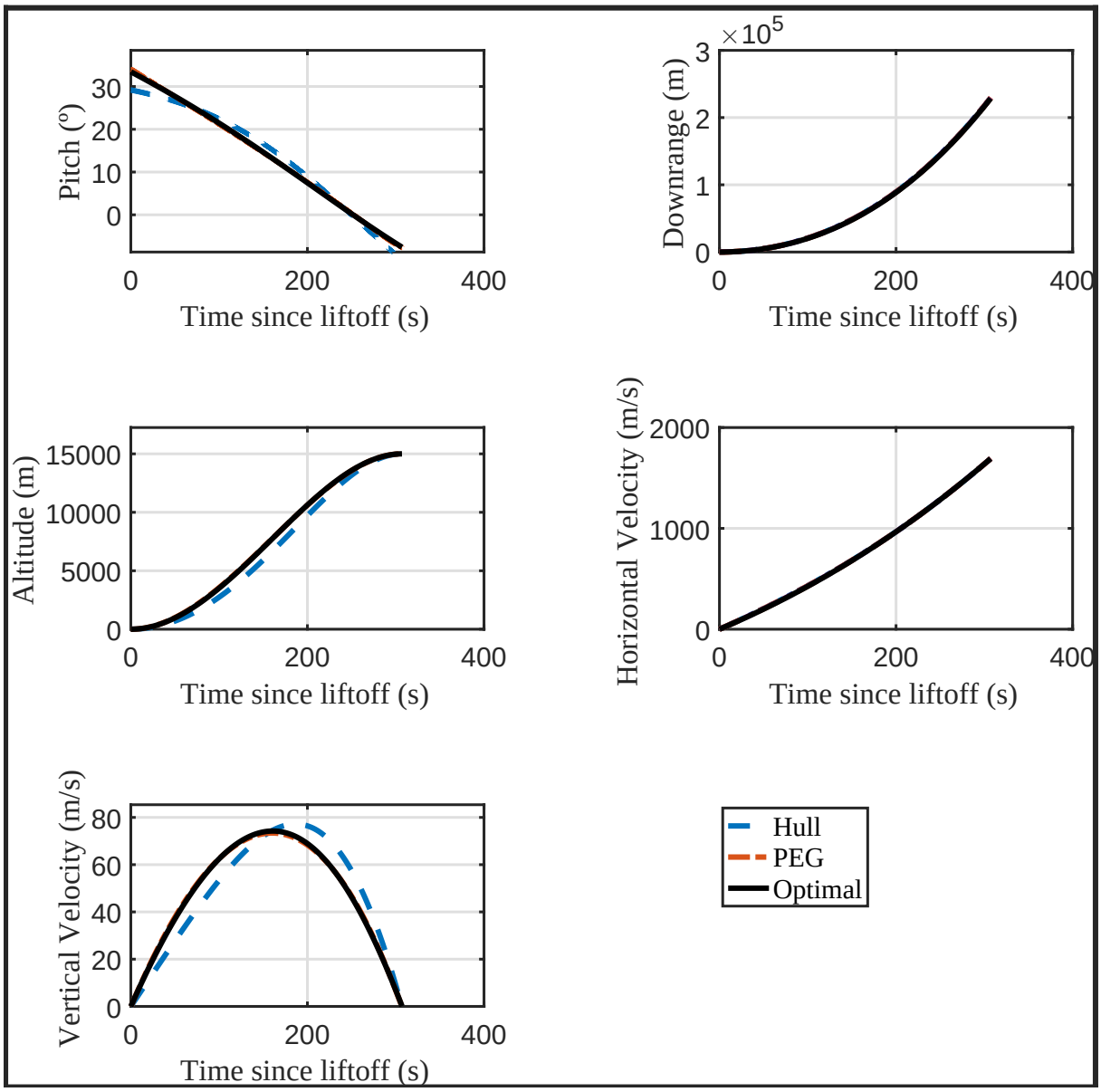

Figure 5.6: Comparison of parameters for 15 km altitude insertion using PEG

Table 5.6: Insertion times [s] comparison for polynomial guidance

	5 km	15 km	30 km	50 km	100 km
Hull	304. 8	307. 4	313. 0	323. 5	363. 3
Polynomal	304. 7	307. 2	313. 3	-	-
Optimal	304. 6	307. 1	312. 7	323. 0	355. 8

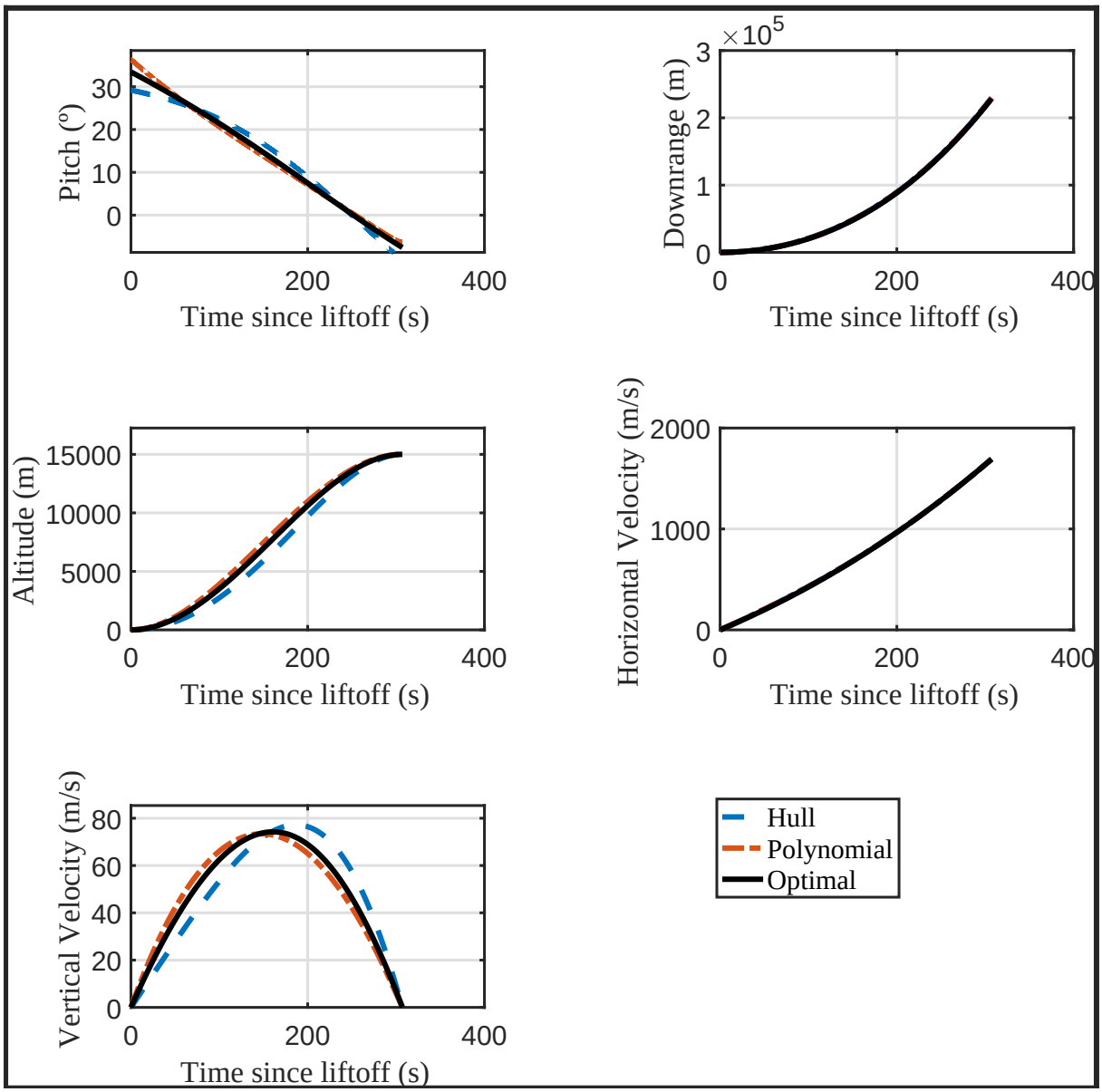

Figure 5.7: Comparison of parameters for 15 km altitude insertion using polynomial guidance

worse for higher altitudes. For the $5\,\mathrm{km}$ insertion altitude, Algorithms II and IV actually manage to have a closer pitch profile to the optimum than all the other tested methods, including this version of PEG, an algorithm that requires solving an equation iteratively. Algorithms II and IV decrease the insertion time in $0.1\,\mathrm{s}$ from Hull's approximation, which is about 0.03%. This translates into about $0.18\,\mathrm{kg}$ saved proppelant.

For the $15\,\mathrm{km}$ insertion altitude, almost all of the new approximations have a close to optimal pitch profile. PEG and polynomial guidance also produce a near optimal pitch profile. Algorithm I can save $0.2\,\mathrm{s}$ in the ascent, which is about 0.06% and it translates into about $0.36\,\mathrm{kg}$ saved proppelant.

The results for $30\,\mathrm{km}$ are very similar to the $15\,\mathrm{km}$ results. The difference is that Algorithm II in this case actually outperfoms PEG and polynomial guidance, instead of just having the same performance.

The results for $50\,\mathrm{km}$ insertion altitude start to have significant differences between the new approximations and Hull's, PEG and polynomial guidance. Both PEG and polynomial guidance actually stop working for this altitude of insertion. There is a $0.4\,\mathrm{s}$ (about 0.12%) in insertion times between Algorithm I and Hull's approximation, leading to $0.72\,\mathrm{kg}$ fuel saving.

The results for $100\,\mathrm{km}$ insertion altitude have very significant difference between the approximations. Using Algorithm I will actually lead to $7\,\mathrm{s}$ (about 2%) saving from Hull's approximation, leading to about $12.6\,\mathrm{kg}$ of fuel saving, while still only staying $0.5\,\mathrm{s}$ away from the optimal insertion. This is a significant improvement. This type of very high orbit insertion will not typically be used on a regular ascent, but it can, for example, be used as contigency plan for enabling a rendezvous.

The linear approximations are at least as good as PEG and polynomial for all the insertions tested, showing a significant improvement for higher altitudes (since PEG and polynomial simply will not work for some altitudes). This happens because the pitch profiles generated by the linear Taylor series and Lagrange polynomial approximations are very similar to the optimal pitch profiles, as can be seen in Figs. 5.2 through 5.7 and in all the Figs. from Appendix D.

Surprisingly the cosine approximation alone does not have a positive impact on some of the trajectories tested, namely the lower altitude insertions. This was unexpected at first, but it makes sense because Hull's approximation for the sine of the angle is an overestimate, i.e. for all values of $\bar{\lambda}_v$ the approximation has a larger absolute value than the actual function. Thus, having an estimate for the remaining burntime smaller than the real one will counter this effect. This also happens in the other approximations for the sine, except for insertion altitudes of $50\,\mathrm{km}$ and $100\,\mathrm{km}$ using the linear Lagrange polynomials and the linear Taylor series approximations. In these cases the real sine of the pitch is actually larger (in absolute value) than the approximation for a large part of the domain, making a more realistic remaining burntime guess work better than than Hull's approximation. However, these insertion altitudes are not common and the improvement using the Padé approximant for the cosine and using the linear approximations for the sine compared to just approximating the sine is small. This is actually good news, because using a contanst approximation for the cosine instead of the Padé approximant is simpler and requires less calculations.

Considering the linear approximations have good performances for all altitudes tested, using them is prefered, since they do not require solving a fourth degree polynomial, only solving a linear system of two

equations. Also, because the linear approximation coefficients can be calculated *a priori*, they require the same amount of computation as Hull's, while performing better all around. Based on the points mentioned before, the best performing approximations for a guidance scheme are Algorithms I and II. This Algorithms are the best compromise between performance and computational cost. In Chapter 5.4 these guidance schemes are tested for three dimensional perturbed trajectories against Hull's scheme and the optimal trajectory.

The difference between the optimal trajectory and the best performing algorithms for a 15 km insertion altitude can be seen in Fig. 5.8

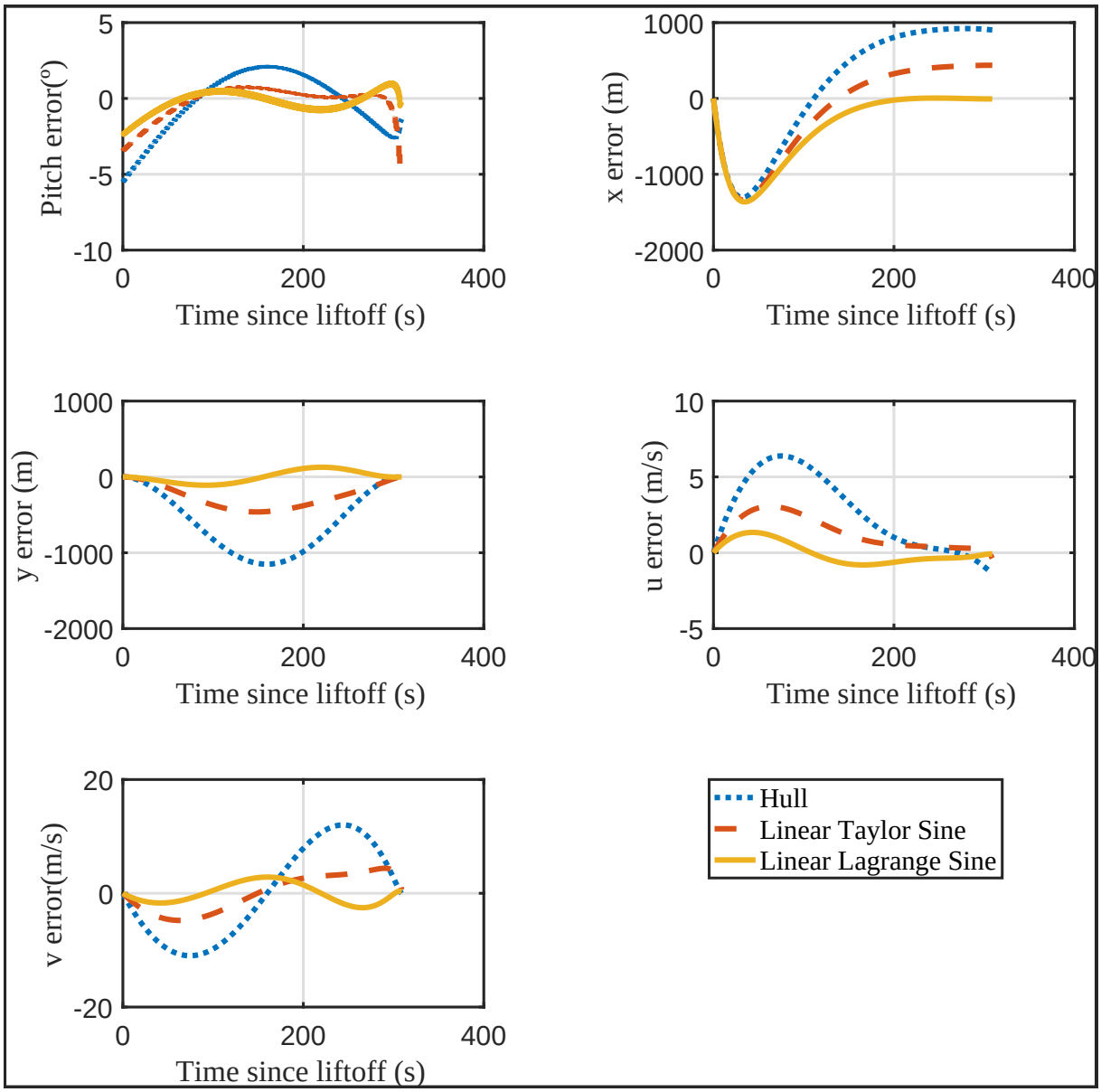

Figure 5.8: Difference of some parameters from the optimal reference trajectory for 15 km altitude insertion using the linear algorithms

5.4 Analysis of Results from Three-Dimensional Simulations with Perturbed Parameters

In order to make sure that the selected approximation is able to handle out of plane perturbations, a 15 km altitude insertion is tested, with different out of plane initial conditions. The yaw angle was plotted and compared with Hull's approximation and the optimal value, to see if the approximations have any effect on the yaw angle profile, compared with the one produced by Hull's algorithm.

Observing at Figs. 5.9, 5.10 and 5.11 it can be seen that the yaw angle is almost exactly the same for all the approximations as the optimal value, hence confirming that changing the approximation of the sine of the pitch angle does not have any effect on the hability of the algorithm to optimally handle out of plane perturbations. In appendix B it can also be seen that the insertion error from the Algorithm II is smaller than Algorithm I, so it might be a better option.

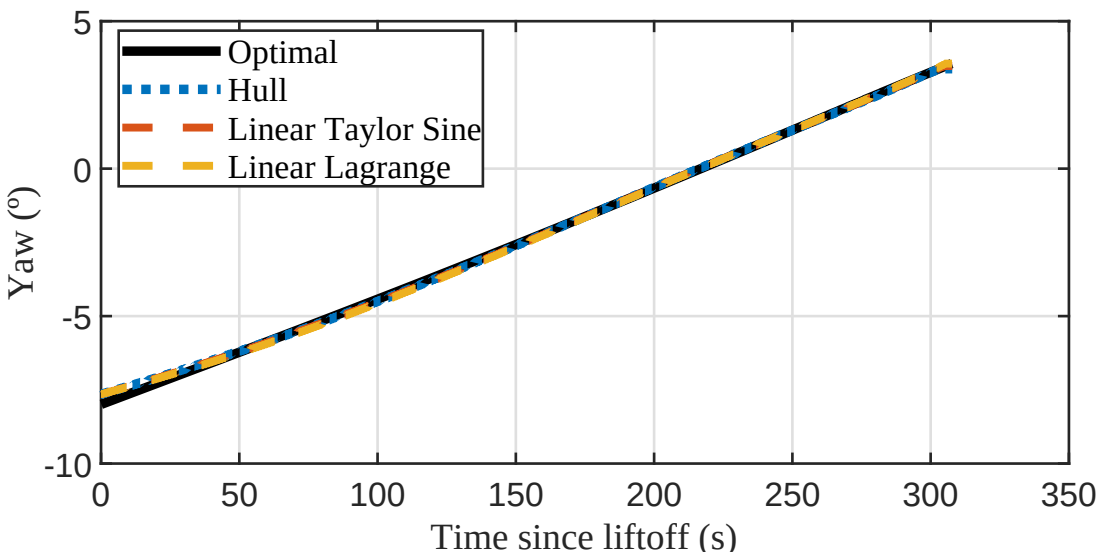

Figure 5.9: Comparison of Yaw angle for 15 km altitude insertion with 50 m s^{-1} out of plane initial velocity

The effect of the J2 perturbations was also be analysed, and once again the 15 km altitude insertion was used. The test assumes that the vehicle is launched from the south pole of the moon into a 90° inclination orbit to calculate the J2 perturbations. From 5.12 it can be seen that the effect of the J2 perturbation, which was the largest pertubation in effect (see Table 2.2), leads to the same insertion time and has no noticeable effect during the ascent, and thus the assumption of not using perturbations to develop the guidance laws and to calculate the optimal trajectory was valid.

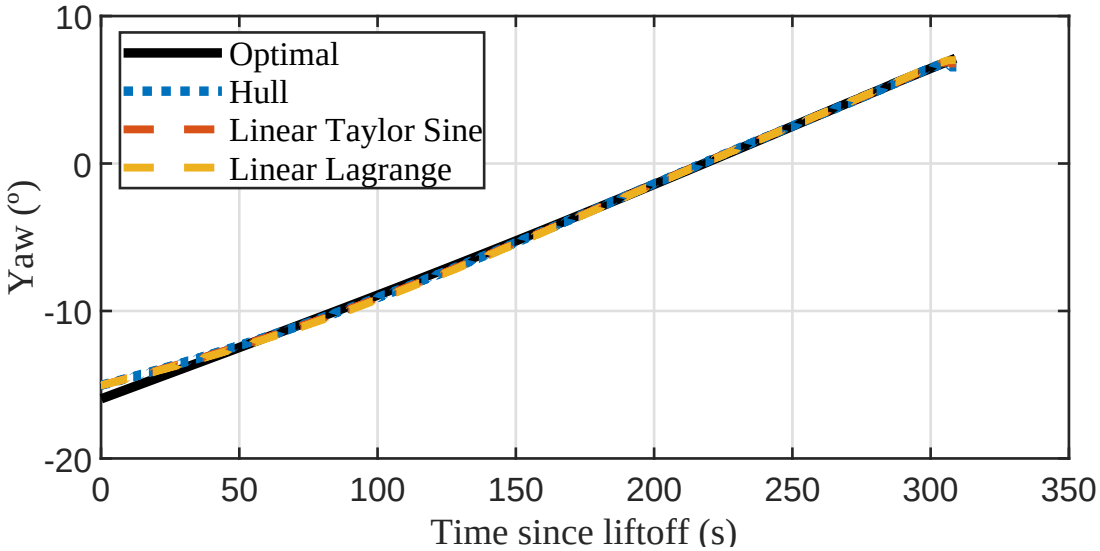

Figure 5.10: Comparison of Yaw angle for 15 km altitude insertion with 100 m s^{-1} out of plane initial velocity

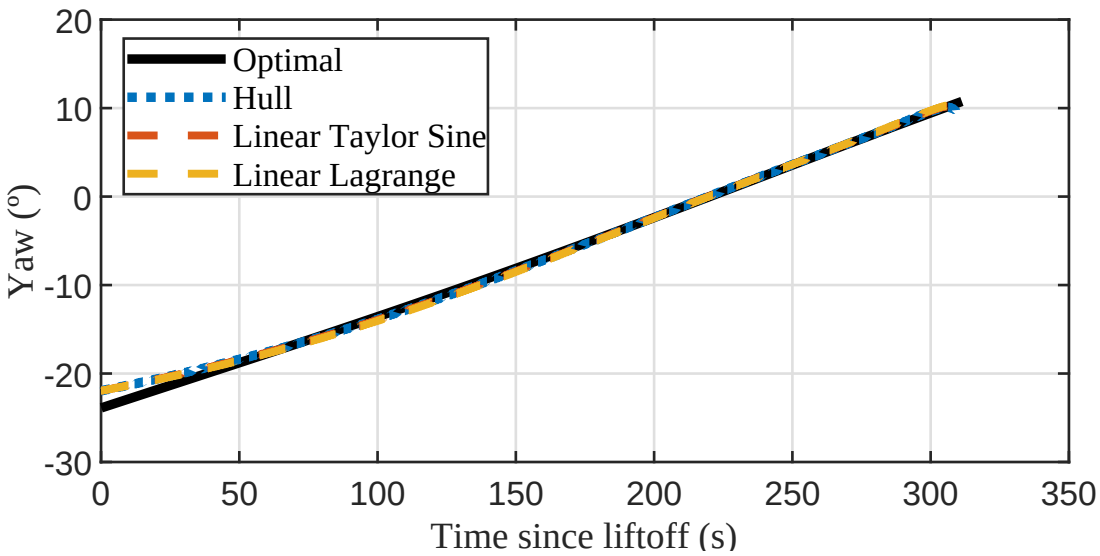

Figure 5.11: Comparison of Yaw angle for 15 km altitude insertion with 150 m s^{-1} out of plane initial velocity

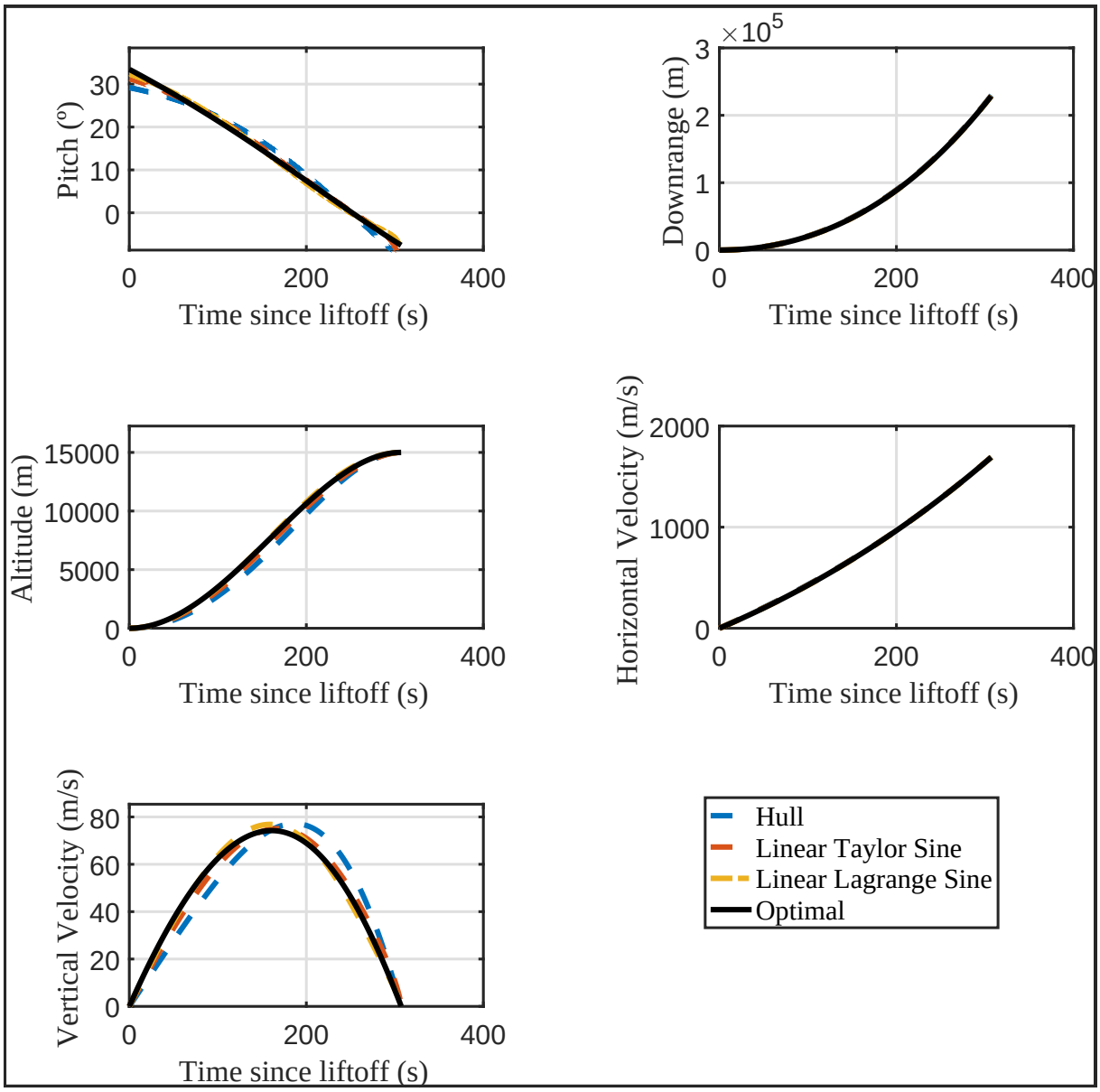

Figure 5.12: Comparison of parameters for 15 km altitude insertion using a linear Lagrange polynomial and linear Taylor series expansions with addition of J2 perturbations

Chapter 6

Conclusions

The objective of this thesis was to develop an optimal, yet simple and explicit, guidance algorithm for a single stage atmosphereless ascent problem. The algorithm should then be applied on the ascent LAE of the HERACLES mission from the surface of the moon to a polar LLO. The difficulty in developing an optimal ascent guidance algorithm is to obtain closed form solutions that are fast and capabable to have performance close to optimal for a variety of different types of orbits. It is still very important to save spacecraft resources, even though today's on board computers can handle numerical guidance. In line with this, the algorithms were developed using prime vector theory and differ from each other by the type of approximations used to estimate the pitch angle. Specifically, a new method for estimating the remaining burntime based on a quadratic approximation for the cosine of the pitch and a Padé approximant for the acceleration integral and four different methods for approximating the sine of the pitch angle were developed. The sine approximations were developed using linear and quadratic Taylor series expansions and linear and quadratic Lagrange polynomials. These were then compared with other methods (PEG, polynomial guidance and Hull's explicit algorithm), and with an optimal numerical closed loop solution. To do this, all the methods were implemented using *Matlab* and *Simulink*.

Out of all the different methods developed for the sine approximation, the ones that showed the best results were the two linear approximations. They exhibited near optimal results for insertions up to $50\,\mathrm{km}$ altitude and decent results for a $100\,\mathrm{km}$ altitude insertion. These methods also require the same computational power as Hull's method, since the necessary coefficients for the sine approximations can be calculated on the ground station. In addition to that, they do not require the quadratic pitch cosine approximation to perfom, i.e. the remaining burntime estimate obtained by approximating the cosine of the pitch by one is good. This means that only the solution of a linear system of two equations is necessary to estimate the pitch, instead of requiring the solution of a fourth degree polynomial. The linear approximations were also capable of handling out of plane perturbations, making them strong candidates for closed loop guidance algorithms. Another indirect conclusion from this work is the possibility of using Padé approximants to calculate the thrust acceleration integrals in order to simplify other types of algorithms.

6.1 Future Work

In this work the hability of the algorithms to handle perturbations was not extensively tested, and no actual control system actuators were simulated, since both the pitch and the yaw responses were assumed to be instantaneous. In the future an actual control system with real actuators should be added to the simulation. In addition to that, a perturbation analysis using something like Monte Carlo simulations would be necessary to understand wether or not the algorithms are capable of performing in a real life scenario. Another thing that can be explored is the expansion of the algorithms to a multiple stage ascent with coasting, making the algorithm usable for larger multiple stage vehicles. Other than that, using Padé approximants for the thrust acceleration integrals should also be analyzed in different missions and different guidance algorithms, instead of the much used Taylor series expansions. The usage of these approximations might decrease the computational cost of some already existing numerical algorithms, or even allow for different explicit solutions.

Bibliography

[1] D. G. Hull. Optimal Guidance for Quasi-planar Lunar Ascent. *Journal of Optimization Theory and Applications*, 151(2):353–372, 2011. ISSN 00223239. doi: 10.1007/s10957-011-9884-5.

[2] S. Garber. Sputnik and the dawn of the space age. https://history.nasa.gov/sputnik/. Accessed: 2018/09/03.

[3] Apollo 11. https://www.nasa.gov/mission_pages/apollo/missions/apollo11.html, . Accessed: 2018/09/03.

[4] Apollo 12. https://www.nasa.gov/mission_pages/apollo/missions/apollo12.html, . Accessed: 2018/09/03.

[5] Apollo 14. https://www.nasa.gov/mission_pages/apollo/missions/apollo14.html, . Accessed: 2018/09/03.

[6] Apollo 15. https://www.nasa.gov/mission_pages/apollo/missions/apollo15.html, . Accessed: 2018/09/03.

[7] Apollo 16. https://www.nasa.gov/mission_pages/apollo/missions/apollo16.html, . Accessed: 2018/09/03.

[8] Apollo 17. https://www.nasa.gov/mission_pages/apollo/missions/apollo17.html, . Accessed: 2018/09/03.

[9] ISECG. The Global Exploration Roadmap. 2018. URL https://www.globalspaceexploration.org/wordpress/wp-content/isecg/GER{_}2018{_}small{_}mobile.pdf.

[10] R. Withley and R. Martinez. Options for Staging Orbits in Cislunar Space. *IEEE Aerospace Conference Proceedings*, 2016-June, 2016.

[11] R. Schonenborg. HERACLES Lunar Ascent Element (LAE). 2017.

[12] B. Hufenbach, C. Lange, R. Martinez, J. Hill, M. Landgraf, and A. Bergamasco. International Missions to the Lunar Vicinity and Surface-near-term Mission Scenario of the Global Space Exploration Roadmap. *66th International Astronautical Congress*, 5 (1):1–11, 2016. ISSN 00741795. URL https://www.lpi.usra.edu/lunar/strategies/HufenbachEtAl{_}IAC2015{_}GERNeartermMissionScenario.pdf.

[13] D. C. Davis, S. A. Bhatt, K. C. Howell, J. W. Jang, R. J. Whitley, F. D. Clark, D. Guzzetti, E. M. Zimovan, and G. H. Barton. Orbit Maintenance and Navigation of Human Spacecraft at Cislunar Near Rectilinear Halo Orbits. *Advances in the Astronautical Sciences*, 160:2257–2276, 2017.

[14] F. V. Bennett and NASA. Lunar descent and ascent trajectories. In *The AIAA 8th Aerospace Sciences Meeting*, New York, New York, 1970. AIAA.

[15] D. C. Chandler and I. E. Smith. Development of the Iterative Guidance Mode with Its Application to Various Vehicles and Missions. *Journal of Spacecraft and Rockets*, 4(7), 1967. ISSN 00224650. doi: 10.2514/6.1966-1861.

[16] F. Teren and NASA. Explicit guidance equations for multistage boost trajectories. 1966.

[17] R. L. Mchenry, A. D. Long, B. F. Cockrell, R. J. Thibodeau III, and T. J. Brand. Space shuttle ascent guidance, navigation, and control. 27(1):1–38, 1979. doi: 10.1063/1.1722828.

[18] D. Zimpfer, P. Hattis, J. Ruppert, and A. Lifetime. Space shuttle gn&c development history and evolution. 09 2011.

[19] P. V. D. Porten, N. Ahmad, and M. Hawkins. Powered Explicit Guidance Modifications & Enhancements for Space Launch System Block - 1 and Block - 1B Vehicles. pages 1–12, 2018.

[20] S. K. Scarritt, T. Fill, and S. Robinson. Advances in orion's on-orbit guidance and targeting ssystem architechture. pages 1–13.

[21] Z. Zhang, S. Gong, and J. Li. The Fuel-optimal Trajectory for Finite-thrust Lunar Ascent. *Aerospace Science and Technology*, 39:675–684, 2014. ISSN 12709638. doi: 10.1016/j.ast.2014.06.011. URL `http://dx.doi.org/10.1016/j.ast.2014.06.011`.

[22] P. Lu and B. Pan. Highly Constrained Optimal Launch Ascent Guidance. *Journal of Guidance, Control, and Dynamics*, 33(2):404–414, 2010. ISSN 0731-5090. doi: 10.2514/1.45632. URL `http://arc.aiaa.org/doi/10.2514/1.45632`.

[23] P. Lu, S. Forbes, and M. Baldwin. A Versatile Powered Guidance Algorithm. In *AIAA Guidance, Navigation, and Control Conference and Exhibit*, pages 1–16, 2012. ISBN AIAA 2002-4559. doi: 10.2514/6.2012-4843.

[24] G. A. Dukeman. Atmospheric ascent guidance for rocket-powered launch vehicles. In *Guidance, Navigation, and Control Conference and Exhibit*, Monterey, California, 2002. AIAA. ISBN AIAA 2002-4559. doi: 10.2514/6.2002-4559.

[25] S. Feeley and J. L. Speyer. Approximate optimal guidance system for the advanced launch. NASA technical report, The University of California at Los Angeles, Los Angeles, CA, United States, 1993.

[26] D. G. Hull and M. W. Harris. Optimal Solutions and Guidance for Quasi-planar Ascent Over a Spherical Moon. *Advances in the Astronautical Sciences*, 143(4):829–841, 2012. ISSN 00653438. doi: 10.2514/1.55443.

[27] M. Valtonen and H. Karttunen. *Astrophysics and the three-body problem*, page 1–19. Cambridge University Press, 2006. doi: 10.1017/CBO9780511616006.002.

[28] X. Dong, C. Hu, T. Long, and Y. Li. Numerical analysis of orbital perturbation effects on inclined geosynchronous SAR. *Sensors (Switzerland)*, 16(9), 2016. ISSN 14248220. doi: 10.3390/s16091420.

[29] Moon fact sheet. `https://nssdc.gsfc.nasa.gov/planetary/factsheet/moonfact.html`. Accessed: 2018/09/03.

[30] R. Y. Kezerashvili and J. F. Vázquez-Poritz. Bound Orbits of Solar Sails and General Relativity. Technical report, Aug. 2010.

[31] P. Lu, B. J. Griffin, G. a. Dukeman, and F. R. Chavez. Rapid Optimal Multiburn Ascent Planning and Guidance. *Journal of Guidance, Control, and Dynamics*, 31(6):1656–1664, 2008. ISSN 0731-5090. doi: 10.2514/1.36084.

[32] E. B. Lee and L. Markus. *Foundations of Optimal Control Theory*. Wiley, 1967.

[33] W. Liu, E. Mooij, J. Guo, and W. Wu. Polynomial versus gravity-turn guidance law for lunar ascent. In *Proceedings of the International Astronautical Congress, IAC*, volume 2, pages 1255–1264, 2012.

[34] E. W. Weisstein. Padé approximant. From MathWorld—A Wolfram Web Resource, 2018. URL `http://mathworld.wolfram.com/Tree.html`. Accessed: 9/8/2018.

[35] MATLAB. Matlab, 2016a. The MathWorks, Natick, MA, USA.

[36] W. R. Inc. Mathematica, Version 11.3. Champaign, IL, 2018.

[37] R. Kulkarni. Unified Method for Solving General Polynomial Equations of Degree Less than Five. *Alabama Journal of Mathematics*, 2006. URL `http://ajmonline.org/2006/Kulkarni.pdf`.

[38] S. Janson. Roots of polynomials of degrees 3 and 4. *ArXiv e-prints*, Sept. 2010.

[39] G. Holt and C. D'Souza. Orion Absolute Navigation System Progress and Challenges. *AIAA Guidance, Navigation, and Control Conference*, pages 1–17, 2012. doi: 10.2514/6.2012-4995. URL `http://arc.aiaa.org/doi/abs/10.2514/6.2012-4995`.

Appendix A

Computer Specifications

Processor	Intel(R) Core(TM) i7-4720HQ CPU @ 2.60GHz
Video Card	NVIDIA GeForce GTX 950M
RAM	8.0 GB
Operating System	Microsoft Windows 10 (build 17134), 64-bit

Figure A.1: Computer specifications used for the runtime simulations

Appendix B

3D Insertion Position Errors

B.1 Out of Plane Errors

Table B.1: Out of plane insertion errors

Out of plane insertion errors for the 3D ascentions for the 15km altitude insertion								
Initial v_z	0m s^{-1}		50m s^{-1}		100m s^{-1}		150m s^{-1}	
	z	v_z	z	v_z	z	v_z	z	v_z
Algorithm I	0	0	-0.0056	-0.0024	0.0200	0.0358	0.1028	0.2386
Algorithm II	0	0	0.0121	0.0265	0.0404	0.0752	0.1445	0.2765

B.2 Vertical Errors

Table B.2: Vertical insertion errors

Vertical insertion errors for the 3D ascentions for the 15km altitude insertion								
Initial v_z	0m s^{-1}		50m s^{-1}		100m s^{-1}		150m s^{-1}	
	y	v_y	y	v_y	y	v_y	y	v_y
Algorithm I	0.1435	0.3934	0.2415	0.4422	0.0358	0.2918	0.1362	0.2241
Algorithm II	0.2599	0.7418	0.4628	0.8672	0.1935	0.5811	0.2742	0.5437

Appendix C

J2 Perturbation in the LVLH Reference Frame

The first step necessary to calculate the J2 perturbation in the LVLH reference frame, is to calculate the MCI reference frame position from the LVLH reference frame. This can be done when the Lift-off point in the MCI frame and the orbital parameters of the target orbit are known. Specifically, the inclination (i) and longitude of the ascending (Ω) node are necessary, since these are the two parameters that will determine the direction of the LVLH frame in the MCI reference frame. The downrange and z perturbation in the LVLH reference frame can be represented by rotations in the MCI reference frame. The altitude in the LVLH frame will translate into the modulus of the position vector in the MCI reference frame. Therefore, the only things that are needed are the rotation angles and reference vectors, in the MCI reference frame. The starting vector will be a vector in the MCI reference frame, with the same direction as the lift-off position vector, but with its radius determined by the altitude

$$P_1 = P_{\text{lift-off}} \frac{R_{☾} + y}{R_{☾}} \tag{C.1}$$

The first rotation, equivalent to the downrange, is about the vector

$$\vec{v}_\chi = \begin{bmatrix} \sin(\Omega)\sin(i) & -\cos(\Omega)\sin(i) & \cos(i) \end{bmatrix}, \tag{C.2}$$

and the rotation angle is

$$\chi = \frac{x}{R_{☾}}. \tag{C.3}$$

The vector produced by this rotation will be denominated P_2. The next step is to make the rotation in the MCI reference frame equivalent to the z perturbation in the LVLH reference frame. For this case, the rotation vector is a unit vector, starting at the origin, rotated 90° clockwise from P_2 on the orbital plane, and, just like the previous case, the rotation angle is

$$\zeta = \frac{z}{R_{☾}}. \tag{C.4}$$

After this rotation the position vector is expressed in the MCI frame, and thus the J_2 gravity acceleration term can be expressed by Eq. 2.9. This vector needs to be rotated back into the LVLH frame to be used in the simulation.

Appendix D

Ascent Flight Plots

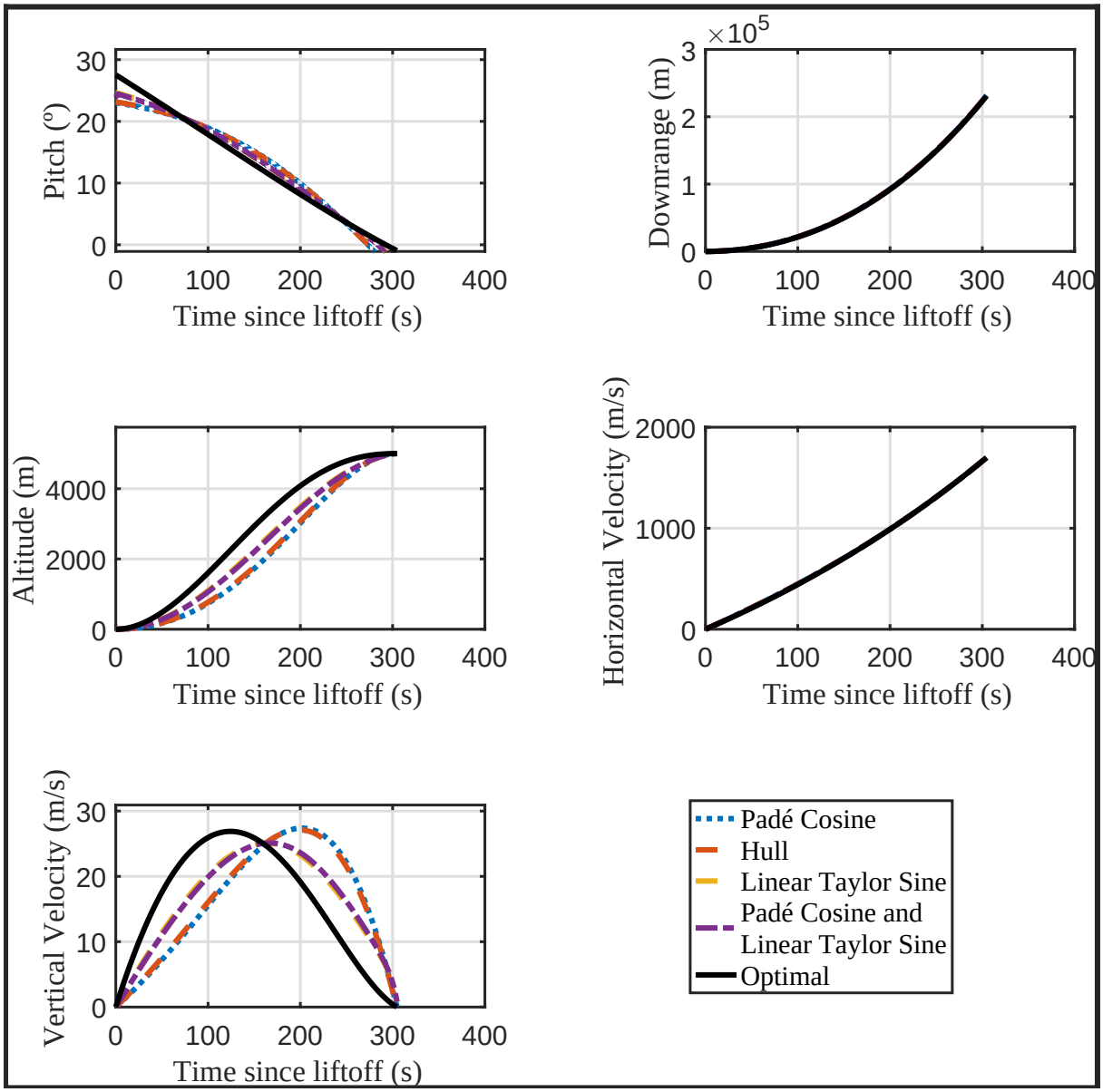

Figure D.1: Comparison of parameters for 5 km altitude insertion using algorithms I and III

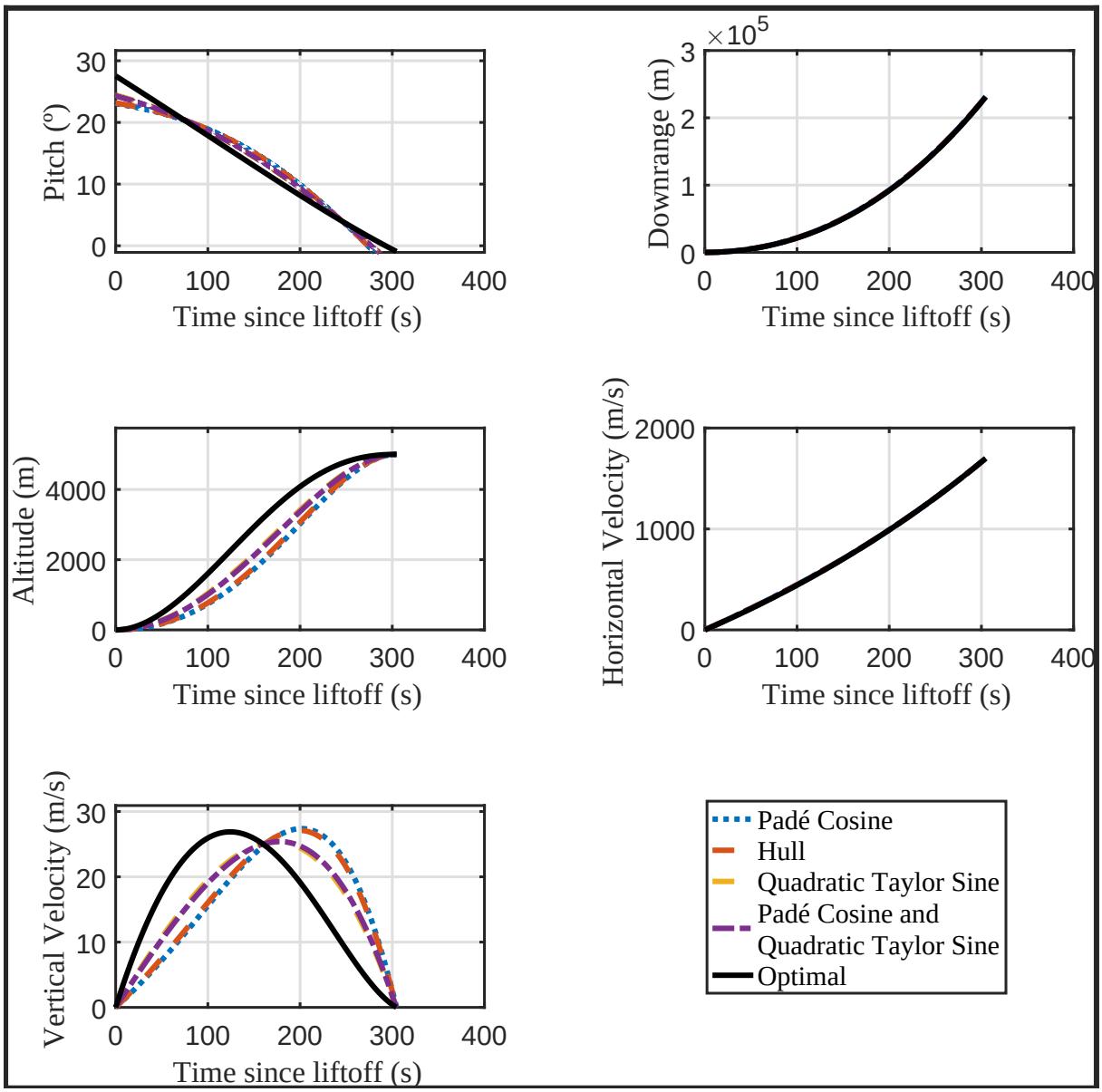

Figure D.2: Comparison of parameters for 5 km altitude insertion using algorithms V and VII

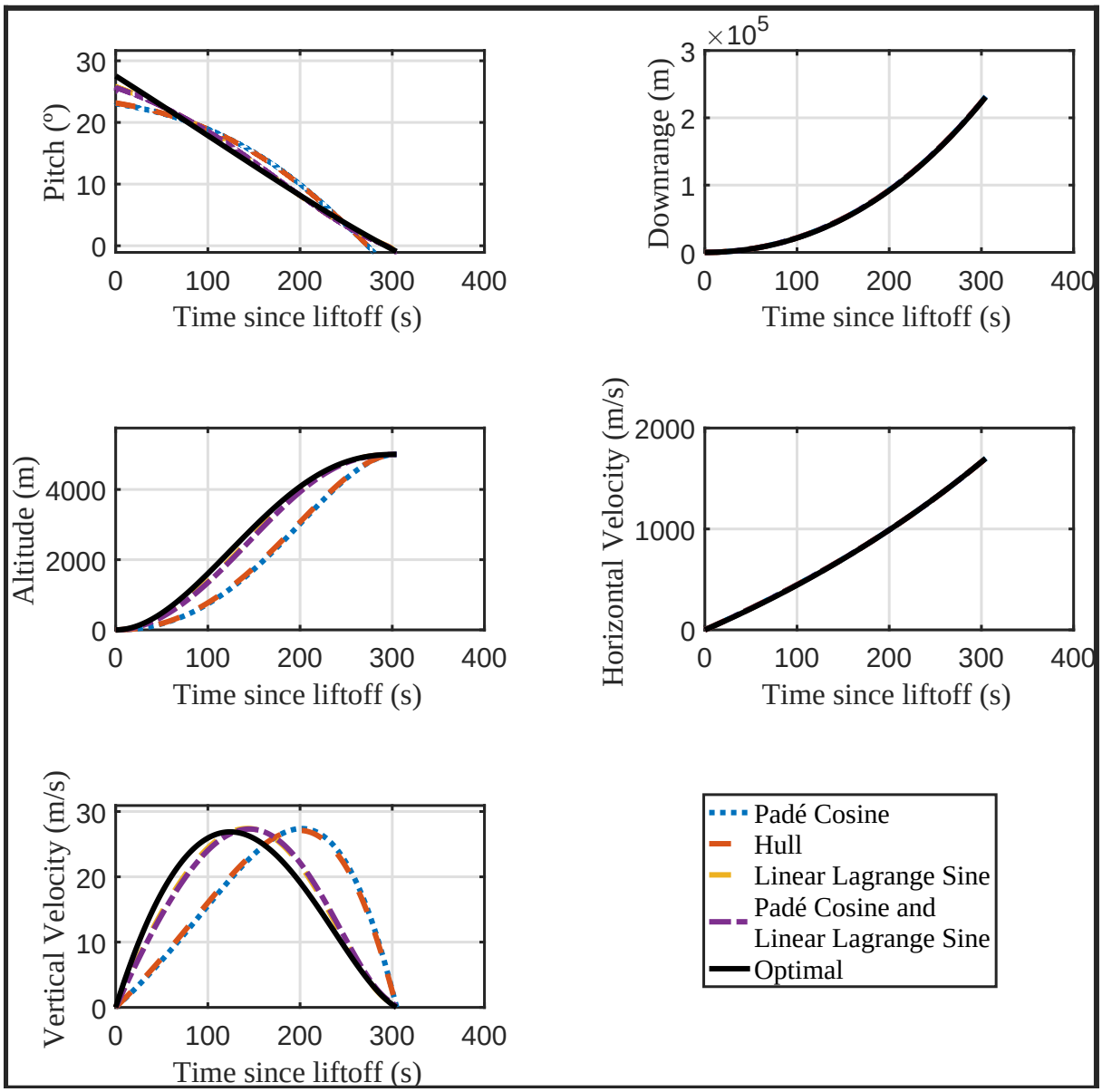

Figure D.3: Comparison of parameters for 5 km altitude insertion using algorithms II and IV

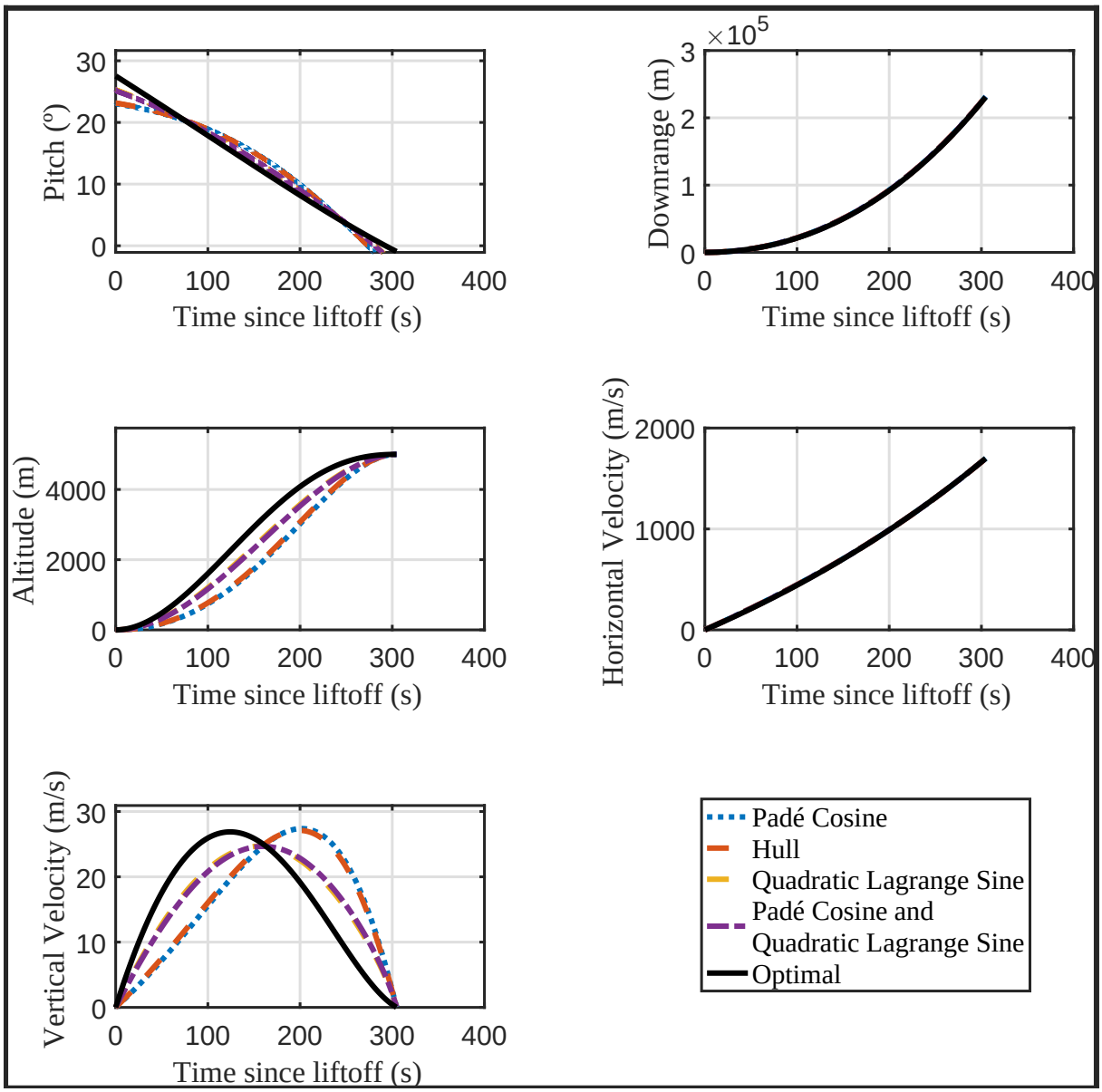

Figure D.4: Comparison of parameters for 5 km altitude insertion using algorithms VI and VIII

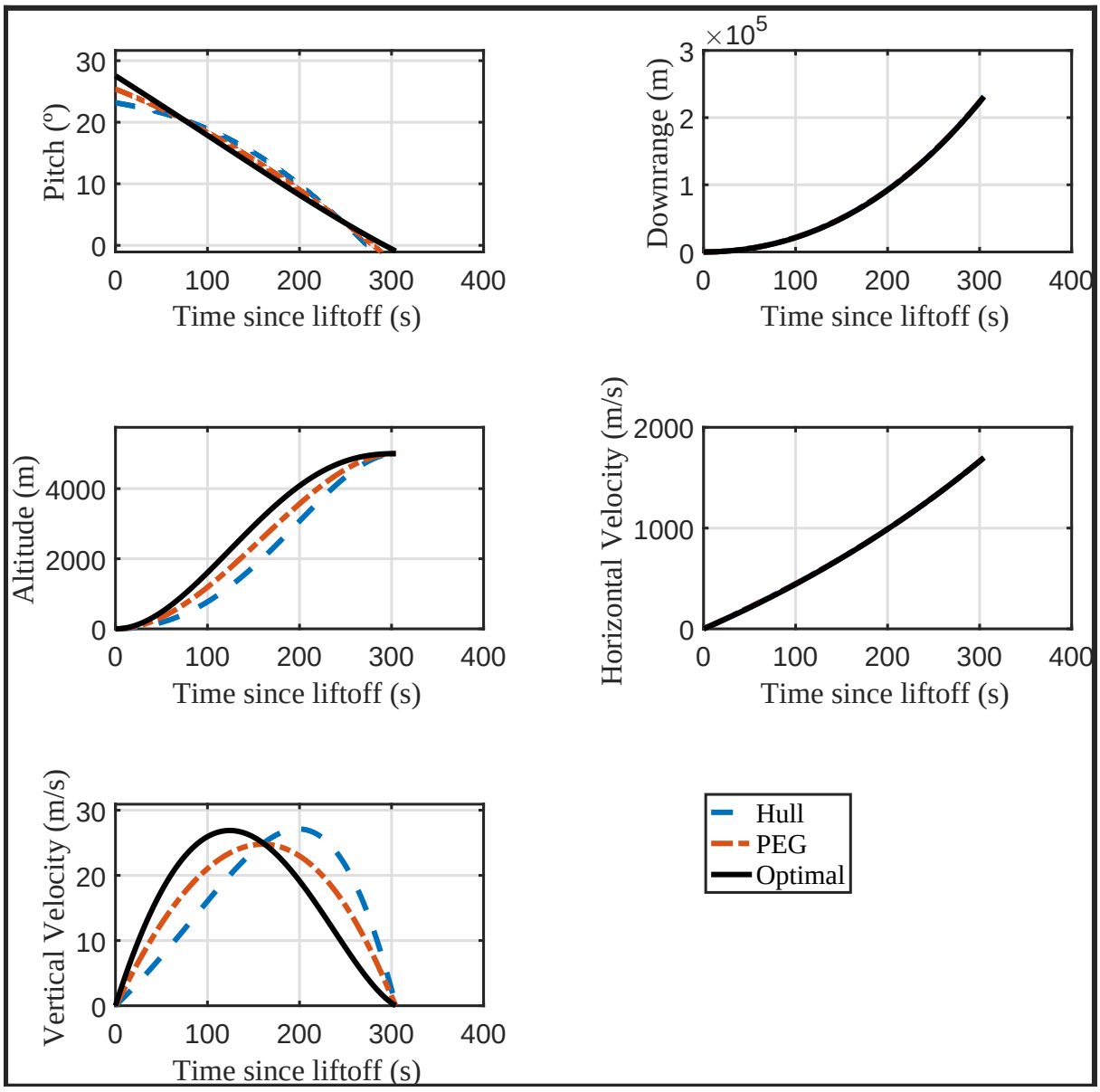

Figure D.5: Comparison of parameters for 5 km altitude insertion using PEG

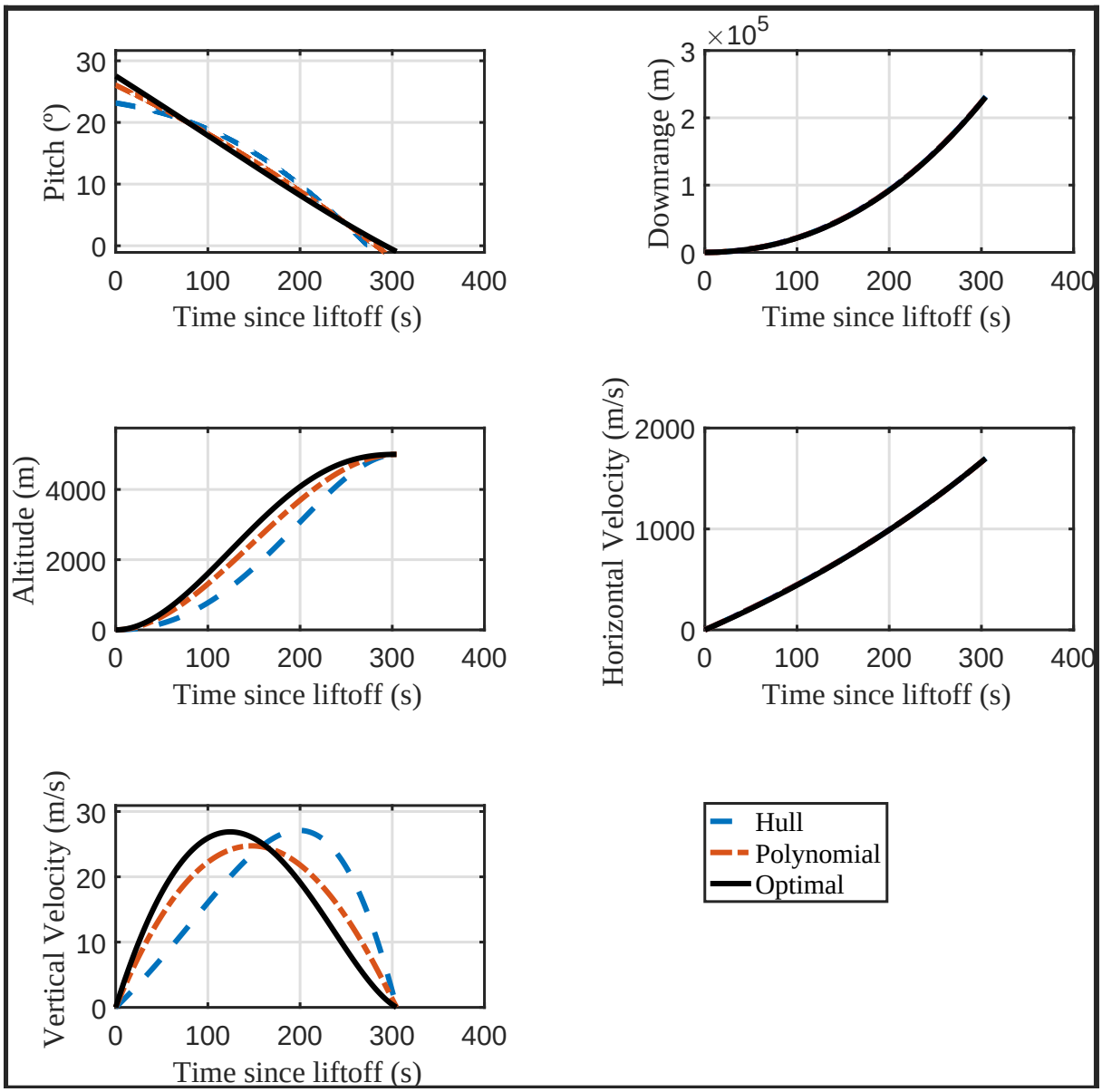

Figure D.6: Comparison of parameters for 5 km altitude insertion using polynomial guidance

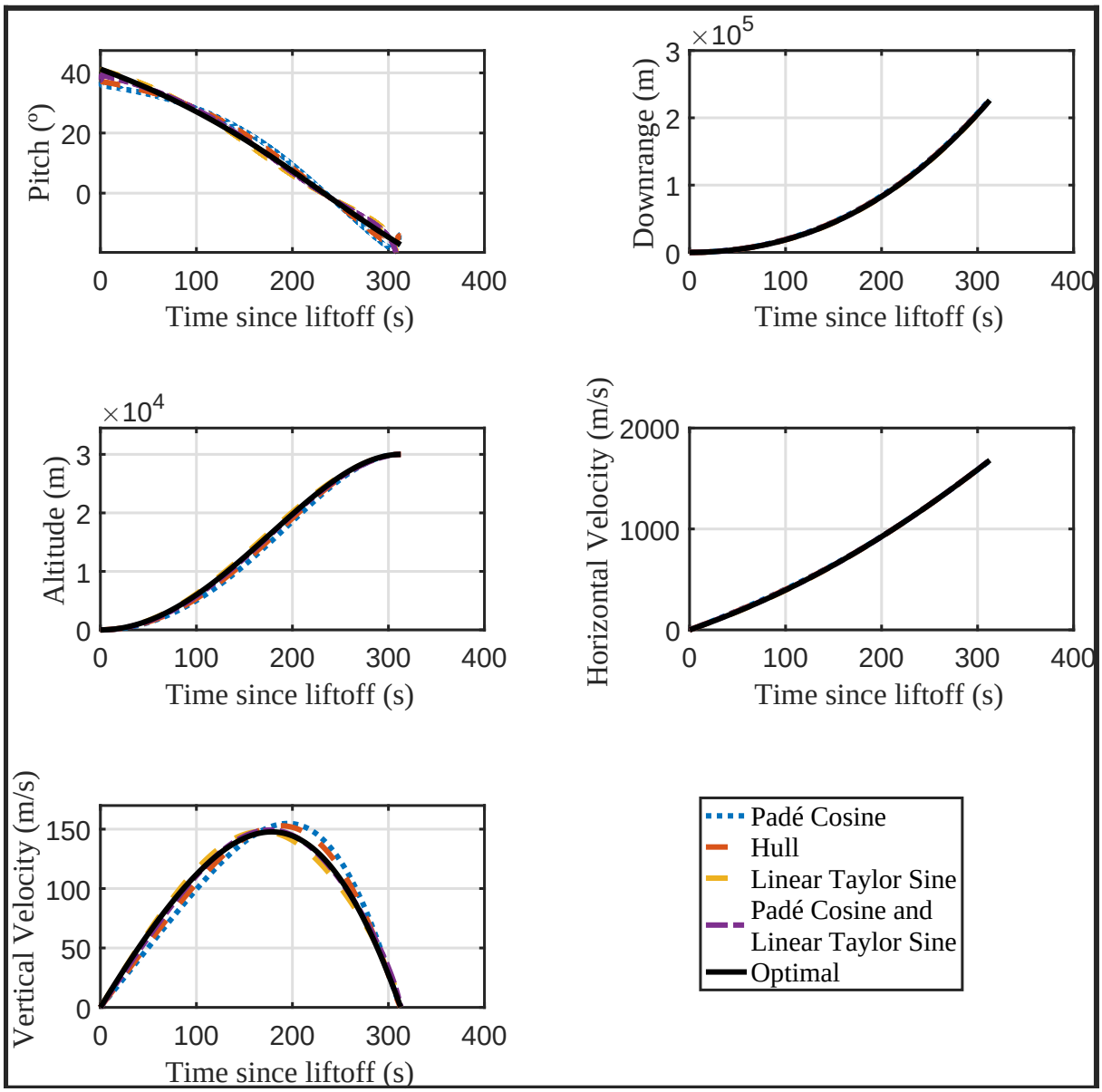

Figure D.7: Comparison of parameters for 30 km altitude insertion using algorithms I and III

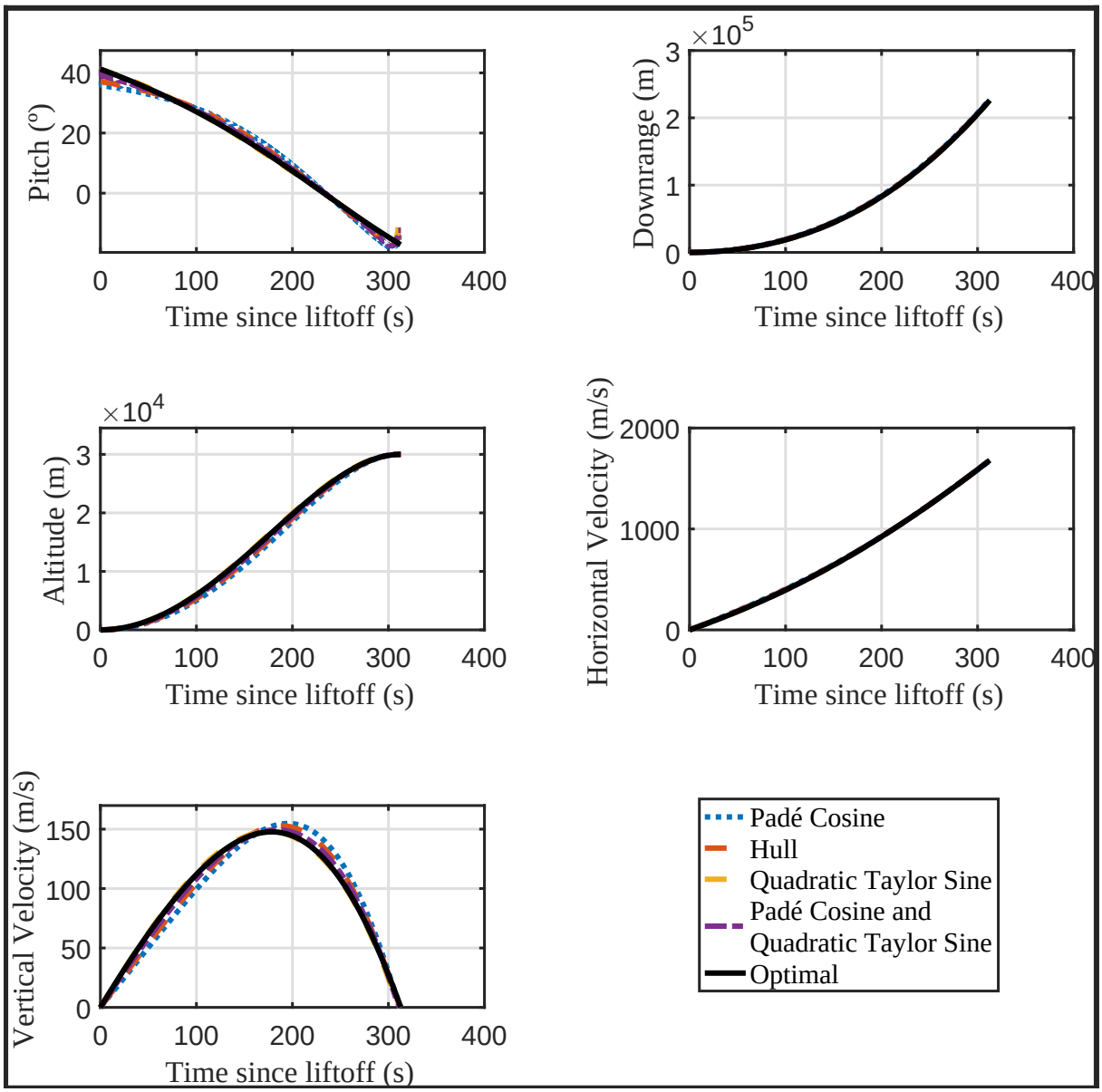

Figure D.8: Comparison of parameters for 30 km altitude insertion using algorithms V and VII

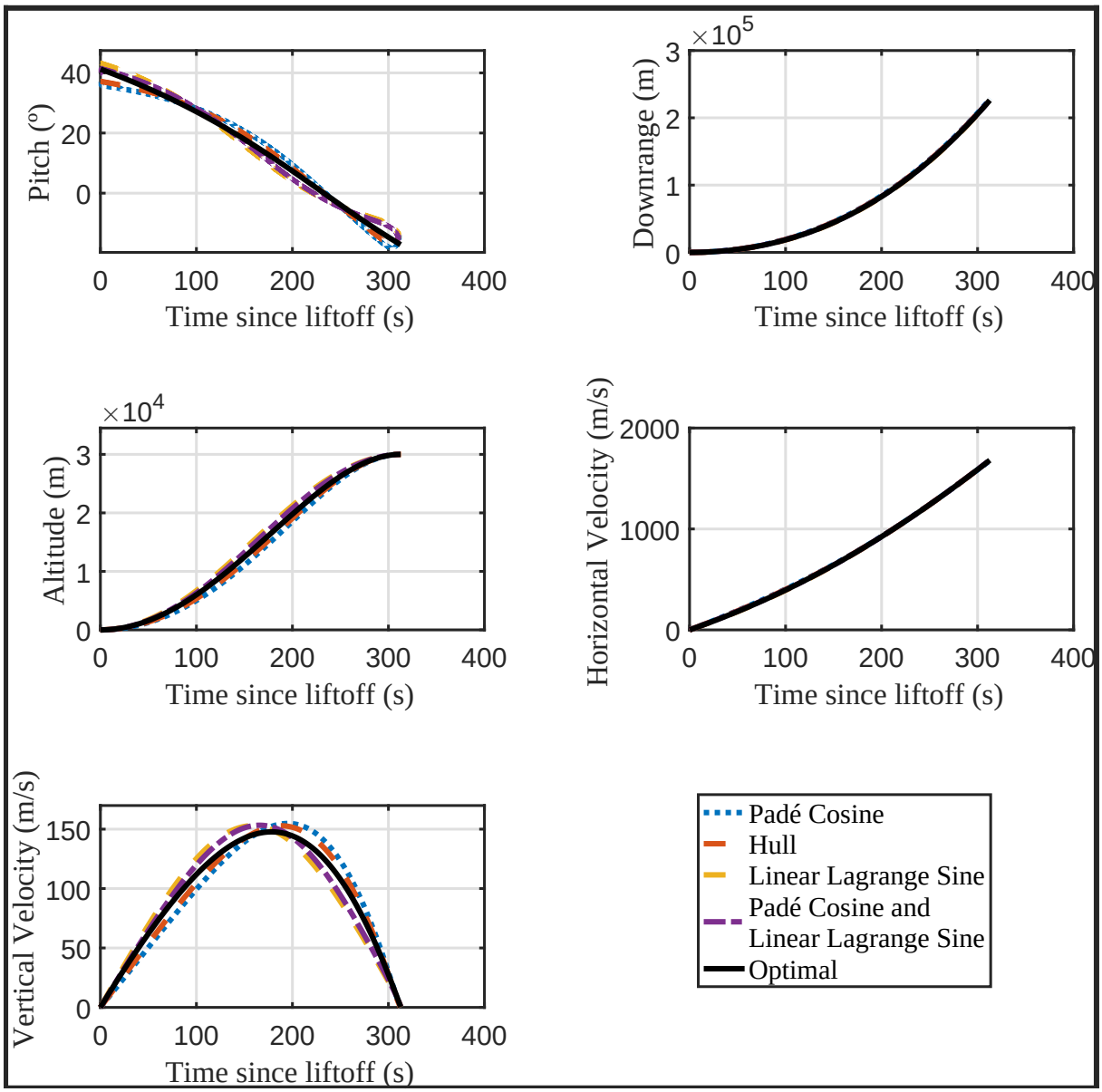

Figure D.9: Comparison of parameters for 30 km altitude insertion using algorithms II and IV

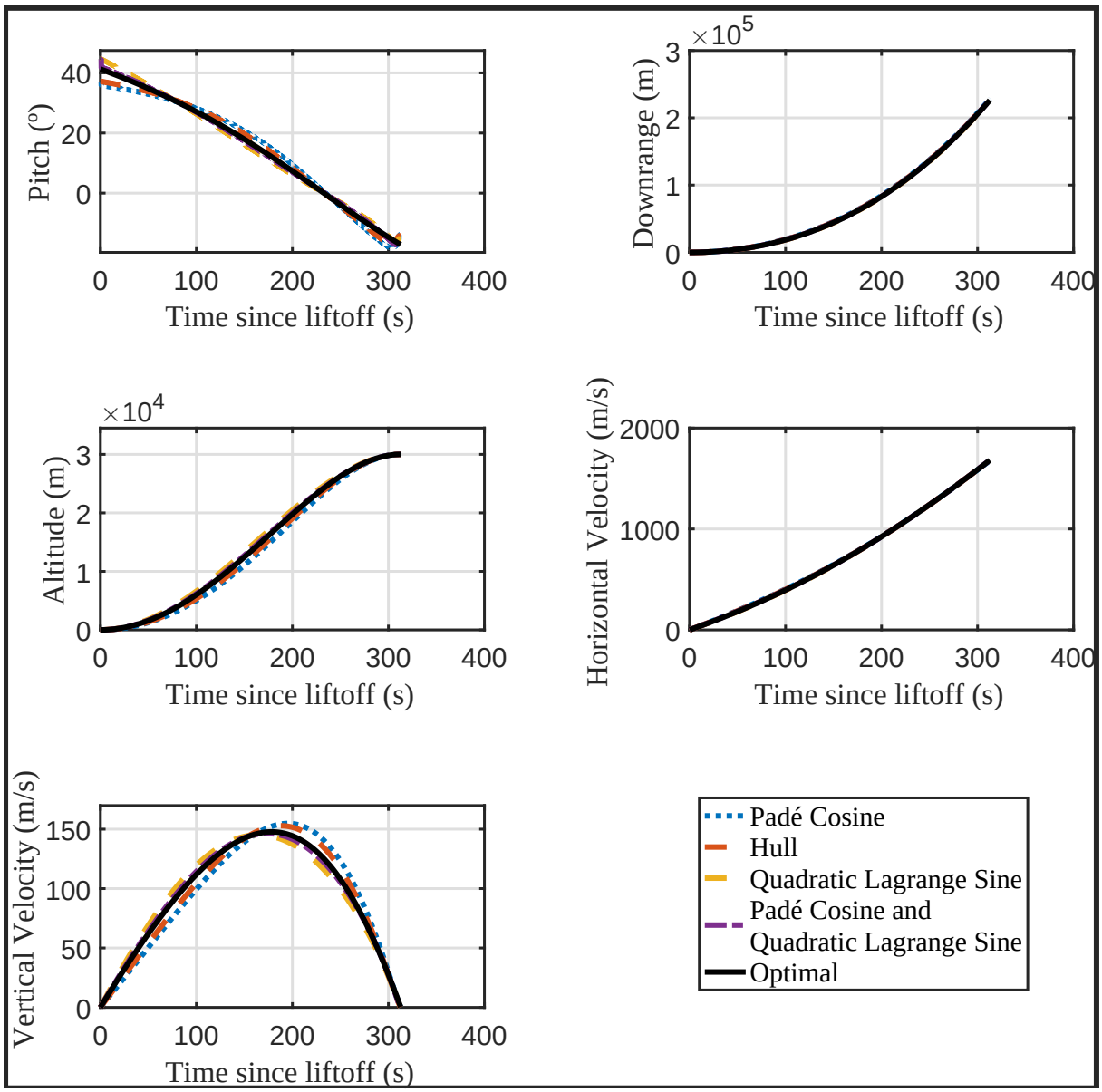

Figure D.10: Comparison of parameters for 30 km altitude insertion using algorithms VI and VIII

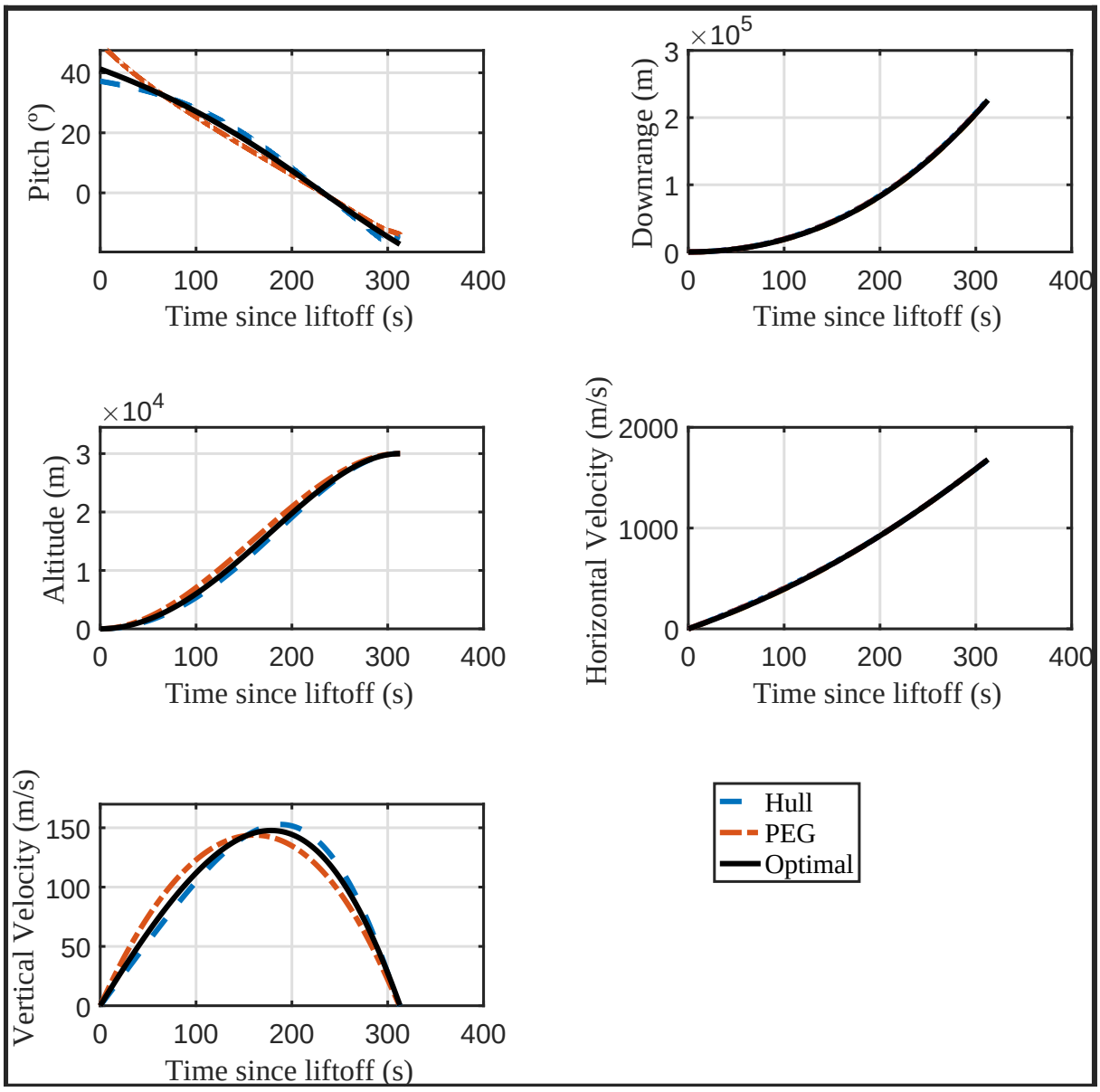

Figure D.11: Comparison of parameters for 30 km altitude insertion using PEG

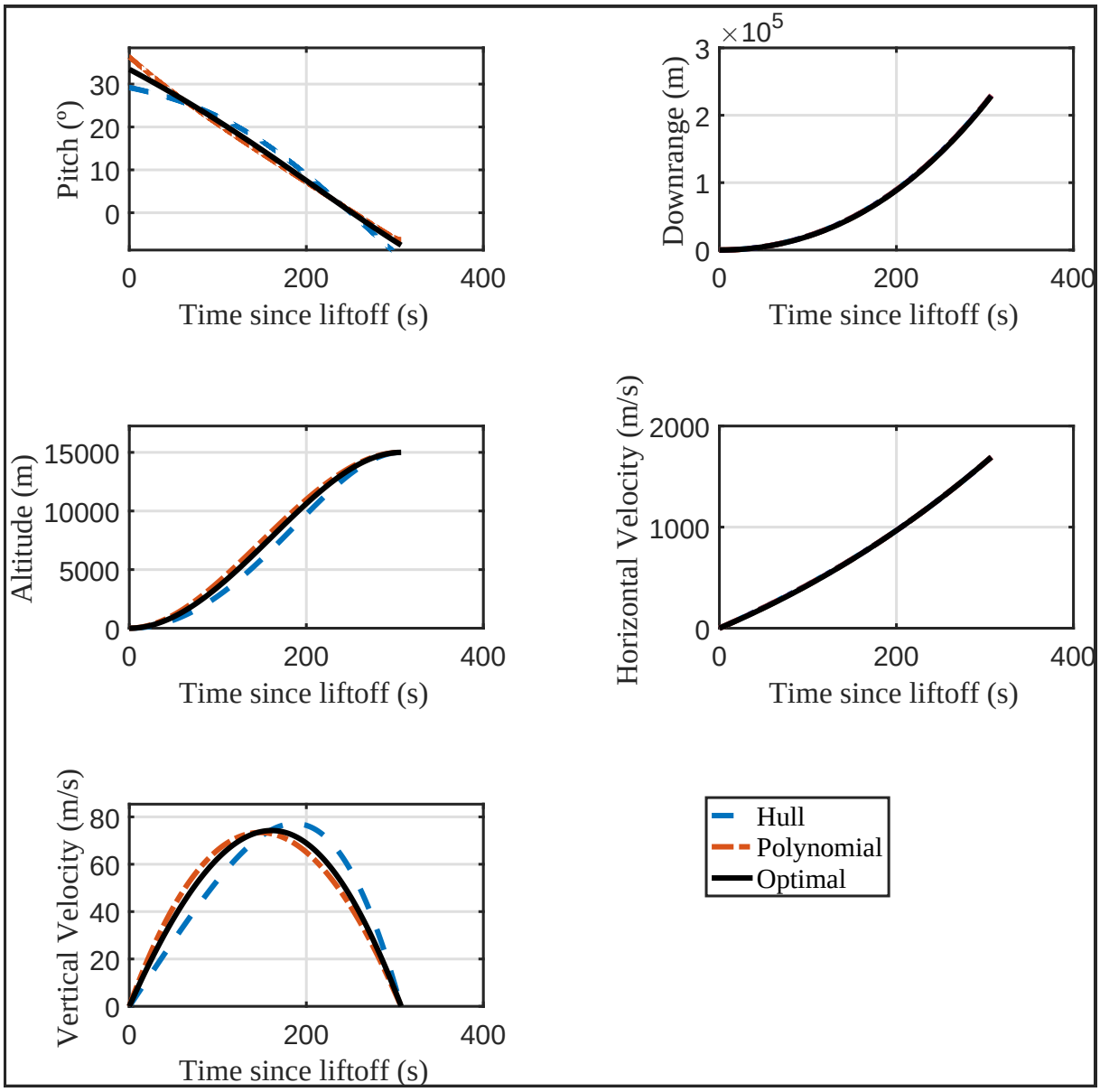

Figure D.12: Comparison of parameters for 30 km altitude insertion using polynomial guidance

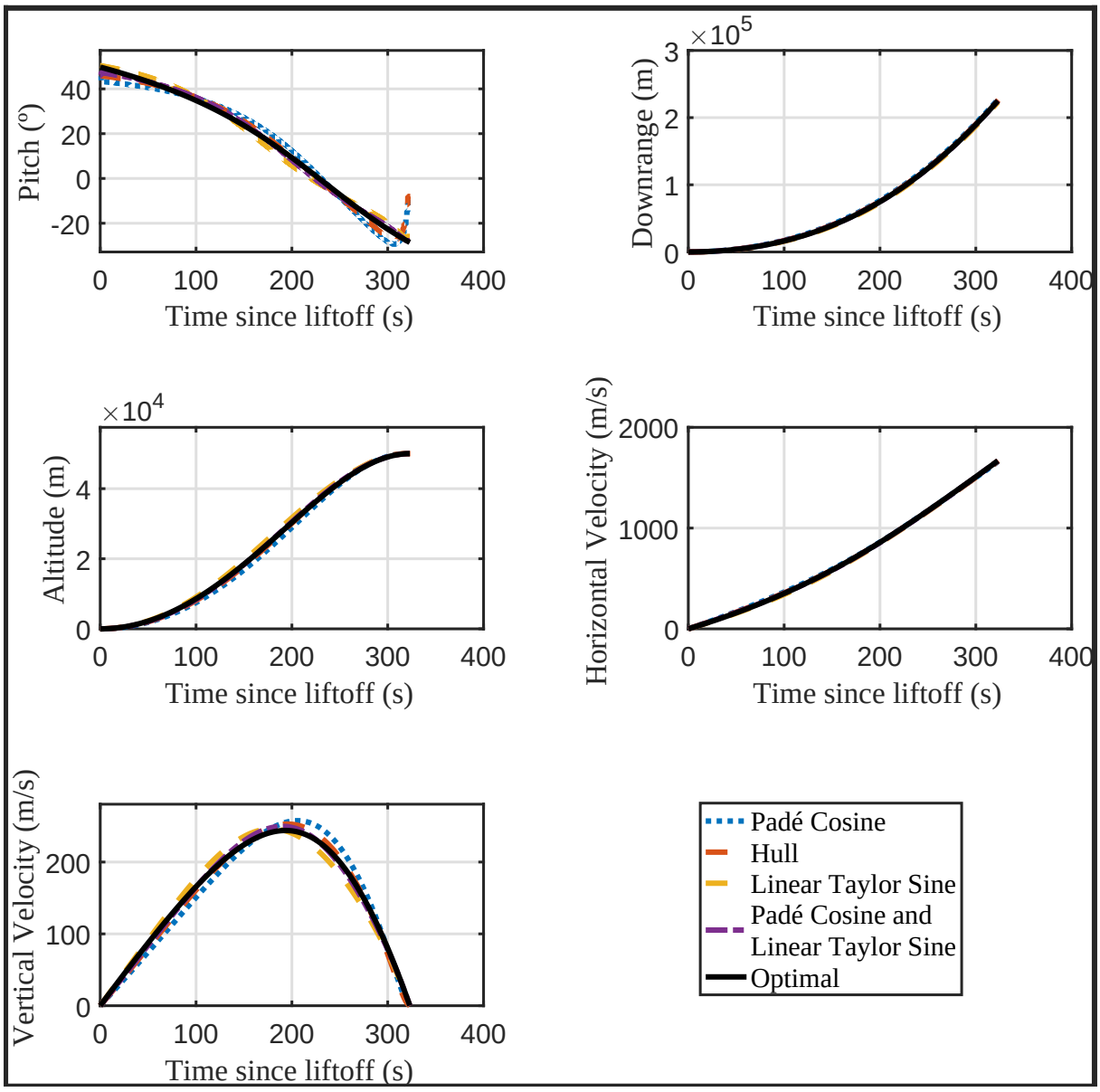

Figure D.13: Comparison of parameters for 50 km altitude insertion using algorithms I and III

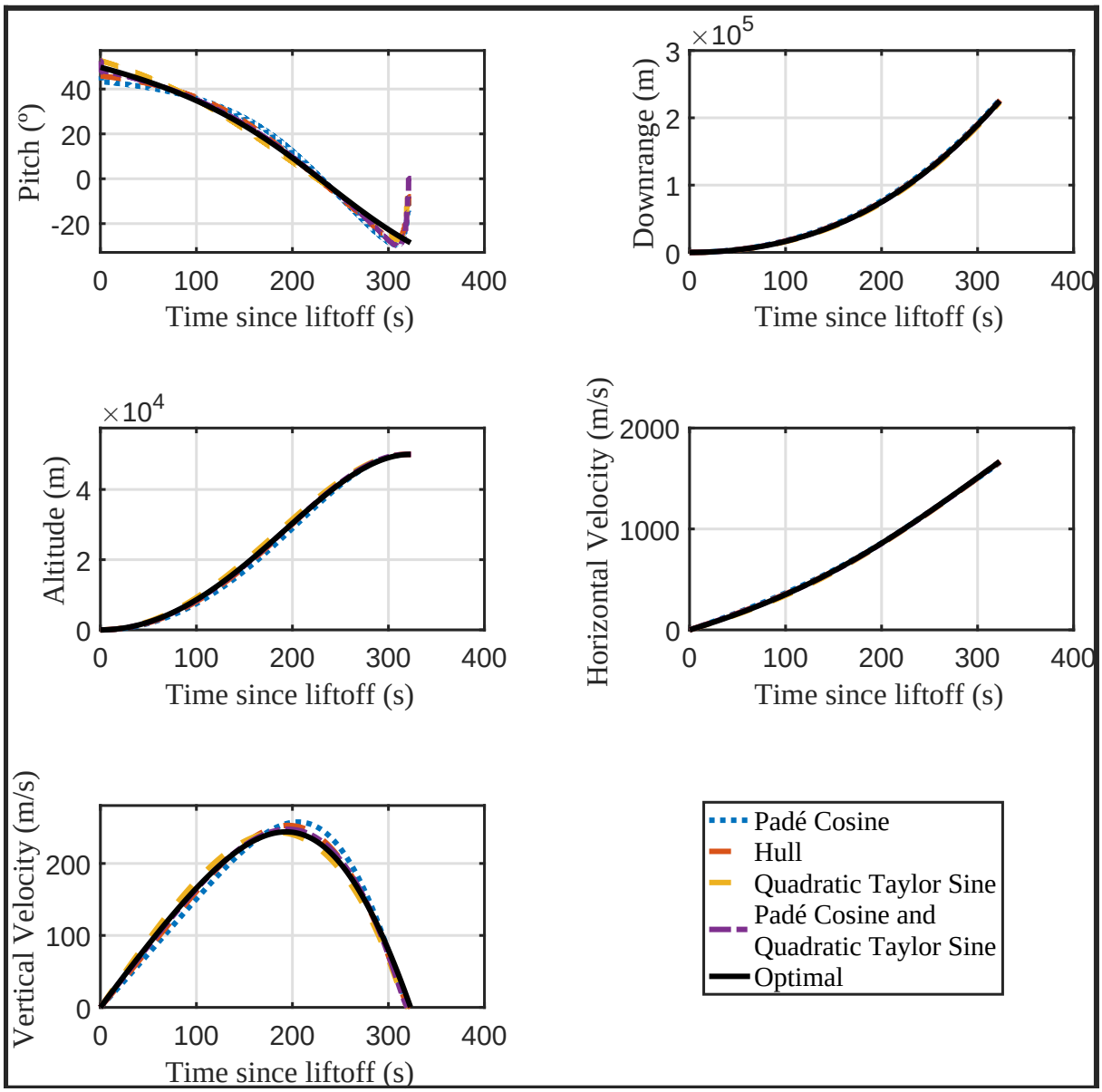

Figure D.14: Comparison of parameters for 50 km altitude insertion using algorithms V and VII

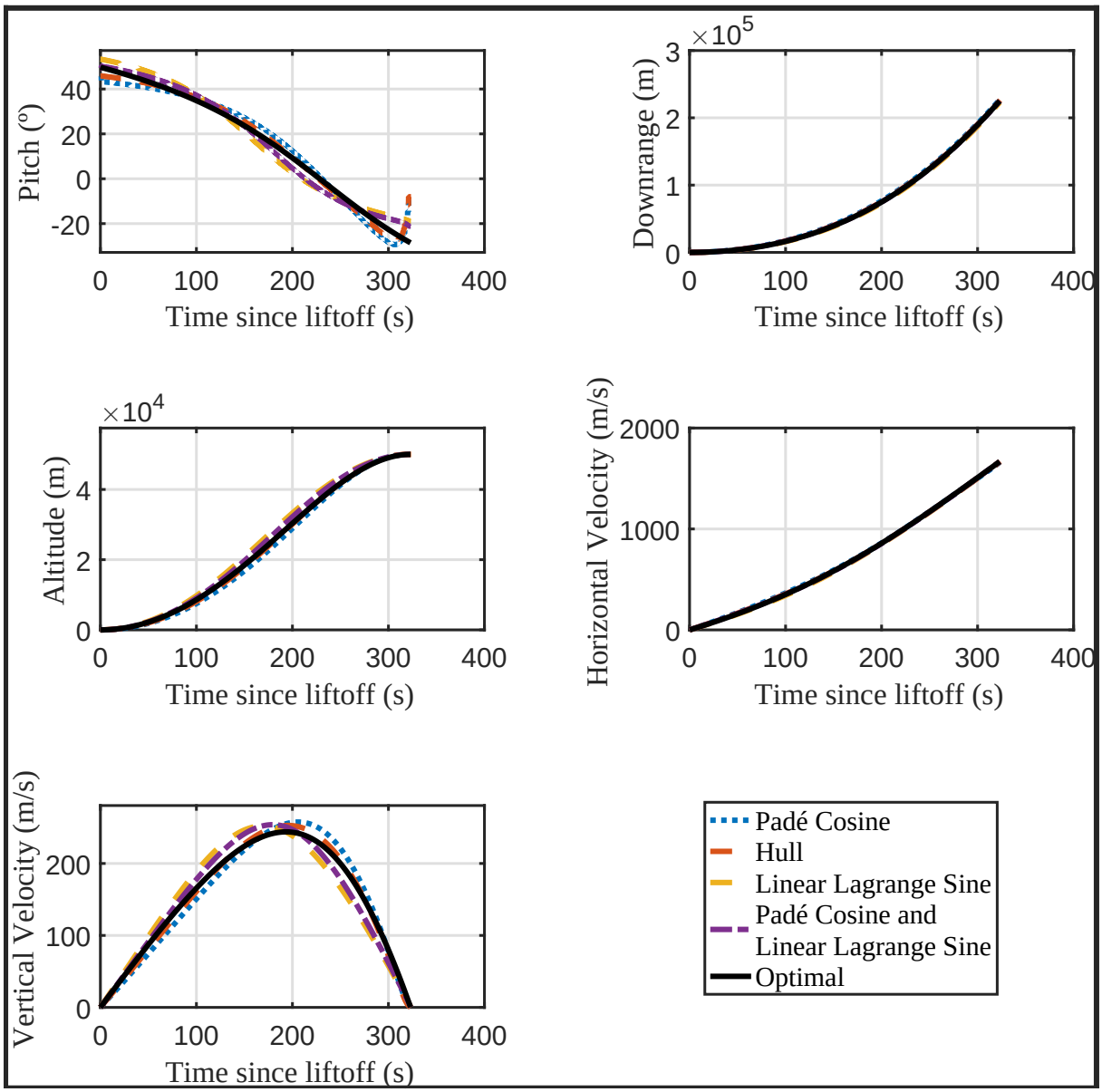

Figure D.15: Comparison of parameters for 50 km altitude insertionusing algorithms II and IV

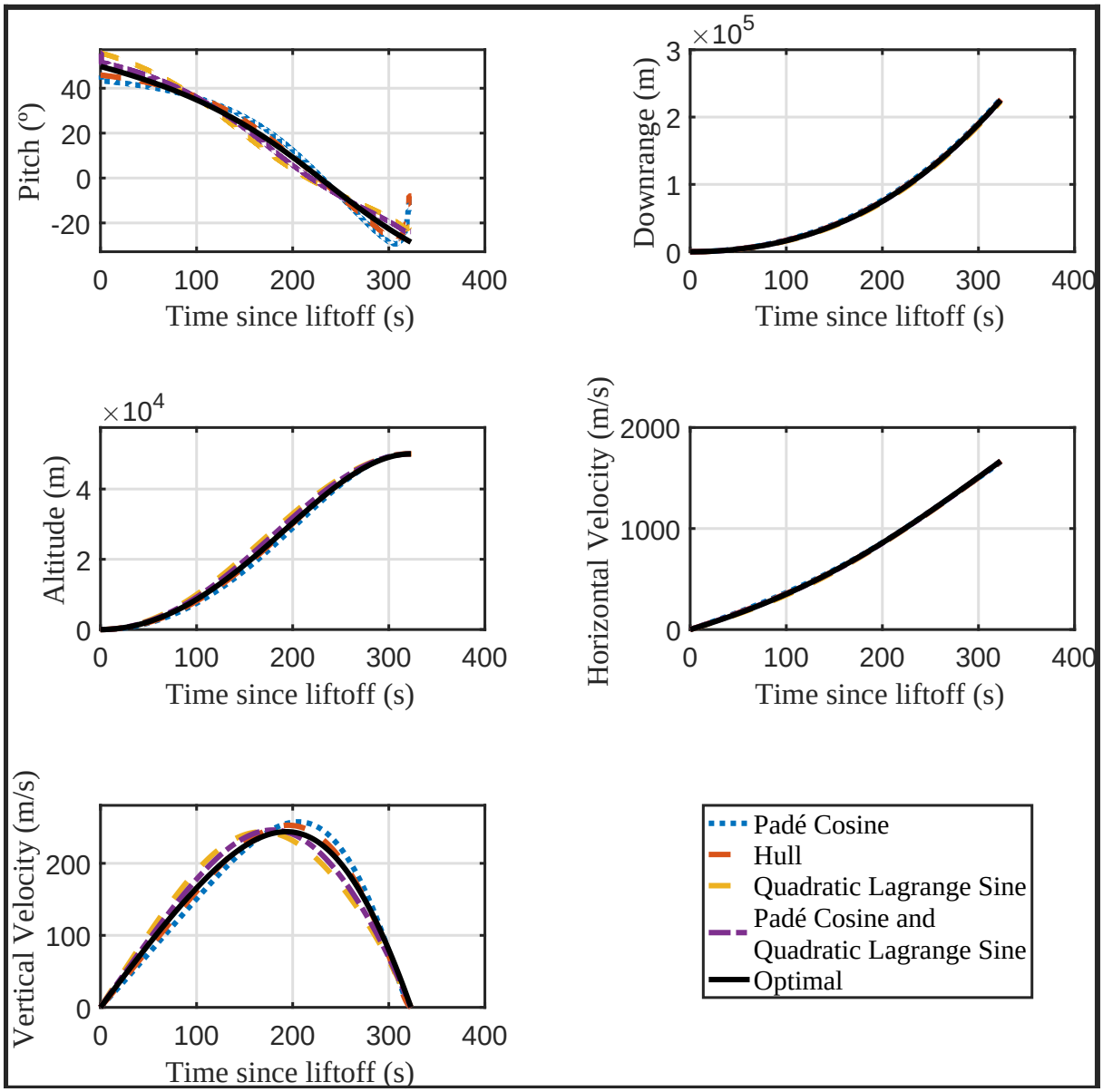

Figure D.16: Comparison of pitch angle, altitude and vertical velocity for 50 km altitude insertion using algorithms VI and VIII

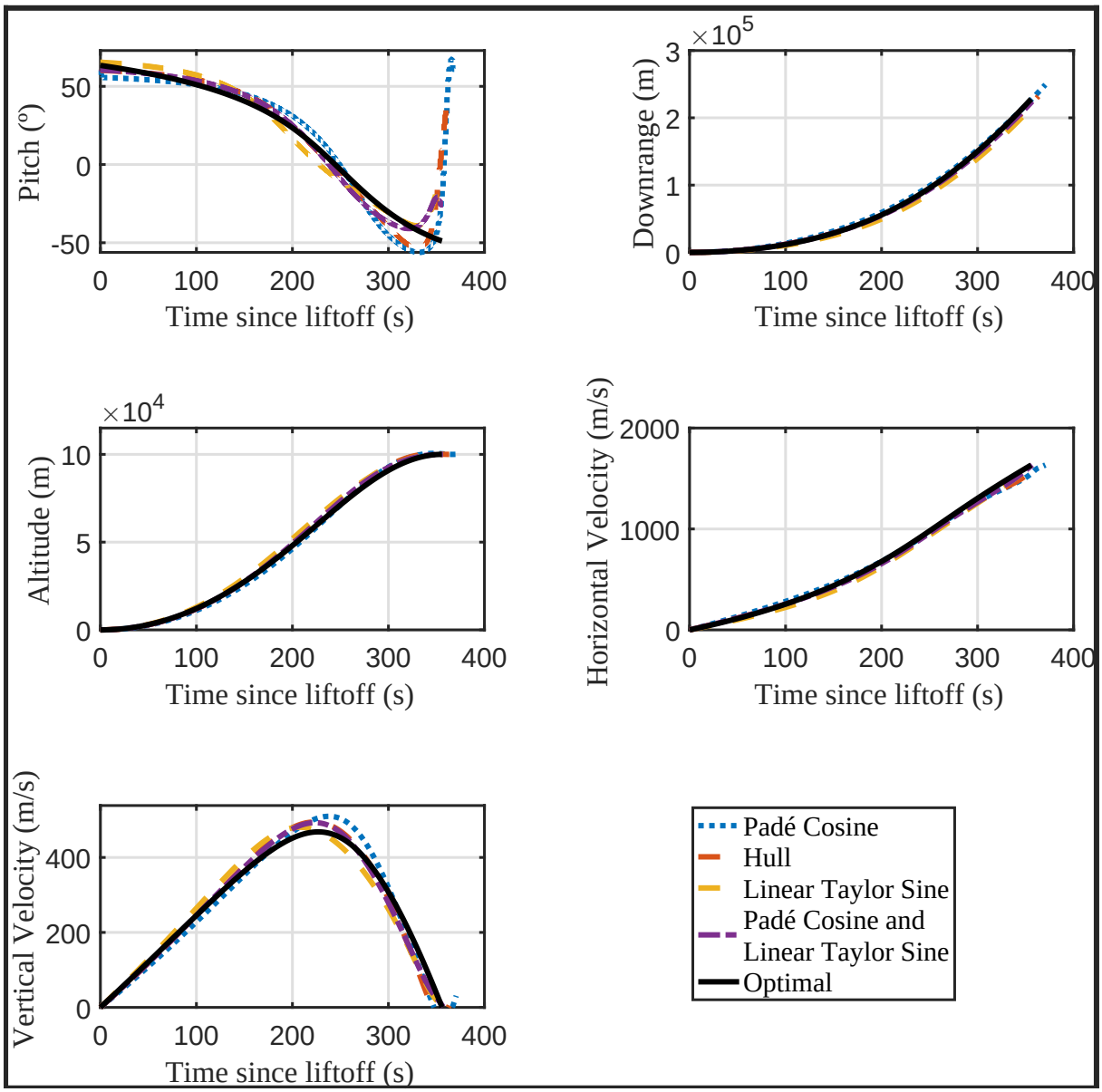

Figure D.17: Comparison of parameters for 100 km altitude insertion using algorithms I and III

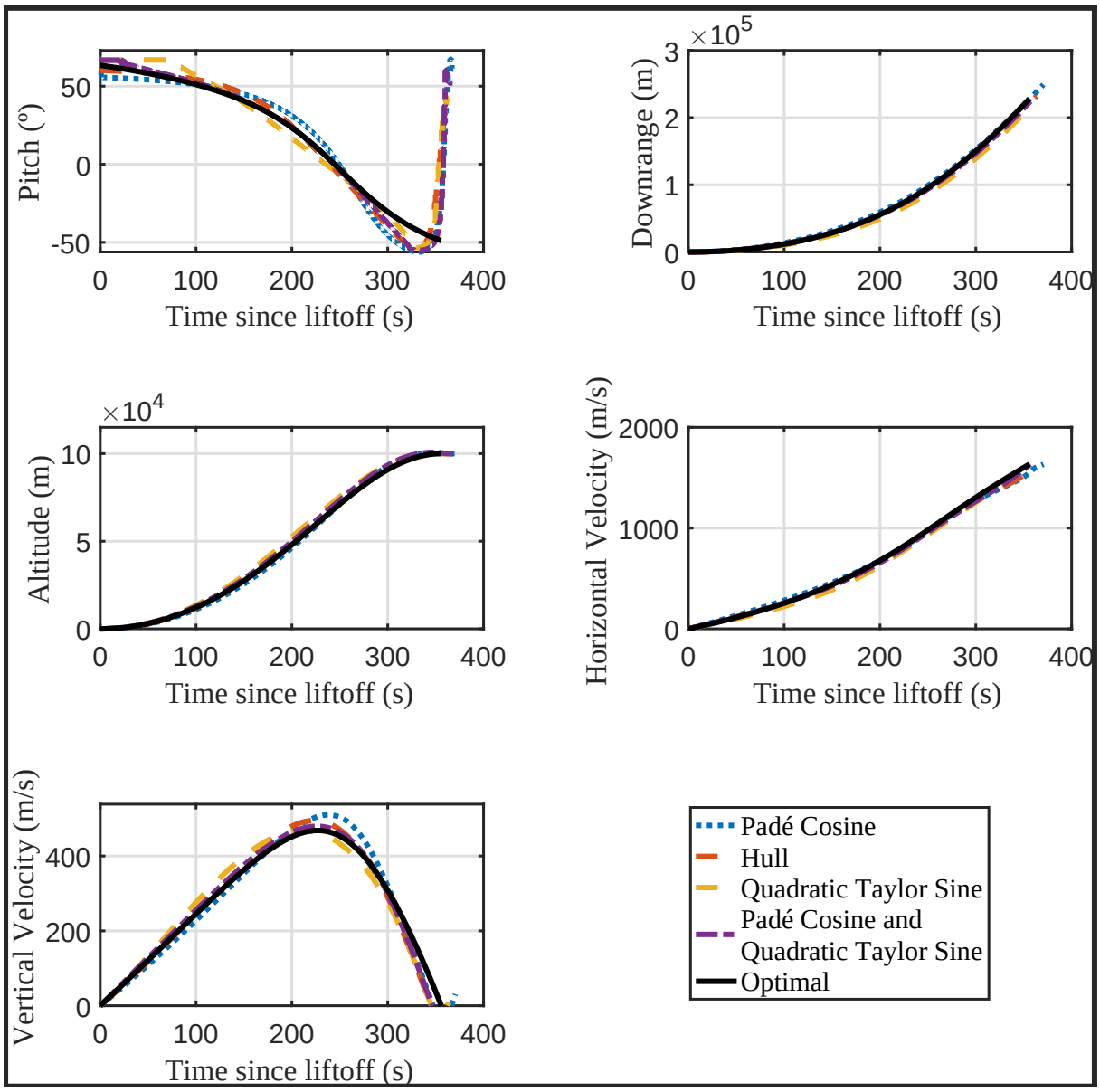

Figure D.18: Comparison of parameters for 100 km altitude insertion using algorithms V and VII

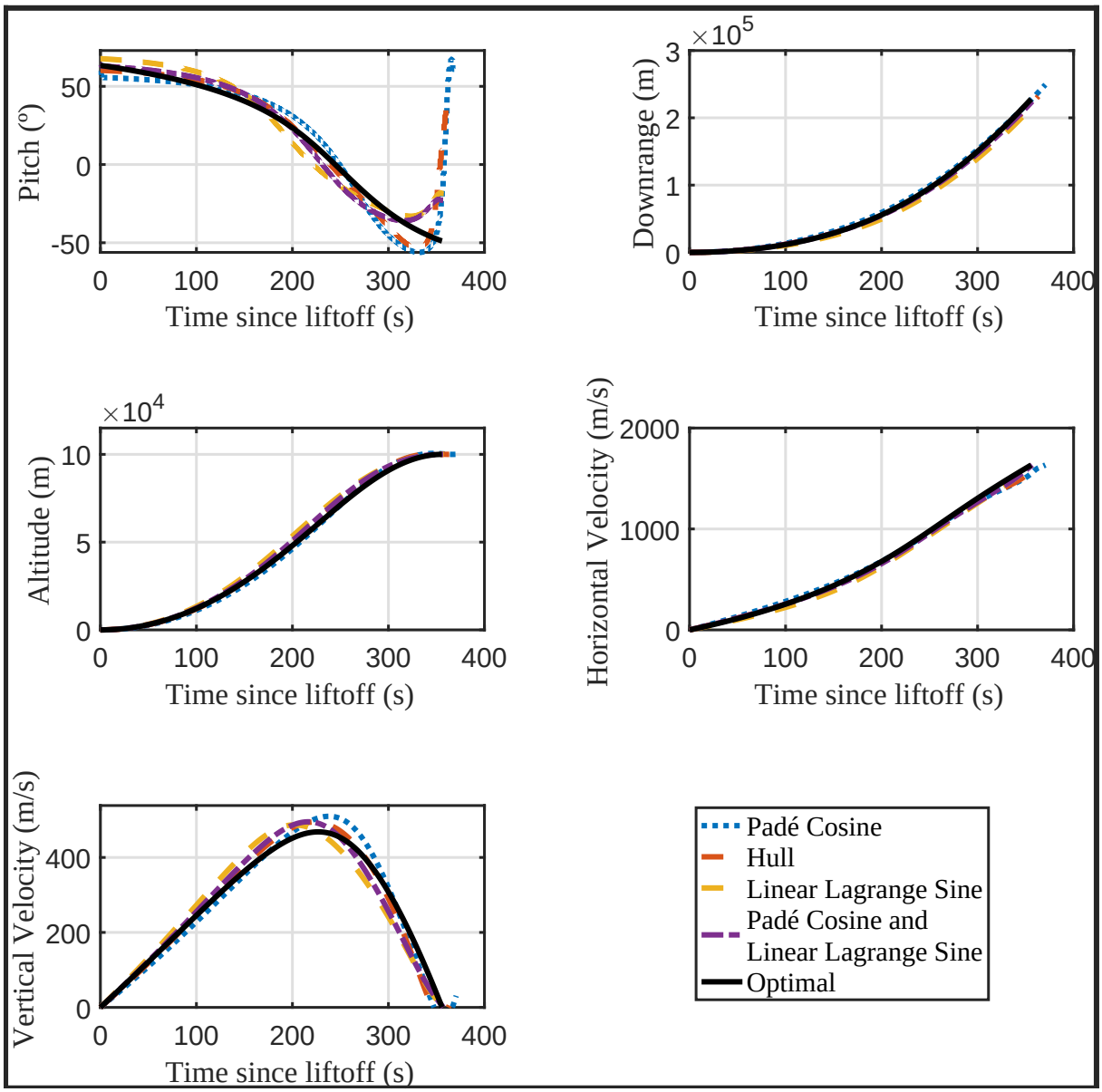

Figure D.19: Comparison of parameters for 100 km altitude insertion using algorithms II and IV

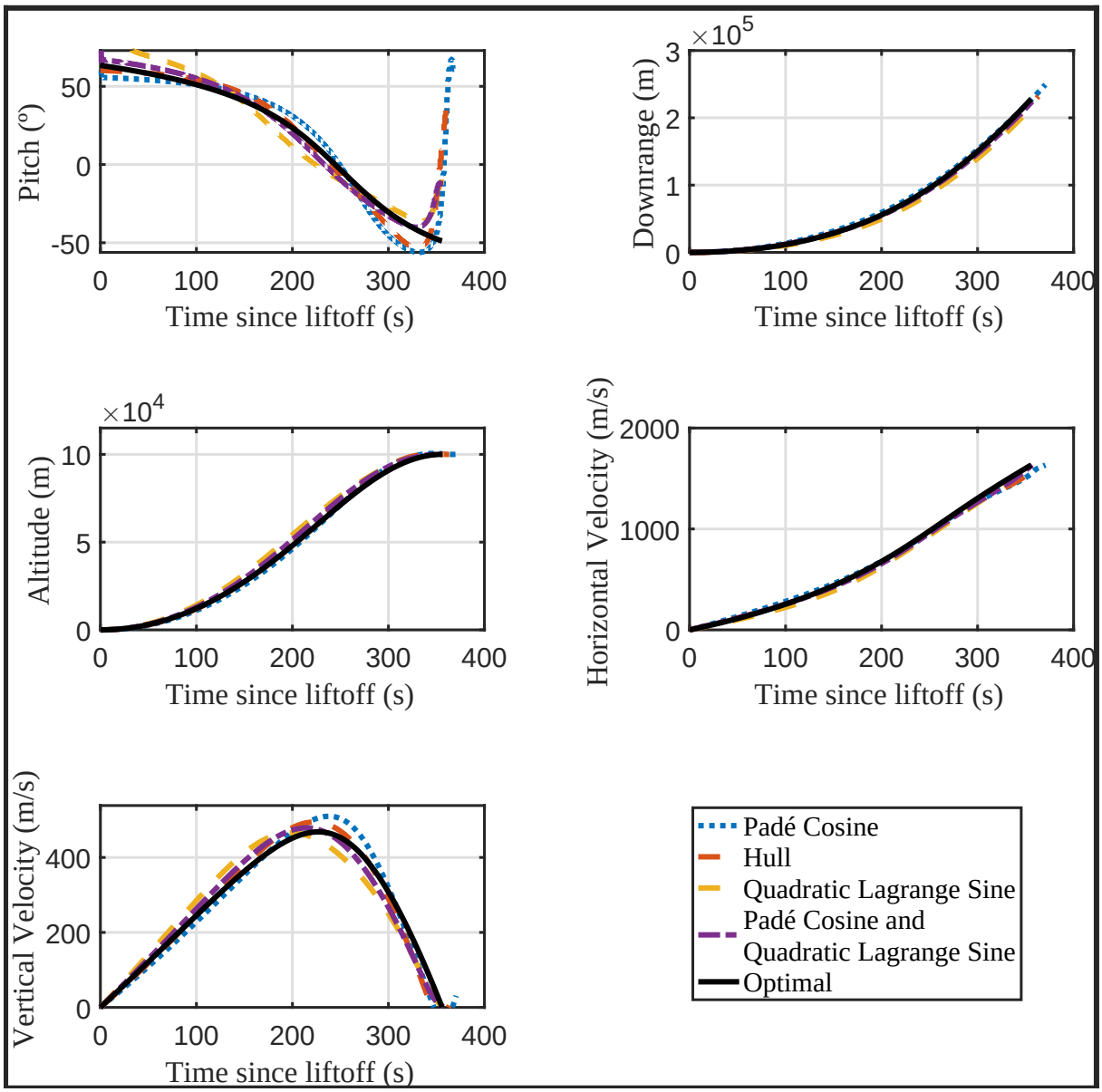

Figure D.20: Comparison of parameters for 100 km altitude insertion using algorithms VI and VIII